

Drivers of plant nutrient acquisition and allocation strategies and their influence
on plant responses to environmental change

by

Evan A. Perkowski, B.S.

A Dissertation

In

Biological Sciences

Submitted to the Graduate Faculty
of Texas Tech University in
Partial Fulfillment of
the Requirements for
the Degree of

Doctor of Philosophy

Approved

Nicholas G. Smith, Ph.D.
Chair of Committee

Aimée T. Classen, Ph.D.

Natasja van Gestel, Ph.D.

Lindsey C. Slaughter, Ph.D.

Dylan W. Schwilk, Ph.D.

Mark Sheridan, Ph.D.
Dean of the Graduate School

May 2023

Copyright 2023, Evan A. Perkowski

Acknowledgements

Placeholder for text

Table of Contents

Acknowledgements	ii
Abstract	vii
List of Tables	viii
List of Figures	x
1. Introduction	1
2. Structural carbon costs to acquire nitrogen are determined by nitrogen and light availability in two species with different nitrogen acquisition strategies	8
2.1 Introduction	8
2.2 Methods	12
2.2.1 <i>Experiment setup</i>	12
2.2.2 <i>Plant measurements and calculations</i>	13
2.2.3 <i>Statistical analyses</i>	14
2.3 Results	16
2.3.1 <i>Carbon costs to acquire nitrogen</i>	16
2.3.2 <i>Whole plant nitrogen biomass</i>	19
2.3.3 <i>Root carbon biomass</i>	21
2.3.4 <i>Root nodule biomass</i>	23
2.4 Discussion	27
3. Soil nitrogen availability modifies leaf nitrogen economies in mature temperate deciduous forests: a direct test of photosynthetic least-cost theory	35
3.1 Introduction	35
3.2 Methods	39
3.2.1 <i>Study site description</i>	39
3.2.2 <i>Experimental design</i>	40
3.2.3 <i>Leaf gas exchange and trait measurements</i>	40
3.2.4 <i>A_{net}/C_i curve-fitting and parameter estimation</i>	43

3.2.5 <i>Proportion of leaf nitrogen allocated to photosynthesis and structure</i>	45
3.2.6 <i>Tradeoffs between nitrogen and water use</i>	46
3.2.7 <i>Soil nitrogen availability and pH</i>	47
3.2.8 <i>Statistical analyses</i>	49
3.3 Results	51
3.3.1 <i>Leaf N content</i>	51
3.3.2 <i>Net photosynthesis and leaf biochemistry</i>	54
3.3.3 <i>Leaf N allocation</i>	57
3.3.4 <i>Tradeoffs between nitrogen and water use</i>	60
3.4 Discussion	63
3.4.1 <i>Soil nitrogen availability modifies tradeoffs between nitrogen and water use</i>	64
3.4.2 <i>Soil pH did not modify tradeoffs between nitrogen and water usage</i>	66
3.4.3 <i>Species identity explains a large amount of variation in leaf and whole plant traits</i>	67
3.4.4 <i>Implications for photosynthetic least-cost theory model development</i>	68
3.4.5 <i>Conclusions</i>	70
4. The relative cost of resource use for photosynthesis drives variance in leaf nitrogen content across climate and soil resource availability gradients	71
4.1 Introduction	71
4.2 Methods	73
4.2.1 <i>Site descriptions and sampling methodology</i>	73
4.2.2 <i>Leaf trait measurements</i>	73
4.2.3 <i>Site climate data</i>	79
4.2.4 <i>Site edaphic characteristics</i>	79
4.2.5 <i>Plant functional group assignments</i>	81
4.2.6 <i>Data analysis</i>	82

4.3 Results	84
4.3.1 Cost to acquire nitrogen relative to water (β)	84
4.3.2 Leaf $C_i:C_a$ (χ)	88
4.3.3 Leaf nitrogen content	91
4.3.4 Structural equation model	95
4.4 Discussion	98
5. Optimal resource investment to photosynthetic capacity maximizes nutrient allocation to whole plant growth under elevated CO₂	99
5.1 Introduction	99
5.2 Methods	104
5.2.1 Seed treatments and experimental design	104
5.2.2 Growth chamber conditions	105
5.2.3 Leaf gas exchange measurements	107
5.2.4 Leaf trait measurements	108
5.2.5 A/C_i curve fitting and parameter estimation	110
5.2.6 Stomatal limitation	110
5.2.7 Proportion of leaf nitrogen allocated to photosynthesis and structure	111
5.2.8 Whole plant traits	113
5.2.9 Statistical analyses	115
5.3 Results	117
5.3.1 Leaf nitrogen content, chlorophyll content, and mass per area	117
5.3.2 Leaf biochemistry and stomatal conductance	121
5.3.3 Leaf nitrogen allocation	125
5.3.4 Whole plant growth and total leaf area	129
5.3.5 Carbon costs to acquire nitrogen	129
5.3.6 Nitrogen fixation	133
5.4 Discussion	137

5.4.1	<i>Soil nitrogen fertilization has divergent effects on leaf and whole plant acclimation responses to CO₂</i>	138
5.4.2	<i>Implications for future model development</i>	142
5.4.3	<i>Study limitations and future directions</i>	143
5.4.4	<i>Conclusions</i>	145
6.	Conclusions	147
	References	149

Abstract

List of Tables

2.1 Analysis of variance results exploring species-specific effects of light availability, nitrogen fertilization, and their interactions on carbon costs to acquire nitrogen, whole-plant nitrogen biomass, and root carbon biomass	17
2.2 Analysis of variance results exploring effects of light availability, nitrogen fertilization, and their interactions on <i>G. max</i> root nodule biomass and the ratio of root nodule biomass to root biomass*	24
2.3 Slopes of the regression line describing the relationship between each dependent variable and nitrogen fertilization at each light level*	25
3.1 Effects of soil N availability, soil pH, and species on leaf N content per unit leaf area (N_{area}), leaf N content per unit leaf mass (N_{mass}), and leaf mass per unit leaf area (M_{area})	52
3.2 Effects of soil N availability, soil pH, species, and N_{area} on leaf biochemistry	55
3.3 Effects of soil N availability, soil pH, and species on the proportion of leaf nitrogen content allocated to photosynthesis, Rubisco, bioenergetics, and structure	58
3.4 Effects of soil N availability, soil pH, species, and N_{area} on tradeoffs between nitrogen and water use	61

4.1	Site locality information, sampling year(s), 2006-2020 mean annual precipitation (MAP; mm), mean annual temperature (MAT; °C), and water holding capacity (WHC; mm)*	77
4.2	Effects of soil moisture, soil nitrogen availability, and plant functional group on β	86
4.3	Effects of soil moisture, soil nitrogen availability, and plant functional group on χ^*	89
4.4	Effects of soil nitrogen fertilization, inoculation, and CO ₂ treatments on N_{area} , N_{mass} , M_{area} , and Chl_{area}	93
4.5	Structural equation model results investigating direct effects of climatic and soil resource availability on N_{area} , N_{mass} , M_{area} , χ , and β	96
5.1	Effects of soil nitrogen fertilization, inoculation, and CO ₂ treatments on N_{area} , N_{mass} , M_{area} , and Chl_{area}	119
5.2	Effects of soil nitrogen fertilization, inoculation, and CO ₂ on leaf biochemistry	123
5.3	Effects of soil N availability, soil pH, species, and N_{area} on leaf nitrogen allocation	127
5.4	Effects of soil N availability, soil pH, species, and N_{area} on total leaf area, whole plant biomass, and costs of nitrogen acquisition	131
5.5	Effects of soil N availability, soil pH, species, and N_{area} on leaf biochemistry	135

List of Figures

2.1 Relationships between soil nitrogen fertilization and light availability on carbon costs to acquire nitrogen in <i>G. hirsutum</i> and <i>G. max</i>	18
2.2 Relationships between soil nitrogen fertilization and light availability on whole-plant nitrogen biomass in <i>G. hirsutum</i> and <i>G. max</i>	20
2.3 Relationships between soil nitrogen fertilization and light availability on root carbon biomass in <i>G. hirsutum</i> and <i>G. max</i>	22
2.4 Effects of shade cover and nitrogen fertilization on root nodule biomass and the ratio of root nodule biomass to root biomass in <i>G. max</i>	26
3.1 Effects of soil N availability and species on leaf N content per unit leaf area, leaf nitrogen content per unit leaf biomass, and leaf mass per leaf area	53
3.2 Effects of soil N availability, species, and leaf N content leaf biochemistry	56
3.3 Effects of soil N availability, species, and leaf N content on the fraction of leaf nitrogen allocated to photosynthesis and structure	59
3.4 Effects of soil N availability, species, and leaf N content on tradeoffs between nitrogen and water use	62

4.1	Maps that detail site locations along 2006-2020 mean annual precipitation (panel A) and mean annual temperature (panel B) gradients in Texas, USA.	78
4.2	Effects of soil nitrogen availability and soil moisture on the unit cost ratio β	87
4.3	Effects of 4-day mean vapor pressure deficit, 2-day soil moisture (per water holding capacity), and soil nitrogen availability on χ	90
4.4	Effects of χ , soil nitrogen availability, and soil moisture on leaf nitrogen content per unit leaf area, leaf nitrogen content per unit leaf biomass, and leaf mass per area.	94
4.5	Structural equation model results exploring direct and indirect drivers of N_{area}	97
5.1	Effects of CO_2 , fertilization, and inoculation on leaf nitrogen per unit leaf area, leaf nitrogen content, leaf mass per unit leaf area, and chlorophyll content per unit leaf area.	120
5.2	Effects of CO_2 , fertilization, and inoculation on maximum rate of Rubisco carboxylation, the maximum rate of RuBP regeneration, and the ratio of the maximum rate of RuBP regeneration to the maximum rate of Rubisco carboxylation leaf mass per unit leaf area, dark respiration, stomatal conductance, and stomatal limitation. . .	124
5.3	Effects of CO_2 , fertilization, and inoculation on the relative fraction of leaf nitrogen allocated to photosynthesis and the fraction of leaf nitrogen allocated to structure.	128

5.4 Effects of CO ₂ , fertilization, and inoculation on total leaf area, total biomass, and structural carbon costs to acquire nitrogen.	132
5.5 Effects of CO ₂ , fertilization, and inoculation on nodule biomass, nodule: root biomass, and percent nitrogen fixed from the atmosphere.	136

1 Chapter 1

2 Introduction

3 Photosynthesis represents the largest carbon flux between the atmosphere
4 and biosphere, and is regulated by complex ecosystem carbon and nutrient cy-
5 cles (Hungate et al. 2003; IPCC 2021). As a result, the inclusion of robust,
6 empirically tested representations of photosynthetic processes is critical in order
7 for terrestrial biosphere models to accurately and reliably simulate carbon and
8 nutrient fluxes between the atmosphere and terrestrial biosphere (Wieder et al.
9 2015; Smith and Dukes 2013; Prentice et al. 2015; Oreskes et al. 1994). Despite
10 evidence that the inclusion of coupled carbon and nutrient cycles can improve
11 model uncertainty, widespread divergence in predicted carbon and nutrient fluxes
12 is still apparent across model products (Arora et al. 2020; Friedlingstein et al.
13 2014; Davies-Barnard et al. 2020). Divergence in predicted carbon and nutrient
14 fluxes across terrestrial biosphere models may be due to an incomplete under-
15 standing of how plants acclimate to changing environments (Smith and Dukes
16 2013; Davies-Barnard et al. 2020), as terrestrial biosphere models are sensitive to
17 the formulation of photosynthetic processes (Ziehn et al. 2011; Bonan et al. 2011;
18 Booth et al. 2012; Smith et al. 2016; Smith et al. 2017; Rogers et al. 2017).

Many terrestrial biosphere models predict leaf-level photosynthesis through linear relationships between area-based leaf nitrogen content and the maximum rate of Ribulose-1,5-bisphosphate carboxylase/oxygenase ("Rubisco"), following from the idea that large fractions of nitrogen allocated to leaf tissue are allocated to the construction and maintenance of Rubisco (Evans 1989). The inclusion of

24 coupled carbon and nutrient cycles in terrestrial biosphere models (Shi et al. 2016;
25 Braghieri et al. 2022) allows for the prediction of leaf nitrogen content through
26 soil nitrogen availability, which causes models to indirectly predict photosynthetic
27 processes through shifts in soil nitrogen availability (Smith et al. 2014; Lawrence
28 et al. 2019). While these patterns are commonly observed in ecosystems globally
29 (Brix 1971; Evans 1989; Liang et al. 2020; Firn et al. 2019), this formulation of
30 photosynthetic processes does not allow for the prediction of leaf and whole plant
31 acclimation responses to changing environments (Smith and Dukes 2013; Rogers
32 et al. 2017; Harrison et al. 2021). Incorporating leaf and whole plant acclimation
33 schemes in terrestrial biosphere models is important (Smith and Dukes 2013),
34 particularly because recent work indicates that variance in leaf nitrogen content
35 and leaf photosynthesis across environmental gradients may be better explained
36 as an integrated product of leaf acclimation responses to changing climates and
37 soil nitrogen availability than soil nitrogen availability alone (Dong et al. 2017;
38 Dong et al. 2020; Smith et al. 2019; Querejeta et al. 2022; Dong et al. 2022;
39 Westerband et al. 2023).

40 Photosynthetic least-cost theory (Prentice et al. 2014; Wang et al. 2017;
41 Smith et al. 2019; Scott and Smith 2022; Harrison et al. 2021) provides a con-
42 temporary framework for predicting leaf and whole plant acclimation responses
43 to environmental change. The theory, which unifies photosynthetic optimal coor-
44 dination (Chen et al. 1993; Maire et al. 2012) and least-cost (Wright et al. 2003)
45 theories, posits that plants optimize photosynthetic processes by minimizing the
46 summed cost of nitrogen and water use (referred to here and in the rest of this
47 dissertation as β). Photosynthetic processes are optimized such that nitrogen is

48 allocated to photosynthetic enzymes in to allow net photosynthesis rates to be
49 equally co-limited by the maximum rate of Rubisco carboxylation and the max-
50 imum rate of Ribulose-1,5-bisphosphate (RuBP) regeneration (Chen et al. 1993;
51 Maire et al. 2012). The theory indicates that costs of nitrogen and water use
52 are substitutable such that, in a given environment, optimal photosynthesis rates
53 can be achieved by sacrificing inefficient use of a relatively more abundant (and
54 less costly to acquire) resource for more efficient use of a relatively less abundant
55 (and more costly to acquire) resource. These predictions imply that acclimation
56 responses to changing environments may be partially driven by tradeoffs between
57 nitrogen and water use, though empirical tests of the theory are sparse.

58 Optimality models leveraging patterns expected from photosynthetic least-
59 cost theory have been developed for both C₃ (Wang et al. 2017; Smith et al. 2019;
60 Stocker et al. 2020) and more recently for C₄ species (Scott and Smith 2022). Such
61 models show broad agreement with patterns observed across environmental gradi-
62 ents (Paillassa et al. 2020; Querejeta et al. 2022; Smith et al. 2019; Westerband
63 et al. 2023), and are capable of reconciling dynamic leaf nitrogen-photosynthesis
64 relationships and acclimation responses to elevated CO₂, temperature, light avail-
65 ability, and vapor pressure deficit (Dong et al. 2017; Dong et al. 2020; Dong et al.
66 2022; Dong et al. 2022; Smith and Keenan 2020; Luo et al. 2021; Peng et al. 2021;
67 Querejeta et al. 2022; Westerband et al. 2023). Current versions of optimality
68 models that invoke patterns expected from photosynthetic least-cost theory hold
69 β constant across growing environments. As growing evidence suggests that costs
70 of nitrogen use change across resource availability and climatic gradients in species
71 with different nutrient acquisition strategies (Fisher et al. 2010; Brzostek et al.

72 2014; Allen et al. 2020; Terrer et al. 2018), one might expect that β should
73 dynamically change across environments and in species with different acquisition
74 strategies. However, manipulative experiments that test mechanisms underlying
75 nitrogen-water use tradeoffs and leaf nitrogen-photosynthesis relationships pre-
76 dicted from theory are rare, and no study has related these patterns to shifts in β
77 or across species with different nutrient acquisition strategies. Understanding the
78 dynamicism of β across different environmental contexts and impacts of β on pat-
79 terns expected from theory are critical for further optimality model development,
80 and is the central motivation for the experiments presented in this dissertation.

81 In this dissertation, I use four experiments to quantify nutrient acquisition
82 and allocation responses under different environmental conditions and in species
83 with different nutrient acquisition strategies. These experiments provide impor-
84 tant empirical data needed to evaluate patterns expected from photosynthetic
85 least-cost theory and test mechanisms that drive such patterns. In the first ex-
86 perimental chapter, I re-analyze data from a greenhouse experiment that grew
87 *Glycine max* L. (Merr) and *Gossypium hirsutum* seedlings under full-factorial
88 combinations of four light treatments and four fertilization treatments. This re-
89 analysis examined the effect of soil nitrogen availability and light availability on
90 structural carbon costs to acquire nitrogen in a species capable of forming associ-
91 ations with symbiotic nitrogen-fixing bacteria (*G. max*) and a species not capable
92 of forming such associations (*G. hirsutum*). I find strong evidence suggesting that
93 increasing light availability increases structural carbon costs to acquire nitrogen
94 and that increasing soil nitrogen fertilization decreases structural carbon costs to
95 acquire nitrogen.

96 In the second experimental chapter, I measure leaf physiological traits in
97 the upper canopy of mature trees growing in a 9-year nitrogen-by-pH field manip-
98 ulation experiment to assess whether changes in soil nitrogen availability or soil
99 pH modify nitrogen-water use tradeoffs expected from photosynthetic least-cost
100 theory. I find strong nitrogen-water use tradeoffs in response to increasing soil ni-
101 trogen availability, indicated by a strong negative relationship between leaf $C_i:C_a$
102 (referred to here and in the rest of this dissertation as χ) and leaf nitrogen content,
103 as well as a strong increase in leaf nitrogen content per unit leaf χ with increas-
104 ing soil nitrogen availability. Interestingly, I also find a null effect of soil pH on
105 nitrogen-water use tradeoffs. These patterns provide strong support for patterns
106 expected from photosynthetic least-cost theory across soil nitrogen availability
107 gradients, and indicate that previous studies which note strong nitrogen-water
108 use tradeoffs in response to soil pH may be driven by covariation between soil
109 nitrogen availability and soil pH (Paillassa et al. 2020; Westerband et al. 2023).

110 In the third experimental chapter, I leverage a broad precipitation and soil
111 nutrient availability gradient in Texan grasslands to investigate primary drivers of
112 leaf nitrogen content. In this chapter, I directly quantify β and χ using leaf $\delta^{13}\text{C}$ to
113 examine primary drivers of leaf nitrogen content and find that leaf nitrogen content
114 is driven through a negative relationship with χ . I also show that soil nitrogen
115 availability is negatively associated with β , and that β is positively associated
116 with χ . I show strong support for patterns expected from theory, showing for
117 the first time that positive effects of increasing soil nitrogen availability on leaf
118 nitrogen content are mediated by changes in β .

119 In the fourth experimental chapter, I use reach-in growth chambers to

120 quantify leaf and whole plant acclimation responses to CO₂ across a soil nitro-
121 gen fertilization gradient, while also manipulating nutrient acquisition strategy
122 by controlling whether seedlings were able to form associations with symbiotic
123 nitrogen-fixing bacteria. Specifically, I measure leaf physiological and whole plant
124 growth responses of 7-week *G. max* seedlings grown under one of two CO₂ treat-
125 ments, one of nine fertilization treatments, and one of two inoculation treatments
126 in a full factorial design. I find a downregulation in leaf nitrogen content and
127 leaf photosynthesis under elevated CO₂, a pattern that is not modified across
128 the fertilization gradient or between inoculation treatments. However, I also find
129 strong stimulations in total leaf area and whole plant growth under elevated CO₂
130 that are enhanced with increasing fertilization. There was no observable effect
131 of inoculation in modifying whole plant growth responses to CO₂, which I spec-
132 ulate is the result of a downregulation in plant investments to nitrogen fixation
133 with increasing fertilization. Results from this experiment provide strong evidence
134 suggesting that leaf acclimation responses to CO₂ were controlled by optimal re-
135 source investment to photosynthetic capacity, following patterns expected from
136 theory, and suggest divergent roles of soil nitrogen fertilization in modifying leaf
137 and whole plant acclimation responses to CO₂.

138 Throughout the four experimental chapters, I find strong and consistent
139 patterns that are supportive of patterns expected from photosynthetic least-cost
140 theory. Specifically, I find strong nitrogen-water use tradeoffs in response to chang-
141 ing climates and soil resources, and that shifts in soil nitrogen availability have
142 strong negative impacts on costs of nitrogen acquisition, and therefore tend to
143 increase β . In a final conclusion chapter, I summarize major findings from each of

144 the four experimental chapters and synthesize common mechanisms that drive leaf
145 and whole plant responses to changing environmental conditions. I conclude this
146 dissertation with brief dialogue on lessons learned throughout the experimental
147 chapters, and propose future experiments that will target additional uncertainties
148 in photosynthetic least-cost theory responses across environmental gradients.

149

Chapter 2

150

Structural carbon costs to acquire nitrogen are determined by
151 nitrogen and light availability in two species with different nitrogen
152 acquisition strategies

153 2.1 Introduction

154

Carbon and nitrogen cycles are tightly coupled in terrestrial ecosystems.

155

This tight coupling influences photosynthesis (Walker et al. 2014; Rogers et al.

156

2017), net primary productivity (LeBauer and Treseder 2008; Thomas et al. 2013),

157

decomposition (Cornwell et al. 2008; Bonan et al. 2013; Sulman et al. 2019), and

158

plant resource competition (Gill and Finzi 2016; Xu-Ri and Prentice 2017). Ter-

159

restrial biosphere models are beginning to include connected carbon and nitrogen

160

cycles to improve the realism of their simulations (Fisher et al. 2010; Brzostek

161

et al. 2014; Wieder et al. 2015; Shi et al. 2016; Zhu et al. 2019). Simula-

162

tions from these models indicate that coupling carbon and nitrogen cycles can

163

drastically influence future biosphere-atmosphere feedbacks under global change,

164

such as elevated carbon dioxide or nitrogen deposition (Thornton et al. 2007;

165

Goll et al. 2012; Wieder et al. 2015; Wieder et al. 2019). Nonetheless, there

166

are still limitations in our quantitative understanding of connected carbon and

167

nitrogen dynamics (Thomas et al. 2015; Meyerholt et al. 2016; Rogers et al.

168

2017; Exbrayat et al. 2018; Shi et al. 2019), forcing models to make potentially

169

unreliable assumptions.

170

Plant nitrogen acquisition is a process in terrestrial ecosystems by which

171

carbon and nitrogen are tightly coupled (Vitousek and Howarth 1991; Delaire

172

et al. 2005; Brzostek et al. 2014). Plants must allocate photosynthetically de-

173 rived carbon belowground to produce and maintain root systems or exchange with
174 symbiotic soil microbes in order to acquire nitrogen (Högberg et al. 2008; Hög-
175 berg et al. 2010). Thus, plants have an inherent carbon cost associated with
176 acquiring nitrogen, which can include both direct energetic costs associated with
177 nitrogen acquisition and indirect costs associated with building structures that
178 support nitrogen acquisition (Gutschick 1981; Rastetter et al. 2001; Vitousek
179 et al. 2002; Menge et al. 2008). Model simulations (Fisher et al. 2010; Brzostek
180 et al. 2014; Shi et al. 2016; Allen et al. 2020) and meta-analyses (Terrer et al.
181 2018) suggest that these carbon costs vary between species, particularly those
182 with different nitrogen acquisition strategies. For example, simulations using iter-
183 ations of the Fixation and Uptake of Nitrogen (FUN) model indicate that species
184 that acquire nitrogen from non-symbiotic active uptake pathways (e.g. mass flow)
185 generally have larger carbon costs to acquire nitrogen than species that acquire
186 nitrogen through symbiotic associations with nitrogen-fixing bacteria (Brzostek
187 et al. 2014; Allen et al. 2020).

188 Carbon costs to acquire nitrogen likely vary in response to changes in soil
189 nitrogen availability. For example, if the primary mode of nitrogen acquisition
190 is through non-symbiotic active uptake, then nitrogen availability could decrease
191 carbon costs to acquire nitrogen as a result of increased per-root nitrogen up-
192 take (Franklin et al. 2009; Wang et al. 2018). However, if the primary mode of
193 nitrogen acquisition is through symbiotic active uptake, then nitrogen availabil-
194 ity may incur additional carbon costs to acquire nitrogen if it causes microbial
195 symbionts to shift toward parasitism along the parasitism–mutualism continuum
196 (Johnson et al. 1997; Hoek et al. 2016; Friel and Friesen 2019) or if it reduces

197 the nitrogen acquisition capacity of a microbial symbiont (van Diepen et al. 2007;
198 Soudzilovskaia et al. 2015; Muñoz et al. 2016). Species may respond to shifts in
199 soil nitrogen availability by switching their primary mode of nitrogen acquisition
200 to a strategy with lower carbon costs to acquire nitrogen in order to maximize
201 the magnitude of nitrogen acquired from a belowground carbon investment and
202 outcompete other individuals for soil resources (Rastetter et al. 2001; Menge et al.
203 2008).

204 Environmental conditions that affect demand to acquire nitrogen to sup-
205 port new and existing tissues could also be a source of variance in plant carbon
206 costs to acquire nitrogen. For example, an increase in plant nitrogen demand could
207 increase carbon costs to acquire nitrogen if this increases the carbon that must be
208 allocated belowground to acquire a proportional amount of nitrogen (Kulmatiski
209 et al. 2017; Noyce et al. 2019). This could be driven by a temporary state of
210 diminishing return associated with investing carbon toward building and main-
211 taining structures that are necessary to support enhanced nitrogen uptake, such
212 as fine roots (Matamala and Schlesinger 2000; Norby et al. 2004; Arndal et al.
213 2018), mycorrhizal hyphae (Saleh et al. 2020), or root nodules (Parvin et al. 2020).
214 Alternatively, if the environmental factor that increases plant nitrogen demand
215 causes nitrogen to become more limiting in the system (e.g. atmospheric CO₂;
216 Luo et al. (2004), LeBauer and Treseder (2008), Vitousek et al. (2010), Liang
217 et al. (2016)), species might switch their primary mode of nitrogen acquisition to
218 a strategy with lower relative carbon costs to acquire nitrogen in order to gain a
219 competitive advantage over species with either different or more limited modes of
220 nitrogen acquisition (Ainsworth and Long 2005; Taylor and Menge 2018).

221 Using a plant economics approach, we examined the influence of plant
222 nitrogen demand and soil nitrogen availability on plant carbon costs to acquire
223 nitrogen. This was done by growing a species capable of forming associations
224 with nitrogen-fixing bacteria (*Glycine max* L. (Merr)) and a species not capable
225 of forming these associations (*Gossypium hirsutum* L.) under four levels of light
226 availability (plant nitrogen demand proxy) and four levels of soil nitrogen fertil-
227 ization (soil nitrogen availability proxy) in a full-factorial, controlled greenhouse
228 experiment. We used this experimental set-up to test the following hypotheses:

- 229 1. An increase in plant nitrogen demand due to increasing light availability will
230 increase carbon costs to acquire nitrogen through a proportionally larger
231 increase in belowground carbon than whole-plant nitrogen acquisition. This
232 will be the result of an increased investment of carbon toward belowground
233 structures that support enhanced nitrogen uptake, but at a lower nitrogen
234 return.
- 235 2. An increase in soil nitrogen availability will decrease carbon costs to acquire
236 nitrogen as a result of increased per root nitrogen uptake in *G. hirsutum*.
237 However, soil nitrogen availability will not affect carbon costs to acquire
238 nitrogen in *G. max* because of the already high return of nitrogen supplied
239 through nitrogen fixation.

240 2.2 Methods

241 2.2.1 *Experiment setup*

242 *Gossypium hirsutum* and *G. max* were planted in individual 3 liter pots
243 (NS-300; Nursery Supplies, Orange, CA, USA) containing a 3:1 mix of unfertil-
244 ized potting mix (Sungro Sunshine Mix #2, Agawam, MA, USA) to native soil
245 extracted from an agricultural field most recently planted with *G. max* at the
246 USDA-ARS Laboratory in Lubbock, TX, USA (33.59°N, -101.90°W). The field
247 soil was classified as Amarillo fine sandy loam (75% sand, 10% silt, 15% clay).
248 Upon planting, all *G. max* pots were inoculated with *Bradyrhizobium japonicum*
249 (Verdesian N-Dure™ Soybean, Cary, NC, USA) to stimulate root nodulation. In-
250 dividuals of both species were grown under similar, unshaded, ambient greenhouse
251 conditions for 2 weeks to germinate and begin vegetative growth. Three blocks
252 were set up in the greenhouse, each containing four light treatments created us-
253 ing shade cloth that reduced incoming radiation by either 0 (full sun), 30, 50,
254 or 80%. Two weeks post-germination, individuals were randomly placed in the
255 four light treatments in each block. Individuals received one of four nitrogen fer-
256 tilization doses as 100ml of a modified Hoagland solution (Hoagland and Arnon
257 1950) equivalent to either 0, 70, 210, or 630 ppm N twice per week within each
258 light treatment. Nitrogen fertilization doses were received as topical agents to
259 the soil surface. Each Hoagland solution was modified to keep concentrations of
260 other macro- and micronutrients equivalent (Supplementary Table S1). Plants
261 were routinely well watered to eliminate water stress.

262 2.2.2 *Plant measurements and calculations*

263 Each individual was harvested after 5 weeks of treatment, and biomass
264 was separated by organ type (leaves, stems, and roots). Nodules on *G. max*
265 roots were also harvested. With the exception of the 0% shade cover and 630
266 ppm N treatment combination, all treatment combinations in both species had
267 lower average dry biomass:pot volume ratios than the 1:1 ratio recommended by
268 Poorter et al. (2012) to minimize the likelihood of pot volume-induced growth
269 limitation (Supplementary Tables S2, S3; Supplementary Fig. S1). All harvested
270 material was dried, weighed, and ground by organ type. Carbon and nitrogen
271 content (g g^{-1}) was determined by subsampling from ground and homogenized
272 biomass of each organ type using an elemental analyzer (Costech 4010; Costech,
273 Inc., Valencia, CA, USA). We scaled these values to total leaf, stem, and root
274 carbon and nitrogen biomass (g) by multiplying dry biomass of each organ type
275 by carbon or nitrogen content of each corresponding organ type. Whole-plant
276 nitrogen biomass (g) was calculated as the sum of total leaf (g), stem (g), and
277 root (g) nitrogen biomass. Root nodule carbon biomass was not included in the
278 calculation of root carbon biomass; however, relative plant investment toward root
279 or root nodule standing stock was estimated as the ratio of root biomass to root
280 nodule biomass (g g^{-1}), following similar metrics to those adopted by Dovrat et al.
281 (2018) and Dovrat et al. (2020).

282 Carbon costs to acquire nitrogen (gC gN^{-1}) were estimated as the ratio of
283 total root carbon biomass (gC) to whole-plant nitrogen biomass (gN). This cal-
284 culation quantifies the relationship between carbon spent on nitrogen acquisition
285 and whole-plant nitrogen acquisition by using root carbon biomass as a proxy for

286 estimating the magnitude of carbon allocated toward nitrogen acquisition. This
287 calculation therefore assumes that the magnitude of root carbon standing stock is
288 proportional to carbon transferred to root nodules or mycorrhizae, or lost through
289 root exudation or turnover. This assumption has been supported in species that
290 associate with ectomycorrhizal fungi (Hobbie 2006; Hobbie and Hobbie 2008), but
291 is less clear in species that acquire nitrogen through non-symbiotic active uptake
292 or symbiotic nitrogen fixation. It is also unclear whether relationships between
293 root carbon standing stock and carbon transfer to root nodules are similar in mag-
294 nitude to carbon lost through exudation or when allocated toward other active
295 uptake pathways. Thus, because of the way we performed our measurements, our
296 proximal values of carbon costs to acquire nitrogen are underestimates.

297 2.2.3 *Statistical analyses*

298 We explored the effects of light and nitrogen availability on carbon costs to
299 acquire nitrogen using separate linear mixed-effects models for each species. Mod-
300 els included shade cover, nitrogen fertilization, and interactions between shade
301 cover and nitrogen fertilization as continuous fixed effects, and also included block
302 as a random intercept term. Three separate models for each species were built
303 with this independent variable structure for three different dependent variables: (i)
304 carbon costs to acquire nitrogen (gC gN^{-1}); (ii) whole-plant nitrogen biomass (de-
305 nominator of carbon cost to acquire nitrogen; gN); and (iii) root carbon biomass
306 (numerator of carbon cost to acquire nitrogen; gC). We constructed two additional
307 models for *G. max* with the same model structure described above to investigate
308 the effects of light availability and nitrogen fertilization on root nodule biomass

309 (g) and the ratio of root nodule biomass to root biomass (unitless).

310 We used Shapiro–Wilk tests of normality to determine whether species-
311 specifc linear mixed-effects model residuals followed a normal distribution. None
312 of our models satisfied residual normality assumptions when models were fit using
313 untransformed data (Shapiro–Wilk: $P<0.05$ in all cases). We attempted to satisfy
314 residual normality assumptions by first fitting models using dependent variables
315 that were natural-log transformed. If residual normality assumptions were still
316 not met (Shapiro–Wilk: $P>0.05$), then models were fit using dependent variables
317 that were square root transformed. All residual normality assumptions were satis-
318 fied when models were fit with either a natural-log or square root transformation
319 (Shapiro–Wilk: $P>0.05$ in all cases). Specifically, we natural-log transformed *G.*
320 *hirsutum* carbon costs to acquire nitrogen and *G. hirsutum* whole-plant nitrogen
321 biomass. We also square root transformed *G. max* carbon costs to acquire nitro-
322 gen, *G. max* whole-plant nitrogen biomass, root carbon biomass in both species,
323 *G. max* root nodule biomass, and the *G. max* ratio of root nodule biomass to root
324 biomass. We used the ‘lmer’ function in the ‘lme4’ R package (Bates et al. 2015)
325 to fit each model and the ‘Anova’ function in the ‘car’ R package (Fox and Weis-
326 berg 2019) to calculate Wald’s χ^2 to determine the significance ($\alpha = 0.05$) of each
327 fixed effect coefficient. Finally, we used the ‘emmeans’ R package (Lenth 2019)
328 to conduct post-hoc comparisons of our treatment combinations using Tukey’s
329 tests. Degrees of freedom for all Tukey’s tests were approximated using the Ken-
330 ward–Roger approach (Kenward and Roger 1997). All analyses and plots were
331 conducted in R version 4.0.1 (R Core Team 2021).

332 2.3 Results

333 2.3.1 *Carbon costs to acquire nitrogen*

334 Carbon costs to acquire nitrogen in *G. hirsutum* increased with increasing
335 light availability ($p < 0.001$; Table 2.1; Fig. 2.1) and decreased with increasing
336 nitrogen fertilization ($p < 0.001$; Table 2.1; Fig. 2.1). There was no interaction
337 between light availability and nitrogen fertilization ($p = 0.486$, Table 2.1; Fig.
338 2.1).

339 Carbon costs to acquire nitrogen in *G. max* also increased with increasing
340 light availability ($p < 0.001$, Table 2.1; Fig. 2.1) and decreased with increasing
341 nitrogen fertilization ($p < 0.001$; Table 2.1; Fig. 2.1). There was no interaction
342 between light availability and nitrogen fertilization ($p = 0.261$, Table 2.1; Fig.
343 2.1).

Table 2.1. Analysis of variance results exploring species-specific effects of light availability, nitrogen fertilization, and their interactions on carbon costs to acquire nitrogen, whole-plant nitrogen biomass, and root carbon biomass

	df	Carbon costs to acquire nitrogen			Whole-plant nitrogen biomass			Root carbon biomass		
		Coefficient	χ^2	p	Coefficient	χ^2	p	Coefficient	χ^2	p
<i>G. hirsutum</i>										
Intercept		1.594	-	-	-3.232	-	-	0.432	-	-
Light (L)	1	-1.09E-02	56.494	<0.001	-6.41E-03	91.275	<0.001	-2.62E-03	169.608	<0.001
Nitrogen (N)	1	-1.34E-03	54.925	<0.001	1.83E-03	118.784	<0.001	1.15E-04	2.901	0.089
L*N	1	3.88E-06	0.485	0.486	-1.34E-05	10.721	0.001	-1.67E-06	3.140	0.076
<i>G. max</i>										
Intercept		1.877	-	-	0.239	-	-	0.438	-	-
Light (L)	1	-7.67E-03	174.156	<0.001	-6.72E-04	39.799	<0.001	-2.55E-03	194.548	<0.001
Nitrogen (N)	1	-2.35E-04	21.948	<0.001	1.55E-04	70.771	<0.001	2.52E-04	19.458	<0.001
L*N	1	-2.89E-06	1.262	0.261	-6.32E-07	1.435	0.231	-3.16E-06	10.803	0.001

*Significance determined using Wald's χ^2 tests ($P=0.05$). P -values<0.05 are in bold and p -values between 0.05 and 0.1 are italicized. Negative coefficients for light treatments indicate a positive effect of increasing light availability on all response variables, as light availability is treated as percent shade cover in all linear mixed-effects models.

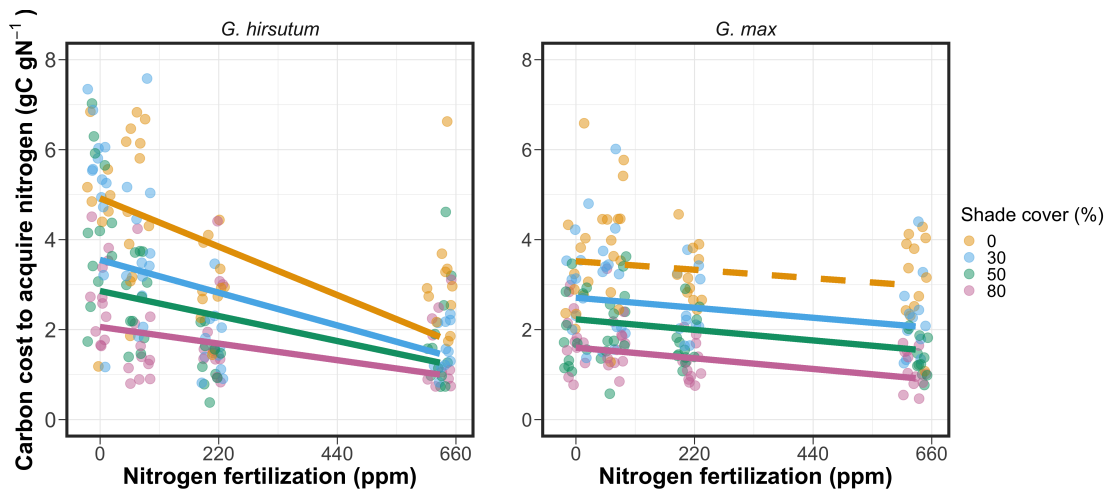


Figure 2.1. Relationships between soil nutrient fertilization and light availability on carbon costs to acquire nitrogen in *G. hirsutum* and *G. max*. Nitrogen fertilization treatments are represented on the x-axis. Shade cover treatments are represented through colored points and trendlines. Trendlines were created by back-transforming marginal mean slopes and intercepts from species-specific linear mixed-effects models. These values were calculated using the ‘emtrends’ and ‘emmeans’ functions in the ‘emmeans’ R package (Lenth, 2019). Points are jittered for visibility. Yellow points and trendlines represent the 0% shade cover treatment, blue points and trendlines represent the 30% shade cover treatment, green points and trendlines represent the 50% shade cover treatment, and purple points and trendlines represent the 80% shade cover treatment. Solid trendlines indicate slopes that are significantly different from zero (Tukey: $p < 0.05$), while dashed trendlines indicate slopes that are not statistically different from zero.

344 2.3.2 *Whole plant nitrogen biomass*

345 Whole-plant nitrogen biomass in *G. hirsutum* was driven by an interaction
346 between light availability and nitrogen fertilization ($p = 0.001$; Table 2.1; Fig.
347 2.2). This interaction indicated a greater stimulation of whole-plant nitrogen
348 biomass by nitrogen fertilization as light levels increased (Table 2.1; Fig. 2.2).

349 Whole-plant nitrogen biomass in *G. max* increased with increasing light
350 availability ($p < 0.001$) and nitrogen fertilization ($p < 0.001$), with no interaction
351 between light availability and nitrogen fertilization ($p = 0.231$; Table 2.1; Fig.
352 2.2).

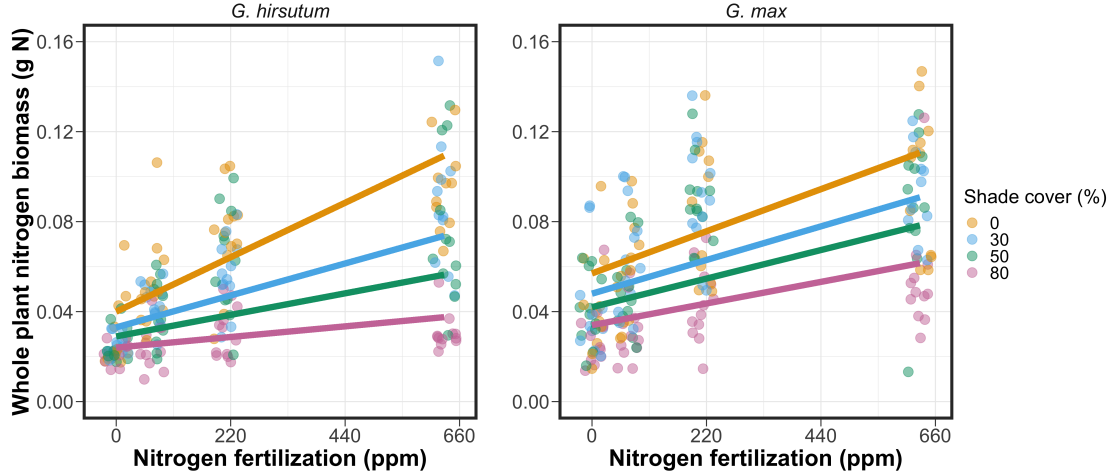


Figure 2.2. Relationships between soil nutrient fertilization and light availability on whole-plant nitrogen biomass in *G. hirsutum* and *G. max*. Whole-plant nitrogen biomass is the denominator of the carbon cost to acquire nitrogen calculation. Nitrogen fertilization treatments are represented on the x-axis. Shade cover treatments are represented through colored points and trendlines. Trendlines were created by back-transforming marginal mean slopes and intercepts from species-specific linear mixed-effects models. These values were calculated using the ‘emtrends’ and ‘emmmeans’ functions in the ‘emmeans’ R package (Lenth 2019). Points are jittered for visibility. Yellow points and trendlines represent the 0% shade cover treatment, blue points and trendlines represent the 30% shade cover treatment, green points and trendlines represent the 50% shade cover treatment, and purple points and trendlines represent the 80% shade cover treatment. Solid trendlines indicate slopes that are significantly different from zero (Tukey: $P < 0.05$), while dashed trendlines indicate slopes that are not statistically different from zero.

353 2.3.3 *Root carbon biomass*

354 Root carbon biomass in *G. hirsutum* significantly increased with increasing
355 light availability ($p < 0.001$; Table 2.1; Fig. 2.3) and marginally increased with
356 nitrogen fertilization ($p = 0.089$; Table 2.1; Fig. 2.3). There was also a marginal
357 interaction between light availability and nitrogen fertilization ($p = 0.076$; Table
358 2.1), driven by an increase in the positive response of root carbon biomass to
359 increasing nitrogen fertilization as light availability increased. This resulted in
360 significantly positive trends between root carbon biomass and nitrogen fertilization
361 in the two highest light treatments (Tukey: $p < 0.05$ in both cases; Table 2.3;
362 Fig. 2.3) and no effect of nitrogen fertilization in the two lowest light treatments
363 (Tukey: $p > 0.05$ in both cases; Table 2.3; Fig. 2.3).

364 There was an interaction between light availability and nitrogen fertiliza-
365 tion on root carbon biomass in *G. max* ($p = 0.001$; Table 2.1; Fig. 2.3). Post-hoc
366 analyses indicated that the positive effects of nitrogen fertilization on *G. max* root
367 carbon biomass increased with increasing light availability (Table 2.3; Fig. 2.3).
368 There were also positive individual effects of increasing nitrogen fertilization ($p <$
369 0.001) and light availability ($p < 0.001$) on *G. max* root carbon biomass (Table
370 2.1; Fig. 2.3).

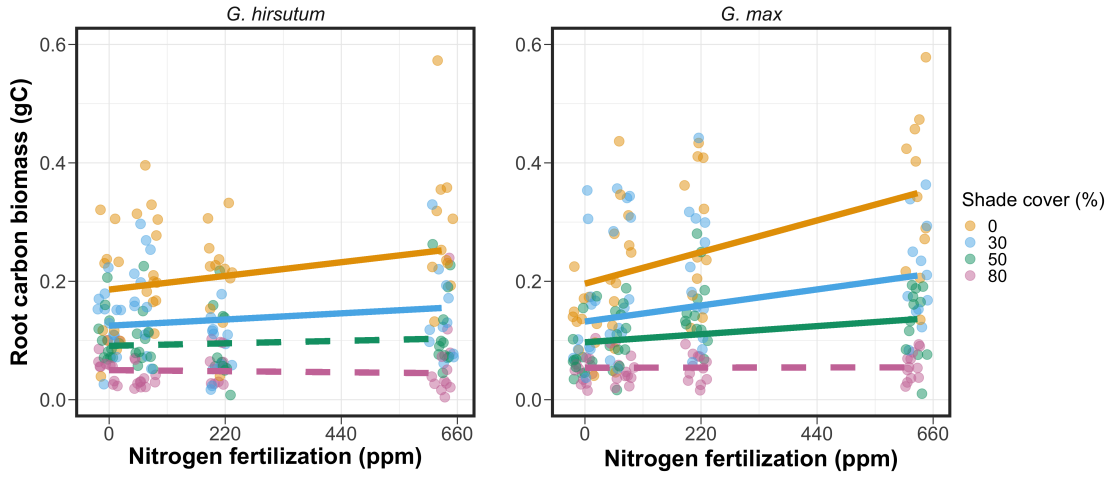


Figure 2.3. Relationships between soil nutrient fertilization and light availability on root carbon biomass in *G. hirsutum* and *G. max*. Root carbon biomass is the numerator of the carbon cost to acquire nitrogen calculation. Nitrogen fertilization treatments are represented on the x-axis. Shade cover treatments are represented through colored points and trendlines. Trendlines were created by back-transforming marginal mean slopes and intercepts from species-specific linear mixed-effects models. These values were calculated using the ‘emtrends’ and ‘emmmeans’ functions in the ‘emmeans’ R package (Lenth 2019). Points are jittered for visibility. Yellow points and trendlines represent the 0% shade cover treatment, blue points and trendlines represent the 30% shade cover treatment, green points and trendlines represent the 50% shade cover treatment, and purple points and trendlines represent the 80% shade cover treatment. Solid trendlines indicate slopes that are significantly different from zero (Tukey: $p < 0.05$), while dashed trendlines indicate slopes that are not statistically different from zero.

371 2.3.4 *Root nodule biomass*

372 Root nodule biomass in *G. max* increased with increasing light availability
373 ($p < 0.001$; Table 2.2; Fig. 2.4A) and decreased with increasing nitrogen fertiliza-
374 tion ($p < 0.001$; Table 2.2; Fig. 2.4A). There was no interaction between nitrogen
375 fertilization and light availability ($p = 0.133$; Table 2.2; Fig. 2.4A). The ratio of
376 root nodule biomass to root biomass did not change in response to light avail-
377 ability ($p = 0.481$; Table 2.2; Fig. 2.4B) but decreased with increasing nitrogen
378 fertilization ($p < 0.001$; Table 2.2; Fig. 2.4B). There was no interaction between
379 nitrogen fertilization and light availability on the ratio of root nodule biomass to
380 root biomass ($p = 0.621$; Table 2.2; Fig. 2.4B).

Table 2.2. Analysis of variance results exploring effects of light availability, nitrogen fertilization, and their interactions on *G. max* root nodule biomass and the ratio of root nodule biomass to root biomass*

	Nodule biomass			Nodule biomass: root biomass			
	df	Coefficient	χ^2	p	coefficient	χ^2	p
(Intercept)		0.302	-	-	0.448	-	-
Light (L)	1	-1.81E-03	72.964	<0.001	-8.76E-05	0.496	0.481
Nitrogen (N)	1	-2.83E-04	115.377	<0.001	-5.09E-04	156.476	<0.001
L*N	1	1.14E-06	2.226	0.133	-7.30E-07	0.244	0.621

*Significance determined using Wald's χ^2 tests ($\alpha = 0.05$). *p*-values less than 0.05 are in bold. Negative coefficients for light treatments indicate a positive effect of increasing light availability on all response variables, as light availability is treated as percent shade cover in all linear mixed-effects models. Root nodule biomass and nodule biomass: root biomass models were only constructed for *G. max* because *G. hirsutum* was not inoculated with *B. japonicum* and is not capable of forming root nodules.

Table 2.3. Slopes of the regression line describing the relationship between each dependent variable and nitrogen fertilization at each light level*

Shade cover	Carbon cost to acquire nitrogen	Whole-plant nitrogen biomass	Root carbon biomass	Root nodule biomass	Nodule biomass root biomass
<i>G. hirsutum</i>					
0%	-1.34E-03^a	1.83E-03^a	1.15E-04^b	-	-
30%	-1.22E-03^a	1.43E-03^a	1.17E-04^b	-	-
50%	-1.14E-03^a	1.17E-03^a	3.12E-05 ^b	-	-
80%	-1.02E-03^a	7.66E-04^a	-1.89E-06 ^b	-	-
<i>G. max</i>					
0%	-2.35E-04 ^b	1.55E-05^b	2.51E-04^b	-2.83E-04^b	-5.09E-04^b
30%	-3.22E-04^b	1.35E-05^b	1.57E-04^b	-2.49E-04^b	-5.31E-04^b
50%	-3.80E-04^b	1.23E-05^b	9.37E-05^b	-2.26E-04^b	-5.45E-04^b
80%	-4.66E-04^b	1.04E-05^b	-9.95E-07 ^b	-1.92E-04^b	-5.67E-04^b

*Slopes represent estimated marginal mean slopes from linear mixed-effects models described in the Methods. Slopes were calculated using the ‘emmeans’ R package (Lenth 2019). Superscripts indicate slopes fit to natural-log (^a) or square root (^b) transformed data. Slopes statistically different from zero (Tukey: $p < 0.05$) are indicated in bold. Marginally significant slopes (Tukey: $0.05 < p < 0.1$) are italicized.

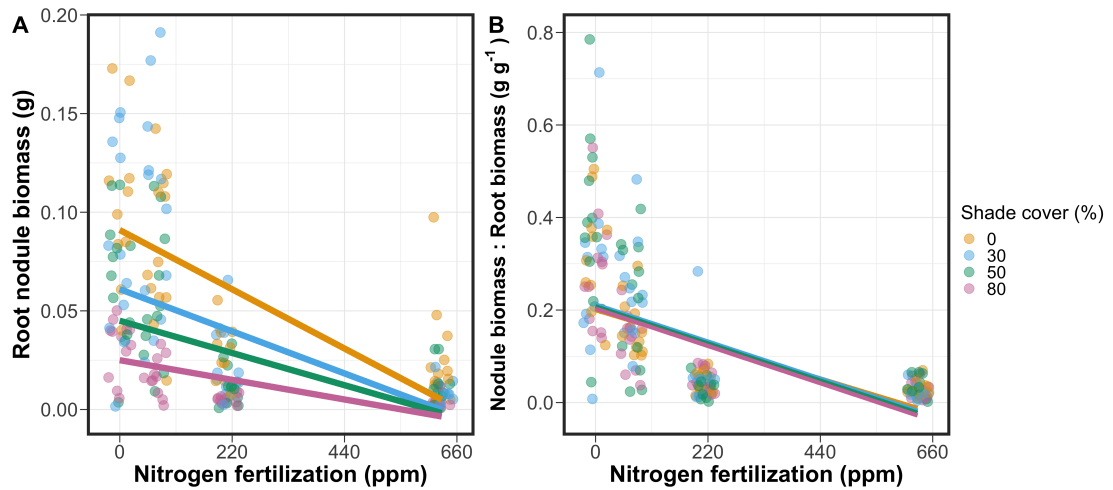


Figure 2.4. Effects of shade cover and nitrogen fertilization on root nodule biomass (A) and the ratio of root nodule biomass to root biomass (B) in *G. max*. Nitrogen fertilization treatments are represented on the x-axis. Shade cover treatments are represented through colored points and trendlines. Trendlines were created by back-transforming marginal mean slopes and intercepts from species-specific linear mixed-effects models. These values were calculated using the ‘emtrends’ and ‘emmeans’ functions in the ‘emmeans’ R package (Lenth 2019). Points are jittered for visibility. Yellow points and trendlines represent the 0% shade cover treatment, blue points and trendlines represent the 30% shade cover treatment, green points and trendlines represent the 50% shade cover treatment, and purple points and trendlines represent the 80% shade cover treatment. Solid trendlines indicate slopes that are significantly different from zero (Tukey: $p < 0.05$), while dashed trendlines indicate slopes that are not statistically different from zero.

381 2.4 Discussion

382 In this chapter, we determined the effects of light availability and soil ni-
383 trogen fertilization on root mass carbon costs to acquire nitrogen in *G. hirsutum*
384 and *G. max*. In support of our hypotheses, we found that carbon costs to acquire
385 nitrogen generally increased with increasing light availability and decreased with
386 increasing soil nitrogen fertilization in both species. These findings suggest that
387 carbon costs to acquire nitrogen are determined by factors that influence plant
388 nitrogen demand and soil nitrogen availability. In contrast to our second hypothe-
389 sis, root nodulation data suggested that *G. max* and *G. hirsutum* achieved similar
390 directional carbon cost responses to nitrogen fertilization despite a likely shift in
391 G.!max allocation from nodulation to root biomass along the nitrogen fertilization
392 gradient (Fig. 2.4B).

393 Both *G. max* and *G. hirsutum* experienced an increase in carbon costs to
394 acquire nitrogen due to increasing light availability. These patterns were driven by
395 a larger increase in root carbon biomass than whole-plant nitrogen biomass. In-
396 creases in root carbon biomass due to factors that increase plant nitrogen demand
397 are a commonly observed pattern, as carbon allocated belowground provides sub-
398 strate needed to produce and maintain structures that satisfy aboveground plant
399 nitrogen demand (Nadelhoffer and Raich 1992; Giardina et al. 2005; Raich et al.
400 2014). Our findings suggest that plants allocate relatively more carbon for acquir-
401 ing nitrogen when demand increases over short temporal scales, which may cause
402 a temporary state of diminishing return due to asynchrony between belowground
403 carbon and whole-plant nitrogen responses to plant nitrogen demand (Kulmatiski
404 et al. 2017; Noyce et al. 2019). These responses might be attributed to a temporal

lag associated with producing structures that enhance nitrogen acquisition. For example, fine roots (Matamala and Schlesinger 2000; Norby et al. 2004; Arndal et al. 2018) and root nodules (Parvin et al. 2020) take time to build and first require the construction of coarse roots. Thus, full nitrogen returns from these investments may not occur immediately (Kayler et al. 2010; Kayler et al. 2017), and may vary by species acquisition strategy. We speculate that increases in nitrogen acquisition from a given carbon investment may occur beyond the 5 week scope of this experiment. A similar study conducted over a longer temporal scale would address this.

Increasing soil nitrogen fertilization generally decreased carbon costs to acquire nitrogen in both species. These patterns were driven by a larger increase in whole-plant nitrogen biomass than root carbon biomass. In *G. hirsutum*, reductions in carbon costs to acquire nitrogen may have been due to an increase in per-root nitrogen uptake, allowing individuals to maximize the amount of nitrogen acquired from a belowground carbon investment. Interestingly, increased soil nitrogen fertilization increased whole-plant nitrogen biomass in *G. max* despite reductions in root nodule biomass that likely reduced the nitrogen-fixing capacity of *G. max* (Andersen et al. 2005; Muñoz et al. 2016). While reductions in root nodulation due to increased soil nitrogen availability are commonly observed (Gibson and Harper 1985; Fujikake et al. 2003), our responses were observed in tandem with increased root carbon biomass, implying that *G. max* shifted relative carbon allocation from nitrogen fixation to soil nitrogen acquisition (Markham and Zekveld 2007; Dovrat et al. 2020). This was likely because there was a reduction in the carbon cost advantage of acquiring fixed nitrogen relative to soil nitrogen, and

429 suggests that species capable of associating with symbiotic nitrogen-fixing bacte-
430 ria shift their relative nitrogen acquisition pathway to optimize nitrogen uptake
431 (Rastetter et al. 2001). Future studies should further investigate these patterns
432 with a larger quantity of phylogenetically related species, or different varieties
433 of a single species that differ in their ability to form associations with symbiotic
434 nitrogen-fixing bacteria to more directly test the impact of nitrogen fixation on
435 the patterns observed in this study.

436 Carbon costs to acquire nitrogen are subsumed in the general discussion of
437 economic analogies to plant resource uptake (Bloom et al. 1985; Rastetter et al.
438 2001; Vitousek et al. 2002; Phillips et al. 2013; Terrer et al. 2018; Henneron et al.
439 2020). Despite this, terrestrial biosphere models rarely include these carbon costs
440 within their framework for predicting plant nitrogen uptake. There is currently
441 one plant resource uptake model, FUN, that quantitatively predicts carbon costs
442 to acquire nitrogen within a framework for predicting plant nitrogen uptake for
443 different nitrogen acquisition strategies (Fisher et al. 2010; Brzostek et al. 2014)

444 (Fisher et al. 2010; Brzostek et al. 2014). Iterations of FUN are currently
445 coupled to two terrestrial biosphere models: the Community Land Model 5.0 and
446 the Joint UK Land Environment Simulator (Shi et al. 2016; Lawrence et al.
447 2019; Clark et al. 2011). Recent work suggests that coupling FUN to CLM 5.0
448 caused a large overprediction of plant nitrogen uptake associated with nitrogen
449 fixation (Davies-Barnard et al. 2020). Thus, empirical data from manipulative
450 experiments that explicitly quantify carbon costs to acquire nitrogen in species
451 capable of associating with nitrogen-fixing bacteria across different environmental
452 contexts is an important step toward identifying potential biases in models such

453 as FUN.

454 Our findings broadly support the FUN formulation of carbon costs to ac-
455 quire nitrogen in response to soil nitrogen availability. FUN calculates carbon
456 costs to acquire nitrogen based on the sum of carbon costs to acquire nitrogen
457 via nitrogen fixation, mycorrhizal active uptake, non-mycorrhizal active uptake,
458 and retranslocation (Fisher et al. 2010; Brzostek et al. 2014). Carbon costs to
459 acquire nitrogen via mycorrhizal or non-mycorrhizal active uptake pathways are
460 derived as a function of nitrogen availability, root biomass, and two parameterized
461 values based on nitrogen acquisition strategy (Brzostek et al. 2014). Due to this,
462 FUN simulates a net decrease in carbon costs to acquire nitrogen with increasing
463 nitrogen availability for mycorrhizal and non-mycorrhizal active uptake pathways,
464 assuming constant root biomass. This was a pattern we observed in *G. hirsutum*
465 regardless of light availability. In contrast, FUN would not simulate a net change
466 in carbon costs to acquire nitrogen via nitrogen fixation due to nitrogen avail-
467 ability. This is because carbon costs to acquire nitrogen via nitrogen fixation are
468 derived from a well-established function of soil temperature, which is independent
469 of soil nitrogen availability (Houlton et al. 2008; Fisher et al. 2010). We observed
470 a net reduction in carbon costs to acquire nitrogen in *G. max*, except when in-
471 dividuals were grown under 0% shade cover (Fig. 2.1). While a net reduction of
472 carbon costs in response to nitrogen fertilization runs counter to nitrogen fixa-
473 tion carbon costs simulated by FUN, these patterns were likely because *G. max*
474 individuals switched their primary mode of nitrogen acquisition from symbiotic
475 nitrogen fixation to a non-symbiotic active uptake pathway (Fig. 2.4B).

476 It should be noted that the metric used in this study to determine carbon

477 costs to acquire nitrogen has several limitations. Most notably, this metric uses
478 root carbon biomass as a proxy for estimating the amount of carbon spent on
479 nitrogen acquisition. While it is true that most carbon allocated belowground
480 has at least an indirect structural role in acquiring soil resources, it remains un-
481 clear whether this assumption holds true for species that acquire nitrogen via
482 symbiotic nitrogen fixation. We also cannot quantify carbon lost through root
483 exudates or root turnover, which may increase due to factors that increase plant
484 nitrogen demand (Tingey et al. 2000; Phillips et al. 2011), and can increase the
485 magnitude of available nitrogen from soil organic matter through priming effects
486 on soil microbial communities (Uselman et al. 2000; Bengtson et al. 2012). It is
487 also not clear whether these assumptions hold under all environmental conditions,
488 such as those that shift belowground carbon allocation toward a different mode of
489 nitrogen acquisition (Taylor and Menge 2018; Friel and Friesen 2019) or between
490 species with different acquisition strategies. In this study, increasing soil nitrogen
491 fertilization increased carbon investment to roots relative to carbon transferred
492 to root nodules (Fig. 2.4B). By assuming that carbon allocated to root carbon
493 was proportional to carbon allocated to root nodules across all treatment com-
494 binations, these observed responses to soil nitrogen fertilization were likely to be
495 overestimated in *G. max*. We encourage future research to quantify these carbon
496 fates independently.

497 Researchers conducting pot experiments must carefully choose pot volume
498 to minimize the likelihood of pot volume-induced growth limitation (Poorter et al.
499 2012). Poorter et al. (2012) indicate that researchers are likely to avoid growth
500 limitations associated with pot volume if measurements are collected when the

501 plant biomass:pot volume ratio is less than 1 g L⁻¹. In this experiment, all treat-
502 ment combinations in both species had biomass:pot volume ratios less than 1 g
503 L⁻¹ except for *G. max* and *G. hirsutum* that were grown under 0% shade cover
504 and had received 630 ppm N. Specifically, *G. max* and *G. hirsutum* had average
505 respective biomass:pot volume ratios of 1.24±0.07 g L⁻¹ and 1.34±0.13 g L⁻¹, when
506 grown under 0% shade cover and received 630 ppm N (Supplementary Tables S2,
507 S3; Supplementary Fig. S1). If growth in this treatment combination was limited
508 by pot volume, then individuals may have had larger carbon costs to acquire ni-
509 trogen than would be expected if they were grown in larger pots. This pot volume
510 induced growth limitation could cause a reduction in per-root nitrogen uptake as-
511 sociated with more densely packed roots, which could reduce the positive effect
512 of nitrogen fertilization on whole-plant nitrogen biomass relative to root carbon
513 biomass (Poorter et al. 2012).

514 Growth limitation associated with pot volume provides a possible explana-
515 tion for the marginally insignificant effect of increasing nitrogen fertilization on *G.*
516 *max* carbon costs to acquire nitrogen when grown under 0% shade cover (Table
517 2.3; Fig. 2.1). This is because the regression line describing the relationship be-
518 tween carbon costs to acquire nitrogen and nitrogen fertilization in *G. max* grown
519 under 0% shade cover would have flattened if growth limitation had caused larger
520 than expected carbon costs to acquire nitrogen in the 0% shade cover, 630 ppm
521 N treatment combination. This may have been exacerbated by the fact that *G.*
522 *max* likely shifted relative carbon allocation from nitrogen fixation to soil nitrogen
523 acquisition, which could have increased the negative effect of more densely packed
524 roots on nitrogen uptake. These patterns could have also occurred in *G. hirsutum*

525 grown under 0% shade cover; however, there was no change in the effect of nitro-
526 gen fertilization on *G. hirsutum* carbon costs to acquire nitrogen grown under 0%
527 shade cover relative to other shade cover treatments. Regardless, the possibility
528 of growth limitation due to pot volume suggests that effects of increasing nitro-
529 gen fertilization on carbon costs to acquire nitrogen in both species grown under
530 0% shade cover could have been underestimated. Follow-up studies using a simi-
531 lar experimental design with a larger pot volume would be necessary in order to
532 determine whether these patterns were impacted by pot volume-induced growth
533 limitation.

534 In conclusion, this study provides empirical evidence that carbon costs to
535 acquire nitrogen are influenced by light availability and soil nitrogen fertilization
536 in a species capable of acquiring nitrogen via symbiotic nitrogen fixation and a
537 species not capable of forming such associations. We show that carbon costs to
538 acquire nitrogen generally increase with increasing light availability and decrease
539 with increasing nitrogen fertilization. This study provides important empirical
540 data needed to evaluate the formulation of carbon costs to acquire nitrogen in
541 terrestrial biosphere models, particularly carbon costs to acquire nitrogen that
542 are associated with symbiotic nitrogen fixation. Our findings broadly support
543 the general formulation of these carbon costs in the FUN biogeochemical model
544 in response to shifts in nitrogen availability. However, there is a need for future
545 studies to explicitly quantify carbon costs to acquire nitrogen under different en-
546 vironmental contexts, over longer temporal scales, and using larger selections of
547 phylogenetically related species. In addition, we suggest that future studies mini-
548 mize the limitations associated with the metric used here by explicitly measuring

549 belowground carbon fates independently.

550 Chapter 3

551 Soil nitrogen availability modifies leaf nitrogen economies in mature
552 temperate deciduous forests: a direct test of photosynthetic least-cost
553 theory

554 3.1 Introduction

Photosynthesis represents the largest carbon flux between the atmosphere and land surface (IPCC 2021), and plays a central role in biogeochemical cycling at multiple spatial and temporal scales (Vitousek and Howarth 1991; LeBauer and Treseder 2008; Kaiser et al. 2015; Wieder et al. 2015). Therefore, carbon and energy fluxes simulated by terrestrial biosphere models are sensitive to the formulation of photosynthetic processes (Ziehn et al. 2011; Bonan et al. 2011; Booth et al. 2012; Smith et al. 2016; Smith et al. 2017) and must be represented using robust, empirically tested processes (Prentice et al. 2015; Wieder et al. 2019).

Current formulations of photosynthesis vary across terrestrial biosphere models (Smith and Dukes 2013; Rogers et al. 2017), which causes variation in modeled ecosystem processes (Knorr 2000; Knorr and Heimann 2001; Bonan et al. 2011; Friedlingstein et al. 2014) and casts uncertainty on the ability of these models to accurately predict terrestrial ecosystem responses and feedbacks to global change (Zaehle et al. 2005; Schaefer et al. 2012; Davies-Barnard et al. 2020).

Terrestrial biosphere models commonly represent C₃ photosynthesis through variants of the Farquhar et al. (1980) biochemical model (Smith and Dukes 2013; Rogers 2014; Rogers et al. 2017). This well-tested photosynthesis model estimates leaf-level carbon assimilation, or photosynthetic capacity, as a function of the maximum rate of Ribulose-1,5-bisphosphate carboxylase-oxygenase (Ru-

574 bisco) carboxylation (V_{cmax}) and the maximum rate of Ribulose-1,5-bisphosphate
575 (RuBP) regeneration (J_{max}) (Farquhar et al. 1980). Many terrestrial biosphere
576 models predict these model inputs based on plant functional group specific linear
577 relationships between leaf nutrient content and V_{cmax} (Smith and Dukes 2013;
578 Rogers 2014; Rogers et al. 2017) under the tenet that a large fraction of leaf
579 nutrients, and nitrogen (N) in particular, are partitioned toward building and
580 maintaining enzymes that support photosynthetic capacity, such as Rubisco (Brix
581 1971; Gulmon and Chu 1981; Evans 1989; Kattge et al. 2009; Walker et al. 2014).
582 Terrestrial biosphere models also predict leaf nutrient content from soil nutrient
583 availability based on the assumption that increasing soil nutrients generally in-
584 creases leaf nutrients (Firn et al. 2019; Li et al. 2020; Liang et al. 2020) which, in
585 the case of N, generally corresponds with an increase in photosynthetic processes
586 (Li et al. 2020; Liang et al. 2020).

587 Recent work calls the generality of relationships between soil nutrient avail-
588 ability, leaf nutrient content, and photosynthetic capacity into question, suggest-
589 ing instead that leaf nutrients and photosynthetic capacity are better predicted as
590 an integrated product of aboveground climate, leaf traits, and soil nutrient avail-
591 ability, rather than soil nutrient availability alone (Dong et al. 2017; Dong et al.
592 2020; Dong et al. 2022; Firn et al. 2019; Smith et al. 2019; Peng et al. 2021).
593 It has been reasoned that this result is because plants allocate added nutrients to
594 growth and storage rather than alterations in leaf chemistry (Smith et al. 2019),
595 perhaps as a result of nutrient limitation of primary productivity (LeBauer and
596 Treseder 2008; Fay et al. 2015). Additionally, recent work suggests that relation-
597 ships between leaf nutrient content and photosynthesis vary across environments,

598 and that the proportion of leaf nutrient content allocated to photosynthetic tis-
599 sue varies over space and time with plant acclimation and adaptation responses
600 to light availability, vapor pressure deficit, soil pH, soil nutrient availability, and
601 environmental factors that influence leaf mass per area (Pons and Pearcy 1994;
602 Niinemets and Tenhunen 1997; Evans and Poorter 2001; Hikosaka and Shigeno
603 2009; Ghimire et al. 2017; Onoda et al. 2017; Luo et al. 2021). The use of linear
604 relationships between leaf nutrient content and Vcmax to predict photosynthetic
605 capacity, as commonly used in terrestrial biosphere models (Rogers 2014), is not
606 capable of detecting such responses.

607 Photosynthetic least-cost theory provides an alternative framework for un-
608 derstanding relationships between soil nutrient availability, leaf nutrient content,
609 and photosynthetic capacity (Harrison et al. 2021). Leveraging a two-input mi-
610 croeconomics approach (Wright et al. 2003), the theory posits that plants accli-
611 mate to a given environment by optimizing leaf photosynthesis rates at the lowest
612 summed cost of using nutrients and water (Prentice et al. 2014; Wang et al. 2017;
613 Smith et al. 2019; Paillassa et al. 2020). Across resource availability gradients,
614 the theory predicts that optimal photosynthetic rates can be achieved by trading
615 less efficient use of a resource that is less costly to acquire (or more abundant)
616 for more efficient use of a resource more costly to acquire (or less abundant). For
617 example, an increase in soil nutrient availability should reduce the cost of acquir-
618 ing and using nutrients (Bae et al. 2015; Eastman et al. 2021; Perkowski et al.
619 2021), which could increase leaf nutrient investments in photosynthetic proteins to
620 allow similar photosynthetic rates to be achieved with higher nutrient use (lower
621 nutrient use efficiency) but lower water use (greater water use efficiency). The

622 theory suggests similar tradeoffs in response to increasing soil pH (Paillassa et al.
623 2020), specifically, that increasing soil pH should reduce the cost of acquiring soil
624 nutrients due to an increase in plant-available nutrient concentration (Paillassa
625 et al. 2020; Dong et al. 2022). The theory is also capable of reconciling dynamic
626 leaf nutrient-photosynthesis relationships at global scales (Luo et al. 2021).

627 Patterns expected from photosynthetic least-cost theory have recently re-
628 ceived empirical support both in global environmental gradient (Smith et al.
629 2019; Paillassa et al. 2020; Luo et al. 2021; Querejeta et al. 2022; Wester-
630 band et al. 2023) and local manipulative invasion (Bialic-Murphy et al. 2021)
631 studies. However, nutrient addition experiments that directly examine nutrient-
632 water use tradeoffs expected from the theory are rare (Guerrieri et al. 2011), and
633 only global gradient studies testing the theory have considered soil pH in their
634 analyses. As a result, there is a need to use nutrient addition and soil pH manu-
635 lation experiments to test mechanisms driving responses predicted by the theory.
636 Such experiments would also be useful to detect whether patterns expected from
637 theory translate to finer spatial scales.

638 In this study, we measured leaf responses to soil N availability in five decid-
639 uous tree species growing in the upper canopy of mature closed canopy temperate
640 forests in the northeastern United States. Soil N availability and pH were manip-
641 ulated through a N-by-pH field manipulation experiment with treatments applied
642 since 2011, eight years prior to measurement. Two different soil N treatments were
643 applied to increase N availability with opposing effects on soil pH. An additional
644 N-free acidifying treatment was expected to decrease soil pH. We hypothesized
645 that increased soil N availability would enable plants to increase nutrient uptake

646 and create more photosynthetic enzymes per leaf, allowing similar photosynthetic
647 rates achieved with lower leaf C_i:C_a and increased leaf N content allocated to
648 photosynthetic leaf tissue. We expected that this response would be driven by a
649 reduction in the cost of acquiring N, which would cause trees to sacrifice efficient
650 N use to enable more efficient use of other limiting resources (i.e., water). We
651 hypothesized similar leaf responses to increasing soil pH.

652 3.2 Methods

653 3.2.1 *Study site description*

654 We conducted this study in summer 2019 at three stands located within
655 a 20-km radius of Ithaca, NY, USA (42.444 °N, 76.502 °W). All stands contain
656 mature, closed-canopy forests dominated by deciduous tree species. Stands con-
657 tained abundant sugar maple (*Acer saccharum* Marshall), American beech (*Fagus*
658 *grandifolia* Ehrh.), and white ash (*Fraxinus americana* L.), accounting for 43%,
659 15%, and 17% of the total aboveground biomass across the three stands, respec-
660 tively, with less frequent red maple (*Acer rubrum* L.; 9% of total aboveground
661 biomass) and red oak occurrences (*Quercus rubra* L.; 10% of total aboveground
662 biomass). Soils at each site were broadly classified as a channery silt loam Incep-
663 tisols using the USDA NRCS Web Soil Survey data product (Soil Survey Staff
664 2022). Between 2006 and 2020, study sites averaged 972 mm of precipitation per
665 year and had an average temperature of 7.9 °C per a weather station located near
666 the Cornell University campus (42.449 °N, 76.449 °W) part of the NOAA NCEI
667 Global Historical Climatology Network (Menne et al. 2012).

668 3.2.2 *Experimental design*

669 Four 40 m x 40 m plots were set up at each site in 2009, each with an
670 additional 10 m buffer along plot perimeters (60 m x 60 m total). The plots
671 were set up as a nitrogen-by-pH field manipulation experiment, with one each of
672 four treatments at each site. Two nitrogen treatments were applied, both at 50
673 kg N ha⁻¹ yr⁻¹, as either sodium nitrate (NaNO₃) to raise soil pH, or ammonium
674 sulfate ((NH₄)₂SO₄) to acidify; an elemental sulfur treatment was selected to acid-
675 ify without N, applied at the same rate of S addition (57 kg S ha⁻¹ yr⁻¹); and
676 control plots received no additions. All amendments were added in pelletized form
677 using hand-held fertilizer spreaders to both the main plots and buffers. Amend-
678 ments were divided into three equal doses distributed across the growing season
679 from 2011-2017 and added as a single dose from 2018 onward. During 2019, plots
680 were fertilized during the week of May 20.

681 3.2.3 *Leaf gas exchange and trait measurements*

682 We sampled one leaf each from 6 to 10 individuals per plot between June
683 25 and July 12, 2019 for gas exchange measurements (Table S1). Leaves were
684 collected from deciduous broadleaf trees represented across all sites and plots and
685 were replicated in efforts to mimic the species abundance of each plot at each
686 site. We also attempted to collect leaves from the upper canopy to reduce differ-
687 ential shading effects on leaf physiology. Leaves were accessed by pulling down
688 small branches using an arborist's slingshot and weighted beanbag attached to a
689 throwline. Branches were immediately recut under deionized water and remained
690 submerged to reduce stomatal closure and avoid xylem embolism (as in Smith &

691 Dukes, 2018) until gas exchange data were collected.

692 Randomly selected leaves with little to no visible external damage were
693 attached to a Li-COR LI-6800 (Li-COR Bioscience, Lincoln, Nebraska, USA)
694 portable photosynthesis machine to measure net photosynthesis (A_{net} ; $\mu\text{mol m}^{-2} \text{s}^{-1}$),
695 stomatal conductance (g_{sw} ; $\text{mol m}^{-2} \text{s}^{-1}$), and intercellular CO_2 concentration
696 (C_i ; $\mu\text{mol mol}^{-1}$) at different reference CO_2 concentrations (C_a ; $\mu\text{mol mol}^{-1}$)
697 concentrations (i.e., an A_{net}/C_i curve) under saturating light conditions (2,000
698 $\mu\text{mol m}^{-2} \text{s}^{-1}$). Reference CO_2 concentrations followed the sequence: 400, 300,
699 200, 100, 50, 400, 400, 600, 800, 1000, 1200, 1500, and 2000 $\mu\text{mol mol}^{-1} \text{CO}_2$. Leaf
700 temperatures were not controlled in the cuvette and ranged from 21.8 °C to 31.7
701 °C (mean±SD: 27.2 ± 2.2 °C). A linear and second order log-polynomial nonlinear
702 regression suggested no effect of temperature on stomatal conductance measured
703 at 400 $\mu\text{mol mol}^{-1} \text{CO}_2$ or net photosynthesis measured at $\mu\text{mol mol}^{-1} \text{CO}_2$ (Ta-
704 ble S2-3; Fig. S1). All A_{net}/C_i curves were generated within one hour of branch
705 severance.

706 Leaf morphological and chemical traits were collected on the same leaf used
707 to generate each A_{net}/C_i curve. Images of each leaf were taken using a flat-bed
708 scanner to determine fresh leaf area using the ‘LeafArea’ R package (Katabuchi
709 2015), which automates leaf area calculations using ImageJ software (Schneider
710 et al. 2012). Each leaf was dried at 65°C for at least 48 hours, weighed, and
711 ground using a Retsch MM200 ball mill grinder (Verder Scientific, Inc., Newtown,
712 PA, USA) until homogenized. Leaf mass per area (M_{area} , g m^{-2}) was calculated
713 as the ratio of dry leaf biomass to fresh leaf area. Using a subsample of ground and
714 homogenized leaf biomass, leaf N content (N_{mass} ; gN g^{-1}) and leaf $\delta^{13}\text{C}$ (‰, rela-

715 tive to VPDB) were measured at the Cornell Stable Isotope Lab with an elemental
 716 analyzer (NC 2500, CE Instruments, Wigan, UK) interfaced to an isotope ratio
 717 mass spectrometer (Delta V Isotope Ratio Mass Spectrometer, ThermoFisher Sci-
 718 entific, Waltham, MA, USA). Leaf N content per unit leaf area (N_{area} ; gN m⁻²)
 719 was calculated by multiplying N_{mass} by M_{area} .

720 We used leaf $\delta^{13}\text{C}$ values to estimate χ (unitless), which is an isotope-
 721 derived estimate of the leaf $C_i:C_a$ ratio. While intercellular and atmospheric CO₂
 722 concentrations were directly measured during each A_{net}/C_i curve, deriving χ from
 723 $\delta^{13}\text{C}$ provides a more integrative estimate of the $C_i:C_a$ over an individual leaf's
 724 lifespan. We derived χ following the approach of Farquhar et al. (1989) described
 725 in Cernusak et al. (2013):

$$\chi = \frac{\Delta^{13}C - a}{b - a} \quad (3.1)$$

726 where $\Delta^{13}\text{C}$ represents the relative difference between leaf $\delta^{13}\text{C}$ (‰) and air $\delta^{13}\text{C}$
 727 (‰), and is calculated from the following equation:

$$\Delta^{13}C = \frac{\delta^{13}C_{\text{air}} - \delta^{13}C_{\text{leaf}}}{1 + \delta^{13}C_{\text{leaf}}} \quad (3.2)$$

728 where $\delta^{13}C_{\text{air}}$ is assumed to be -8‰ (Keeling et al. 1979; Farquhar et al. 1989), a
 729 represents the fractionation between ¹²C and ¹³C due to diffusion in air, assumed
 730 to be 4.4‰, and b represents the fractionation caused by Rubisco carboxylation,
 731 assumed to be 27‰ (Farquhar et al. 1989).

732 3.2.4 A_{net}/C_i curve-fitting and parameter estimation

733 We fit A_{net}/C_i curves of each individual using the ‘fitaci’ function in the
734 ‘plantecophys’ R package (Duursma 2015). This function estimates the maximum
735 rate of Rubisco carboxylation V_{cmax} ; $\mu\text{mol m}^{-2} \text{s}^{-1}$) and maximum rate of electron
736 transport for RuBP regeneration (J_{max} ; $\mu\text{mol m}^{-2} \text{s}^{-1}$) based on the Farquhar,
737 von Caemmerer, and Berry biochemical model of C₃ photosynthesis (Farquhar
738 et al. 1980). For each curve fit, we included triose phosphate utilization (TPU)
739 limitation to avoid underestimating J_{max} (Gregory et al. 2021). Curves were
740 visually examined to confirm the likely presence of TPU limitation.

741 We determined Michaelis-Menten coefficients for Rubisco affinity to CO₂
742 (K_c ; $\mu\text{mol mol}^{-1}$) and O₂ (K_o ; $\mu\text{mol mol}^{-1}$), and the CO₂ compensation point
743 (Γ^* ; $\mu\text{mol mol}^{-1}$) using leaf temperature and equations described in Medlyn et al.
744 (2002) and derived in Bernacchi et al. (2001). Specifically, K_c and K_o were
745 calculated as:

$$K_c = 404.9 * \exp^{\frac{79430(T_k - 298)}{298RT_k}} \quad (3.3)$$

746 and

$$K_o = 278.4 * \exp^{\frac{36380(T_k - 298)}{298RT_k}} \quad (3.4)$$

747 while Γ^* was calculated as:

$$\Gamma^* = 42.75 * \exp^{\frac{37830(T_k - 298)}{298RT_k}} \quad (3.5)$$

748 In all three equations, T_k is the leaf temperature (in Kelvin) during each A_{net}/C_i

749 curve and R is the universal gas constant ($8.314 \text{ J mol}^{-1} \text{ K}^{-1}$).

750 We standardized V_{cmax} and J_{max} estimates to 25°C using a modified Ar-

751 rhenius equation (Kattge and Knorr 2007):

$$k_{25} = \frac{k_{\text{obs}}}{e^{\frac{H_a(T_{\text{obs}} - T_{\text{ref}})}{T_{\text{ref}}RT_{\text{obs}}}} * \frac{1+e^{\frac{T_{\text{ref}}\Delta S - H_d}{T_{\text{obs}}}}}{1+e^{\frac{T_{\text{obs}}\Delta S - H_d}{T_{\text{obs}}}}}} \quad (3.6)$$

752 k_{25} represents the standardized V_{cmax} or J_{max} rate at 25°C , k_{obs} represents

753 the V_{cmax} or J_{max} estimate at the average leaf temperature measured inside the

754 cuvette during the A_{net}/C_i curve. H_a is the activation energy of V_{cmax} ($71,513$

755 J mol^{-1}) Kattge and Knorr (2007) or J_{max} ($49,884 \text{ J mol}^{-1}$) (Kattge and Knorr

756 2007). H_d represents the deactivation energy of both V_{cmax} and J_{max} ($200,000 \text{ J}$

757 mol^{-1}) (Medlyn et al. 2002), and R represents the universal gas constant (8.314

758 $\text{J mol}^{-1} \text{ K}^{-1}$). T_{ref} represents the standardized temperature of 298.15 K (25°C)

759 and T_{obs} represents the mean leaf temperature (in K) during each A_{net}/C_i curve.

760 ΔS is an entropy term that (Kattge and Knorr 2007) derived as a linear relation-

761 ship with average growing season temperature (T_g ; $^\circ\text{C}$), where:

$$\Delta S_{v_{\text{cmax}}} = -1.07 T_g + 668.39 \quad (3.7)$$

762 and

$$\Delta S_{j_{\text{max}}} = -0.75 T_g + 659.70 \quad (3.8)$$

763 We estimated T_g in Equations 3.7 and 3.8 based on mean daily (24-hour) air
764 temperature of the 30 days leading up to the day of each sample collection using
765 the same weather station reported in the site description. We then used V_{cmax25}
766 and J_{max25} estimates to calculate the ratio of J_{max25} to V_{cmax25} ($J_{max25}:V_{cmax25}$;
767 unitless).

768 3.2.5 *Proportion of leaf nitrogen allocated to photosynthesis and structure*

769 We used equations from Niinemets and Tenhunen (1997) to estimate the
770 proportion of leaf N content allocated to Rubisco and bioenergetics. The propor-
771 tion of leaf N allocated to Rubisco (ρ_{rub} ; gN gN⁻¹) was calculated as a function
772 of V_{cmax25} and N_{area} :

$$\rho_{rubisco} = \frac{V_{cmax25} N_r}{V_{cr} N_{area}} \quad (3.9)$$

773 where N_r is the amount of nitrogen in Rubisco, set to 0.16 gN (gN in Rubisco)⁻¹
774 and V_{cr} is the maximum rate of RuBP carboxylation per unit Rubisco protein,
775 set to 20.5 μmol CO₂ (g Rubisco)⁻¹. The proportion of leaf nitrogen allocated to
776 bioenergetics (ρ_{bioe} ; gN gN⁻¹) was similarly calculated as a function of J_{max25} and
777 N_{area} :

$$\rho_{bioe} = \frac{J_{max25} N_b}{J_{mc} N_{area}} \quad (3.10)$$

778 where N_b is the amount of nitrogen in cytochrome f, set to 0.12407 gN (μmol
779 cytochrome f)⁻¹ assuming a constant 1: 1: 1.2 cytochrome f: ferredoxin NADP
780 reductase: coupling factor molar ratio (Evans and Seemann 1989; Niinemets and

781 Tenhunen 1997), and J_{mc} is the capacity of electron transport per cytochrome f,
782 set to $156 \mu\text{mol electron} (\mu\text{mol cytochrome f})^{-1}\text{s}^{-1}$.

783 We estimated the proportion of leaf N content allocated to photosynthetic
784 tissue (ρ_{photo} ; gN gN^{-1}) as the sum of ρ_{rub} and ρ_{bioe} . This calculation is an un-
785 derestimate of the proportion of leaf N allocated to photosynthetic tissue because
786 it does not include N allocated to light harvesting proteins. This leaf N pool was
787 not included because we did not perform chlorophyll extractions on focal leaves.
788 However, the proportion of leaf N content allocated to light harvesting proteins
789 tends to be small relative to ρ_{rub} and ρ_{bioe} , and may scale with changes in ρ_{rub}
790 and ρ_{bioe} (Niinemets and Tenhunen 1997).

791 Finally, we estimated the proportion of leaf N content allocated to struc-
792 tural tissue (ρ_{str} ; gN gN^{-1}) using an empirical equation from Onoda et al. (2017):

$$N_{cw} = 0.000355 * M_{area}^{1.39} \quad (3.11)$$

793 where N_{cw} is the leaf N content allocated to cell walls (gN m^{-2}). ρ_{str} was estimated
794 by dividing N_{cw} by N_{area} .

795 3.2.6 *Tradeoffs between nitrogen and water use*

796 Photosynthetic nitrogen use efficiency (PNUE; $\mu\text{mol CO}_2 \text{ mol}^{-1} \text{ N s}^{-1}$)
797 was calculated by dividing A_{net} by N_{area} , first converting N_{area} to mol N m^{-2}
798 using the molar mass of N (14 g mol^{-1}). We used χ as an indicator of water
799 use efficiency, which exploratory analyses suggest had similar responses to soil N
800 availability and pH as intrinsic water use efficiency measured from gas exchange

801 (A_{net}/g_s). Tradeoffs between nitrogen and water use were determined by cal-
802 culating the ratio of N_{area} to χ ($N_{\text{area}}:\chi$; g N m⁻²) and V_{cmax25} to χ ($V_{\text{cmax25}}:\chi$;
803 $\mu\text{mol m}^{-2} \text{s}^{-1}$). This approach is similar to tradeoff calculations in which nitrogen-
804 water use tradeoffs are measured as the ratio of N_{area} or V_{cmax25} to g_s (Paillassa
805 et al. 2020; Bialic-Murphy et al. 2021). In this study, we quantify these re-
806 lationships using χ in lieu of g_s because g_s rapidly changes with environmental
807 conditions and therefore may have been altered by recent tree branch severance
808 and/or placement in the cuvette.

809 3.2.7 *Soil nitrogen availability and pH*

810 To characterize soil N availability at the time of our leaf gas exchange
811 measurements, we used mixed bed resin bags to quantify mobile ammonium-N
812 and nitrate-N concentrations in each plot. Lycra mesh bags were filled with 5 g
813 of Dowex® Marathon MR-3 hydrogen and hydroxide form resin (MilliporeSigma,
814 Burlington, MA USA) and sealed with a zip tie. Each bag was activated by
815 soaking in 0.5 M HCl for 20 minutes, then in 2 M NaCl until pH of the saline
816 solution stabilized, as described in Allison et al. (2008). Five resin bags were
817 inserted about 10 cm below the soil surface at each plot on June 25, 2019: one
818 near each of the four plot corners and one near the plot center. All resin bags
819 were collected 24 days later on July 19, 2019 and were frozen until extracted.

820 Prior to anion and cation extraction, each resin bag was rinsed with ul-
821 trapure water (MilliQ IQ 7000; Millipore Sigma, Burlington, MA) to remove any
822 surface soil residues. Anions and cations were extracted from surface-cleaned resin
823 bags by individually soaking and shaking each bag in 100 mL of a 0.1 M HCl/2.0

824 M NaCl matrix for one hour. Using a microplate reader (Biotek Synergy H1;
825 Biotek Instruments, Winooski, VT USA), nitrate-N concentrations were quanti-
826 fied spectrophotometrically at 540 nm with the end product of a single reagent
827 vanadium (III) chloride reaction (Doane and Horwáth 2003), and ammonium-N
828 concentrations quantified at 650 nm with the end product of a modified phenol-
829 hypochlorite reaction (Weatherburn 1967; Rhine et al. 1998). Both the single
830 reagent vanadium (III) chloride and modified phenol-hypochlorite methodologies
831 have been well established for determining nitrate-N and ammonium-N concen-
832 trations in resin bag extracts (Arnone 1997; Allison et al. 2008). We used a
833 series of negative and positive controls throughout each well plate to verify the
834 accuracy and precision of our measurements, assaying each resin bag extract and
835 control in triplicate. Soil N availability was estimated as the sum of the nitrate-N
836 and ammonium-N concentration in each resin bag, normalized per g of resin and
837 duration in the field ($\mu\text{g N g}^{-1} \text{ resin d}^{-1}$), then subsequently averaged across all
838 resin bags in a plot for a plot-level mean.

839 Soil pH was measured on 0-10 cm mineral soil samples collected prior to
840 fertilization in 2019. Near each of the four plot corners, three 5.5 cm diameter soil
841 cores were collected after first removing the forest floor where present. Each set
842 of three cores was placed in a plastic bag, and later composited by hand mixing
843 and sieved to 4mm. Soil pH was determined for a 1:2 soil:water slurry (10 g field-
844 moist soil to 20 mL DI water) of each sample using an Accumet AB15 pH meter
845 with flushable junction probe (Fisher Scientific; Hampton, NH, USA), and was
846 estimated at the plot level as the mean soil pH within each plot.

847 3.2.8 *Statistical analyses*

848 We built two separate series of linear mixed-effects models to explore effects
849 of soil N availability, soil pH, species, and leaf N content on leaf physiological
850 traits. In the first series of linear mixed-effects models, we explored the effect
851 of soil N availability, soil pH, and species on leaf N content, leaf photosynthesis,
852 stomatal conductance, and nitrogen-water use tradeoffs. Models included plot-
853 level soil N availability and plot-level soil pH as continuous fixed effects, species
854 as a categorical fixed effect, and site as a categorical random intercept term.
855 Interaction terms between fixed effects were not included due to the small number
856 of experimental plots. We built a series of separate models with this independent
857 variable structure to quantify individual effects of soil N availability, soil pH,
858 and species on N_{area} , M_{area} , N_{mass} , A_{net} , V_{cmax25} , J_{max25} , $J_{\text{max25}}:V_{\text{cmax25}}$, ρ_{rubisco} ,
859 $\rho_{\text{bioenergetics}}$, ρ_{photo} , $\rho_{\text{structure}}$, χ , PNUE, $N_{\text{area}}:\chi$, and $V_{\text{cmax25}}:\chi$.

860 A second series of linear mixed-effects models were built to investigate
861 relationships between leaf N content and photosynthetic parameters. Statistical
862 models included N_{area} as a single continuous fixed effect with species and site des-
863 ignated as individual random intercept terms. We used this independent variable
864 structure to quantify individual effects of leaf N content on A_{net} , V_{cmax25} , J_{max25} ,
865 $J_{\text{max25}}:V_{\text{cmax25}}$, and χ .

866 For all linear mixed-effects models, we used Shapiro-Wilk tests of normal-
867 ity to determine whether linear mixed-effects models satisfied residual normality
868 assumptions. If residual normality assumptions were not met, then models were
869 fit using dependent variables that were natural log transformed. If residual nor-
870 mality assumptions were still not met (Shapiro-Wilk: $p < 0.05$), then models were

871 fit using dependent variables that were square root transformed. All residual nor-
872 mality assumptions for both sets of models that did not originally satisfy residual
873 normality assumptions were met with either a natural log or square root data
874 transformation (Shapiro-Wilk: $p > 0.05$ in all cases).

875 In the first series of models, models for N_{area} , M_{area} , N_{mass} , V_{cmax25} , J_{max25} ,
876 χ , $N_{\text{area}}:\chi$, and $V_{\text{cmax25}}:\chi$, ρ_{rubisco} , $\rho_{\text{bioenergetics}}$, ρ_{photo} , $\rho_{\text{structure}}$ satisfied residual
877 normality assumptions without data transformations (Shapiro-Wilk: $p > 0.05$ in
878 all cases). The model for $J_{\text{max25}}:V_{\text{cmax25}}$ satisfied residual normality assumptions
879 with a natural log data transformation, while models for A_{net} and PNUE each
880 satisfied residual normality assumptions with square root data transformations.
881 In the second series of models, models for V_{cmax25} , J_{max25} , χ , and $V_{\text{cmax25}}:\chi$ satisfied
882 residual normality assumptions without data transformations (Shapiro-Wilk: p
883 > 0.05 in all cases). The model for $J_{\text{max25}}:V_{\text{cmax25}}$ required a natural log data
884 transformation and the model for A_{net} required a square root data transformation
885 (Shapiro-Wilk: $p > 0.05$ in both cases).

886 In all models, we used the ‘lmer’ function in the ‘lme4’ R package (Bates
887 et al. 2015) to fit each model and the ‘Anova’ function in the ‘car’ R package (Fox
888 and Weisberg 2019) to calculate Type II Wald’s χ^2 and determine the significance
889 level ($\alpha = 0.05$) of each fixed effect coefficient. Finally, we used the ‘emmeans’
890 R package (Lenth, 2019) to conduct post-hoc comparisons using Tukey’s tests,
891 where degrees of freedom were approximated using the Kenward-Roger approach
892 (Kenward and Roger 1997). All analyses and plots were conducted in R version
893 4.1.1 (R Core Team 2021)). All figure regression lines and associated 95% confi-
894 dence interval error bars were plotted using predictions generated across the soil

895 nitrogen availability gradient using the ‘emmeans’ R package (Lenth 2019).

896 3.3 Results

897 3.3.1 *Leaf N content*

898 Increasing soil N availability generally increased N_{area} (Table 3.1; Fig.
899 3.1a). This pattern was driven by an increase in N_{mass} (Table 3.1; Fig. 3.1c)
900 and a marginal increase in M_{area} (Table 3.1; Fig. 3.1e) with increasing soil N
901 availability. There was no effect of soil pH on N_{area} , N_{mass} , or M_{area} (Table 3.1);
902 however, we did observe strong differences in N_{area} (Fig. 3.1b), N_{mass} (Fig. 3.1d),
903 and M_{area} (Fig. 3.1e) between species (Table 3.1).

Table 3.1. Effects of soil N availability, soil pH, and species on leaf N content per unit leaf area (N_{area}), leaf N content per unit leaf mass (N_{mass}), and leaf mass per unit leaf area (M_{area})

	df	N_{area}			N_{mass}			M_{area}		
		Coefficient	χ^2	p	Coefficient	χ^2	p	Coefficient	χ^2	p
Intercept	-	9.03E-01	-	-	1.68E+00	-	-	4.60E+01	-	-
Soil N	1	1.68E-02	11.990	0.001	1.25E-02	6.902	0.009	4.87E-01	4.143	0.042
Soil pH	1	9.28E-02	0.836	0.361	8.08E-02	0.663	0.415	4.05E+00	0.653	0.419
Species	4	-	72.128	<0.001	-	35.074	<0.001	-	29.869	<0.001

*Significance determined using Type II Wald χ^2 tests ($\alpha = 0.05$). P-values < 0.05 are in bold.

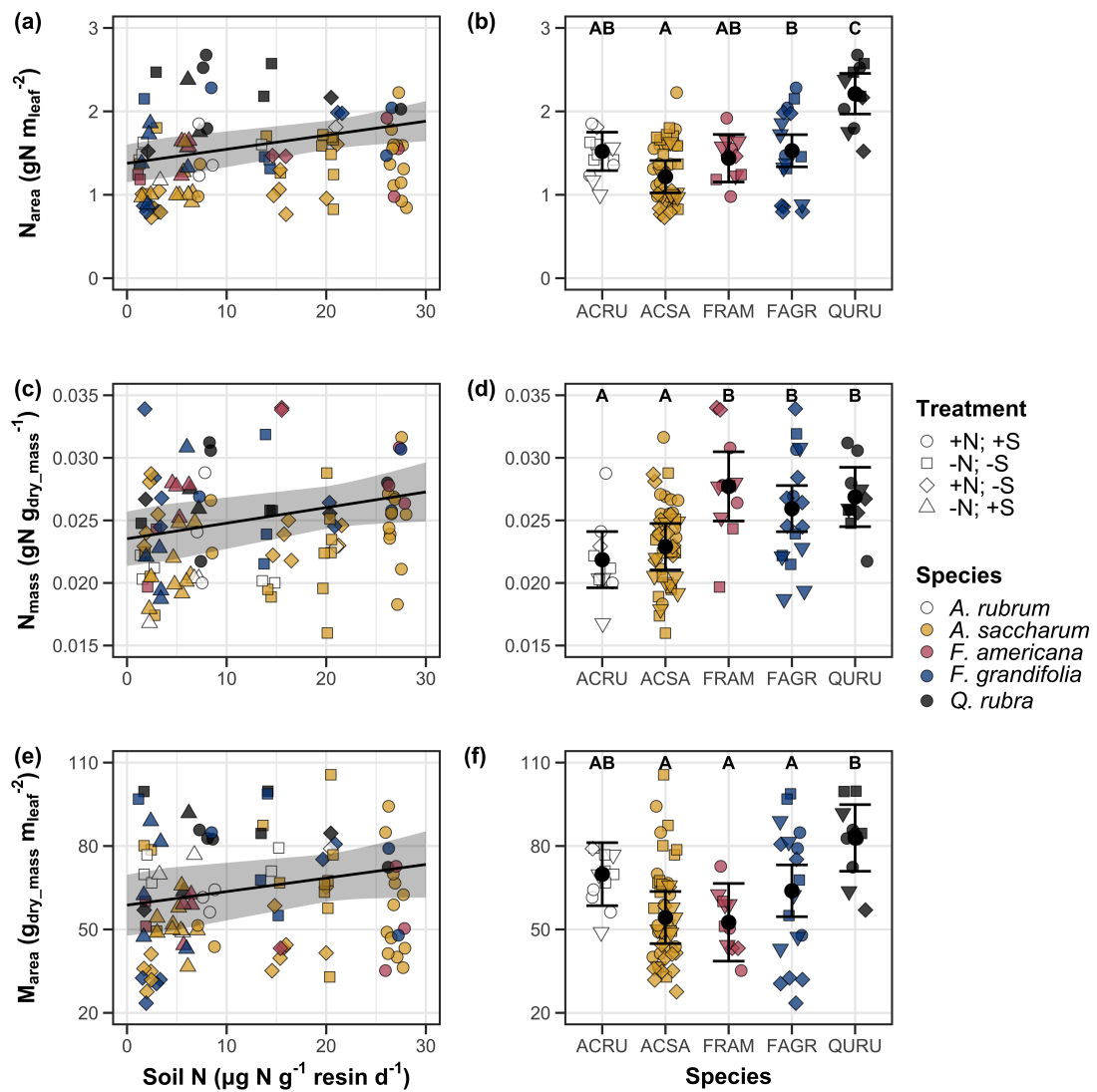


Figure 3.1. Effects of soil N availability and species on leaf N content per unit leaf area (a-b), leaf nitrogen content per unit leaf biomass (c-d), and leaf mass per unit leaf area (e-f). Soil N availability is represented on the x-axis in the left column of panels, while species is represented on the x-axis in the right column of panels. Tree species are represented as colored points and treatment plots are represented as shaped points, jittered for visibility. Species are abbreviated in the right column of panels through their assigned NRCS PLANTS Database symbol (USDA NRCS 2022), grouped along the x-axis per common mycorrhizal association, where the first three species commonly associate with arbuscular mycorrhizae (ACRU, ASCA, FAGR) and the second two species with ectomycorrhizae (FAGR, QURU). Trendlines are only included when the regression slope is statistically different from zero ($p < 0.05$).

904 3.3.2 *Net photosynthesis and leaf biochemistry*

905 Increasing soil N availability generally had no effect on A_{net} , V_{cmax25} , J_{max25} ,
906 or $J_{\text{max25}}:V_{\text{cmax25}}$ (Table 3.2, Figs. 3.2a, 3.2d, 3.2g). We also observed strong
907 species effects on all measured leaf photosynthetic traits (Table 3.2; Figs. 3.2b,
908 3.2e, 3.2h). Increasing soil pH had a marginal negative effect on A_{net} , but had no
909 effect on V_{cmax25} , J_{max25} , or $J_{\text{max25}}:V_{\text{cmax25}}$ (Table 3.2). There was a weak positive
910 effect of increasing N_{area} on A_{net} (Fig. 3.2c), but quite strong positive effects of
911 increasing N_{area} on V_{cmax25} and J_{max25} (Table 3.2; Fig. 3.2f and 3.2i).

Table 3.2. Effects of soil N availability, soil pH, species, and N_{area} on leaf biochemistry

	A_{net}			V_{cmax25}			J_{max25}			
	df	Coefficient	χ^2	p	Coefficient	χ^2	p	Coefficient	χ^2	p
(Intercept)	-	3.29E+00 ^b	-	-	6.38E+01	-	-	1.12E+02	-	-
Soil N	1	-1.23E-03 ^b	1.798	0.180	-3.84E-01	1.745	0.187	-6.70E-01	2.172	0.141
Soil pH	1	-3.09E-01 ^b	3.312	0.069	-4.91E+00	0.655	0.418	-8.18E+00	0.742	0.389
Species	4	-	11.838	0.019	-	31.748	<0.001	-	27.291	<0.001
(N_{area} int.)	-	6.59E-01 ^b	-	-	1.45E-01	-	-	2.86E+01	-	-
N_{area}	4	3.13E-01 ^b	4.790	0.029	2.43E+01	22.616	<0.001	4.04E+01	28.259	<0.001

	$J_{\text{max25}}:V_{\text{cmax25}}$			
	df	Coefficient	χ^2	p
(Intercept)	-	6.59E-01 ^a	-	-
Soil N	1	7.04E-04 ^a	0.088	0.767
Soil pH	1	-7.84E-03 ^a	0.025	0.874
Species	4	-	12.745	0.013
(N_{area} int.)	-	6.69E-01 ^a	-	-
N_{area}	4	-4.69E-02 ^a	1.142	0.285

*Significance determined using Type II Wald χ^2 tests ($\alpha = 0.05$). P -values < 0.05 are in bold, while p -values between 0.05 and 0.1 are italicized. Superscript letters indicate model coefficients fit to natural-log (^a) or square-root (^b) transformed data. Relationships between N_{area} and each response variable were fit using the second series of bivariate mixed-effects models, so model coefficients and results are independent from model coefficients and results reported for relationships between soil N, soil pH, and species for each response variable. Key: A_{net} – light saturated net photosynthesis rate; V_{cmax25} – maximum rate of Rubisco carboxylation at 25°C; J_{max25} – maximum rate of electron transport for RuBP regeneration at 25°C, $J_{\text{max25}}:V_{\text{cmax25}}$ – the ratio of J_{max25} to V_{cmax25} .

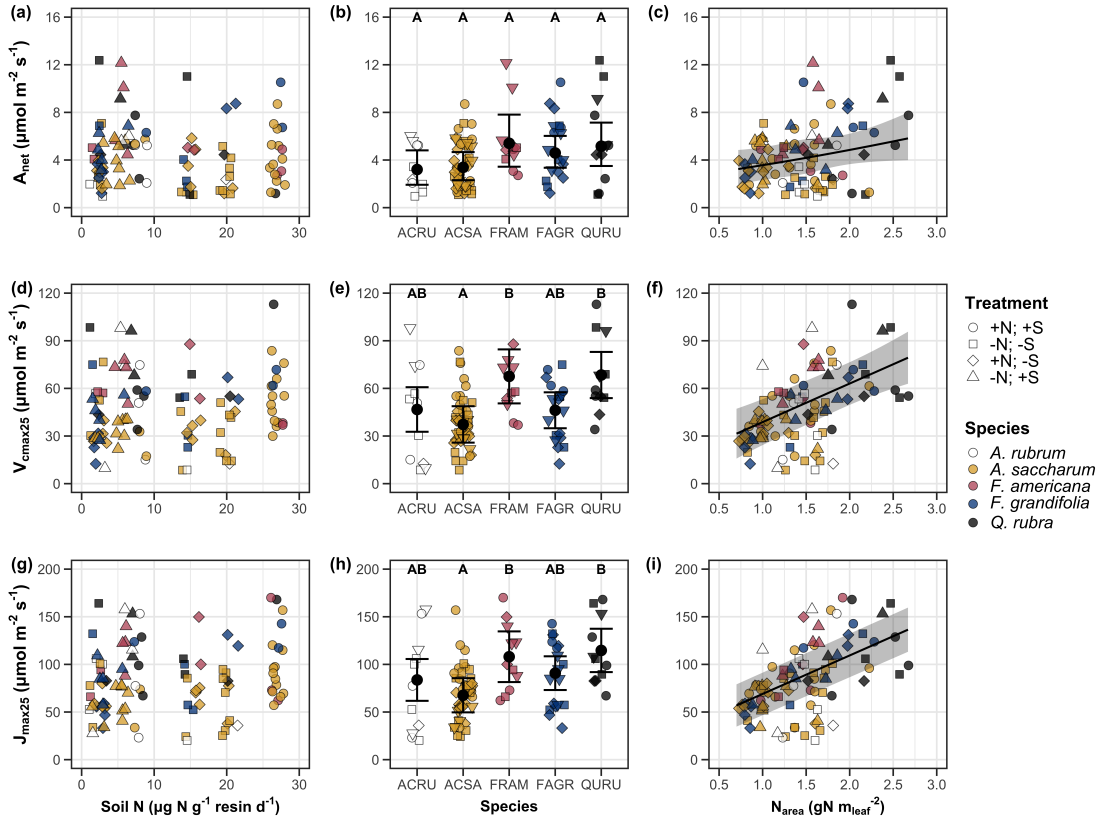


Figure 3.2. Effects of soil N availability (left column of panels), species (middle column of panels), and leaf N content per unit leaf area (right column of panels) on net photosynthesis (a-c), maximum Rubisco carboxylation rate (d-f), and maximum RuBP regeneration rate (g-i). Soil N availability is represented on the x-axis in the left column of panels, species is represented on the x-axis in the middle column of panels, and leaf N content per unit leaf area is represented continuously on the x-axis in the right column of panels. Species abbreviations and position along the x-axis in the middle column of panels, colored points, shapes, and trendlines are as explained in Figure 3.1.

912 3.3.3 *Leaf N allocation*

913 Neither soil N availability nor soil pH affected the proportion of leaf N
914 allocated to Rubisco or bioenergetics (Table 3.3; Fig. 3.3a, Fig. 3.3c), nor was
915 there any subsequent effect on the proportion of leaf N allocated to photosynthesis
916 (Table 3.3; Fig. 3.3f). We also found no effect of soil N availability or soil pH on
917 the proportion of leaf N allocated to structure (Table 3.3; Fig 3.3g). Species varied
918 in the proportion of leaf N allocated to Rubisco, photosynthesis, and structure (Fig
919 3.3b, Fig. 3.3d, Fig 3.3h), with no detectable species effect on the proportion of
920 leaf N allocated to bioenergetics (Table 3.3).

Table 3.3. Effects of soil N availability, soil pH, and species on the proportion of leaf nitrogen content allocated to photosynthesis, Rubisco, bioenergetics, and structure

	ρ_{photo}			ρ_{rub}			ρ_{bioe}			
	df	Coefficient	χ^2	p	Coefficient	χ^2	p	Coefficient	χ^2	p
Intercept	-	4.93E-01	-	-	4.17E-01	-	-	7.64E-02	-	-
Soil N	1	-1.23E-03	0.521	0.470	-1.04E-03	0.501	0.479	-1.77E-04	0.557	0.455
Soil pH	1	-4.37E-02	1.581	0.209	-3.70E-02	1.511	0.219	-6.84E-03	1.941	0.164
Species	4	-	13.106	0.011	-	14.152	0.007	-	7.300	0.121

	ρ_{str}			
	df	Coefficient	χ^2	p
Intercept	-	9.77E-02	-	-
Soil N	1	-2.29E-04	1.165	0.280
Soil pH	1	-1.87E-03	0.179	0.672
Species	4	-	16.428	0.002

*Significance determined using Type II Wald χ^2 tests ($\alpha = 0.05$). P-values < 0.05 are in bold. Key: ρ_{photo} - proportion of leaf nitrogen content allocated to photosynthesis; ρ_{rub} - proportion of leaf nitrogen content allocated to Rubisco; ρ_{bioe} - proportion of leaf nitrogen content allocated to bioenergetics; ρ_{str} - proportion of leaf nitrogen content allocated to structure.

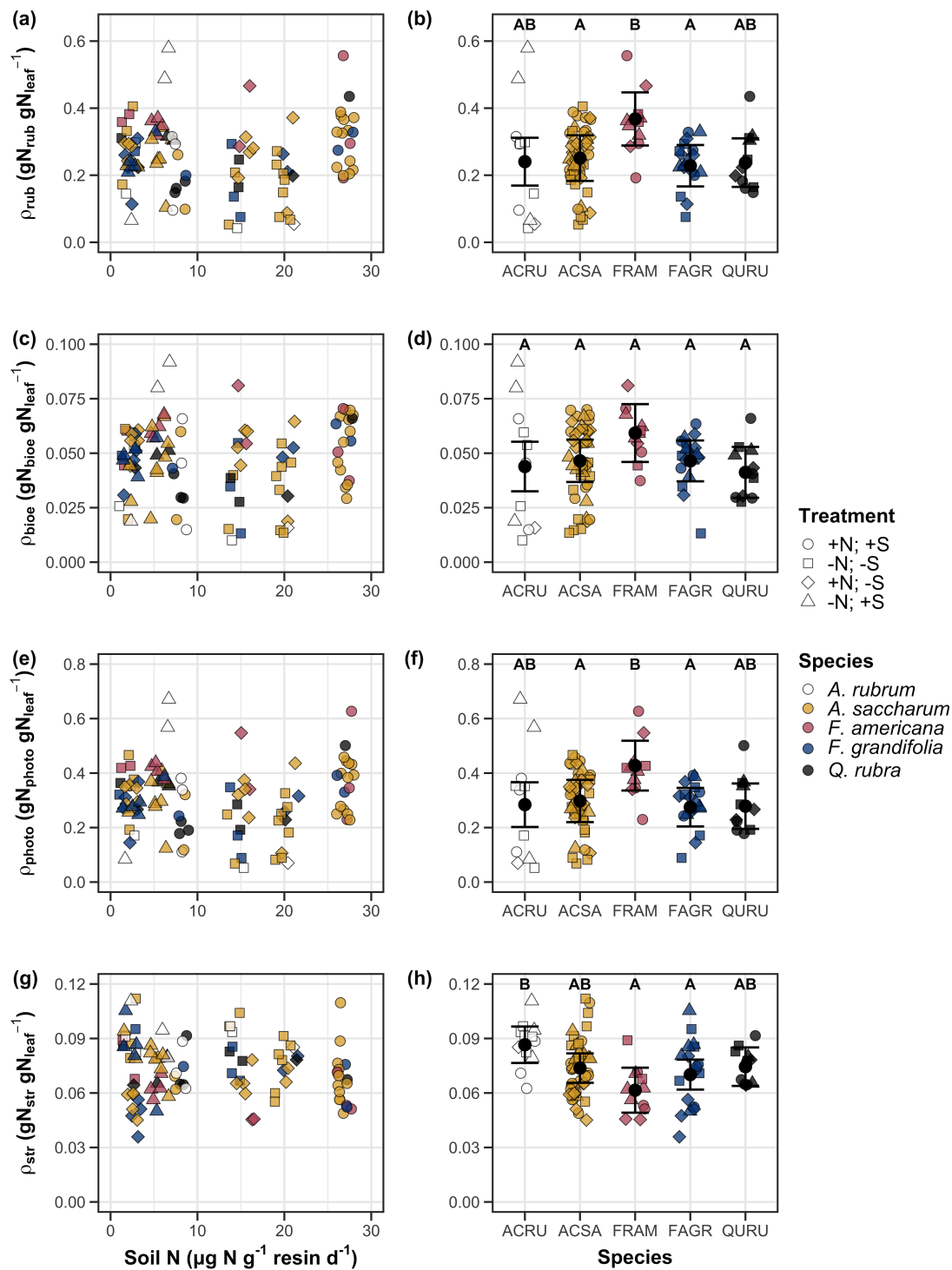


Figure 3.3. Effects of soil nitrogen availability and species on the proportion of leaf nitrogen content allocated to Rubisco (a-b), bioenergetics (c-d), photosynthesis (e-f), and structure (g-h)

921 3.3.4 *Tradeoffs between nitrogen and water use*

922 Although soil N availability did not affect χ (Table 3.4; Fig. 3.4a), increasing
923 soil N availability decreased PNUE (Table 3.4; Fig. 3.4d) and increased the
924 ratio of $N_{\text{area}}:\chi$ (Table 3.4; Fig. 3.4f). Specifically, this response yielded a 26%
925 reduction in PNUE and 37% stimulation in $N_{\text{area}}:\chi$ across the soil nitrogen avail-
926 ability gradient. There was no apparent effect of soil N availability on $V_{\text{cmax25}}:\chi$
927 (Table 3.4; Fig. 3.4h). Increasing soil pH had a weak marginal negative effect
928 on PNUE, but did not influence χ , $N_{\text{area}}:\chi$, or $V_{\text{cmax25}}:\chi$ (Table 3.4). We also
929 observed differences in χ (Fig. 3.4b), PNUE (Fig. 3.4e), $N_{\text{area}}:\chi$ (Fig. 3.4g), and
930 $V_{\text{cmax25}}:\chi$ (Fig. 3.4i) between species (Table 3.4). Finally, increasing N_{area} had a
931 strong negative effect on χ (Table 3.4; Fig. 3.4c) and a strong positive effect on
932 $V_{\text{cmax25}}:\chi$ (Table 3.4; Fig. 3.4j).

Table 3.4. Effects of soil N availability, soil pH, species, and N_{area} on tradeoffs between nitrogen and water use

	χ			PNUE			$N_{\text{area}}:\chi$			
	df	Coefficient	χ^2	p	Coefficient	χ^2	p	Coefficient	χ^2	p
(Intercept)	-	8.12E-01	-	-	9.57E+00	-	-	9.19E-01	-	-
Soil N	1	-1.14E-03	1.698	0.193	-6.63E-02	6.396	0.011	2.60E-02	9.533	0.002
Soil pH	1	-1.91E-02	1.087	0.297	-9.25E-01	2.843	<i>0.092</i>	2.03E-01	1.321	0.250
Species	4	-	18.843	0.001	-	13.454	0.009	-	52.983	<0.001
(N_{area} int.)	-	8.93E-01	-	-	-	-	-	-	-	-
N_{area}	1	-1.11E-01	80.606	<0.001	-	-	-	-	-	-

	$V_{\text{cmax25}}:\chi$			
	df	Coefficient	χ^2	p
(Intercept)	-	7.20E+01	-	-
Soil N	1	3.99E-01	0.963	0.326
Soil pH	1	-3.12E+00	0.138	0.711
Species	4	-	31.450	<0.001
(N_{area} int.)	-	1.18E+01	-	-
N_{area}	4	3.87E+01	32.797	<0.001

61

*Significance determined using Type II Wald χ^2 tests ($\alpha = 0.05$). P -values < 0.05 are in bold, while p -values between 0.05 and 0.1 are italicized. Superscript letters indicate model coefficients fit to natural-log ^(a) or square-root ^(b) transformed data. Relationships between N_{area} and each response variable were fit using the second series of bivariate mixed-effects models, so model coefficients and results are independent from model coefficients and results reported for relationships between soil N, soil pH, and species for each response variable. Key: χ - isotope-derived estimate of the $C_i:C_a$; PNUE - photosynthetic N use efficiency, ratio of net photosynthesis to leaf N content per unit leaf area; $N_{\text{area}}:\chi$ - ratio of N_{area} to χ ; $V_{\text{cmax25}}:\chi$ - ratio of V_{cmax25} to χ .

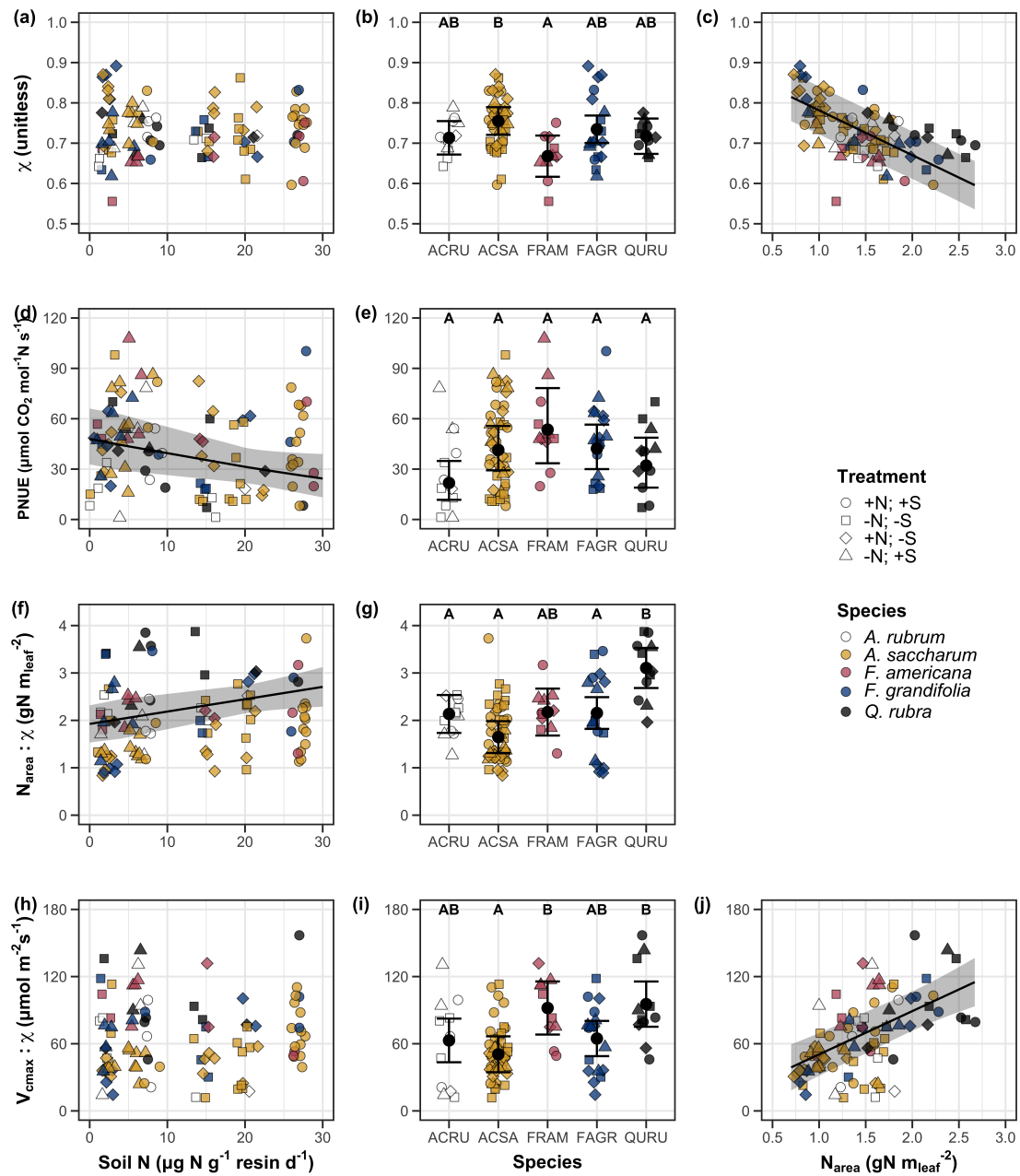


Figure 3.4. Effects of soil nitrogen availability and species on the proportion of leaf nitrogen content allocated to Rubisco (a-b), bioenergetics (c-d), photosynthesis (Rubisco + bioenergetics; e-f), and structure (g-h). Soil nitrogen availability is represented on the x-axis in the left column of panels and species are represented on the x-axis in the right column of panels. Species abbreviations and position along the x-axis in the middle column of panels, colored points, shapes, trendlines, error bars, and compact lettering are as explained in Figure 3.1.

933 3.4 Discussion

934 Photosynthetic least-cost theory provides an explanation for understand-
935 ing relationships between soil nutrient availability, leaf nutrient allocation, and
936 photosynthetic capacity. The theory suggests that plants acclimate to a given
937 environment by optimizing leaf photosynthesis rates at the lowest summed cost
938 of using nutrients and water Prentice et al. (2014), Wang et al. (2017), Smith
939 et al. (2019), Paillassa et al. (2020). The theory predicts that an increase in
940 soil nutrient availability should allow similar photosynthesis rates to be achieved
941 with increased leaf nutrient content and photosynthetic capacity (i.e., V_{cmax25} and
942 J_{max25}) at lower leaf $C_i:C_a$ (χ), resulting in an increase in water use efficiency,
943 decrease in nutrient use efficiency, and increase in both leaf nutrient content and
944 photosynthetic capacity per unit χ . The theory predicts similar leaf responses to
945 increasing soil pH under acidic conditions, presumably due to generally faster nu-
946 trient cycle dynamics and consequent reductions in the cost of acquiring nutrients
947 relative to water with increasing soil pH (Wang et al. 2017; Paillassa et al. 2020;
948 Dong et al. 2020).

949 Supporting the theory, we showed that increasing soil N availability was
950 associated with increased leaf N content (Fig 3.1a, 3.1c), a pattern that reduced
951 photosynthetic N use efficiency (Fig 3.4d) and increased leaf N content per unit
952 χ (Fig 3.4f). Increasing soil N coincided with slight, but non-significant decreases
953 in χ and increases in V_{cmax25} and J_{max25} ($p < 0.2$, Table 3.2). The positive trend
954 between soil N availability and photosynthetic capacity was supported by the con-
955 current strong increase in leaf N content with increasing soil N availability, which
956 resulted in no change in the proportion of leaf N content allocated to photosynthe-

957 sis across the soil N availability gradient. Additionally, leaf N content exhibited a
958 strong negative correlation with χ , indicative of strong nitrogen-water use trade-
959 offs at the leaf level. Responses tended to vary more due to soil N availability
960 than soil pH. Overall, these findings are consistent with the nutrient-water use
961 tradeoffs predicted from theory.

962 3.4.1 *Soil nitrogen availability modifies tradeoffs between nitrogen and water use*

963 In support of expected least-cost outcomes and past environmental gradient
964 studies (Dong et al. 2017; Paillassa et al. 2020), we found that increasing soil N
965 availability was associated with increased leaf N content. Soil N availability had
966 smaller impacts on measures of net photosynthesis and χ , which led to reductions
967 in PNUE and increases in leaf N content per unit χ , as expected from theory.
968 Photosynthetic least-cost theory suggests that reductions in PNUE should be
969 driven by an increase in the proportion of leaf N allocated to photosynthetic tissue,
970 a pattern that should allow plants to achieve optimal photosynthetic rates with
971 greater photosynthetic capacity to make better use of available light. Contrasting
972 theory predictions, we found no effect of soil N availability on photosynthetic
973 capacity. However, photosynthetic capacity did tend to increase with increasing
974 soil N availability ($p < 0.20$; Table 3.2) resulting in no effect of soil N availability on
975 the relative fraction of leaf N allocated to photosynthesis, Rubisco, or bioenergetics
976 (Fig. 3.3). These lines of evidence support the idea that trees use additional N
977 to support increased leaf N allocation toward photosynthetic tissue and enhance
978 photosynthetic capacity (Wright et al. 2003).

979 Soil N availability had a stronger effect on leaf N than photosynthetic ca-

980 pacity. This pattern suggests that additional plant N uptake due to increased
981 soil N availability was also being used to support non-photosynthetic N pools,
982 possibly to structural tissue or stress-induced amino acid and polyamine synthe-
983 sis (Minocha et al. 2000; Onoda et al. 2004; Bubier et al. 2011). While we
984 found no change in the proportion of leaf N allocated to leaf structural tissue, the
985 overall stimulation in leaf N content with increasing soil N availability suggests an
986 increase in the net amount of N invested in leaf structural tissue along the N avail-
987 ability gradient. Importantly, leaf N allocated to structure was calculated using
988 an empirical relationship between M_{area} and the amount of leaf N allocated to cell
989 walls (Onoda et al. 2017). As the generality of relationships between M_{area} and
990 the amount of leaf N allocated to cell walls has been called into question (Harrison
991 et al. 2009), future work should consider explicitly measuring N allocation to cell
992 wall tissue and stress-induced amino acid synthesis to confirm these patterns.

993 In opposition to patterns expected from least cost theory, increasing soil
994 N availability had no apparent effect on χ (Fig. 3.4a). Interestingly, despite
995 the null effect of soil N availability on χ , we observed a strong negative effect of
996 increasing N_{area} on χ (Fig. 3.4c), consistent with the nitrogen-water use tradeoffs
997 expected from theory. The null response of χ to increasing soil N availability may
998 have been due to a lack of water limitation in the system, given that the area
999 received approximately 20% more precipitation (1167 mm) during the 12-month
1000 period leading up to our measurement period than normally expected (972 mm).
1001 However, droughts can and do occur in temperate forests of the northeastern
1002 United States (Sweet et al. 2017), so the observed increase in leaf N content
1003 with increasing soil N availability could be a strategy that allows trees to hedge

1004 bets against drier than normal growing seasons (Onoda et al. 2004; Onoda et al.
1005 2017; Hallik et al. 2009). As was suggested in Paillassa et al. (2020), and more
1006 recently by Querejeta et al. (2022), negative effects of soil N availability on χ may
1007 increase with increasing aridity. This strategy would be especially advantageous if
1008 it allows individuals growing in arid regions to maintain carbon assimilation rates
1009 with reduced water loss. Future work should attempt to quantify interactive roles
1010 of climate and soil nitrogen availability on nitrogen-water use tradeoffs, which
1011 could be done by leveraging coordinated and multi-factor nutrient (Borer et al.
1012 2014) and water (Knapp et al. 2017) manipulation experiments across broad
1013 climatic gradients.

1014 3.4.2 *Soil pH did not modify tradeoffs between nitrogen and water usage*

1015 While the primary purpose of this study was to examine the role of soil N
1016 availability on nitrogen-water use tradeoffs, our experimental design manipulated
1017 both soil N and pH, providing an opportunity to isolate the roles of these variables.
1018 Previous correlational studies along environmental gradients identified soil pH as
1019 a particularly important factor that can modify tradeoffs between nutrient and
1020 water use (Smith et al. 2019; Paillassa et al. 2020; Westerband et al. 2023)
1021 and the proportion of leaf nitrogen allocated to photosynthesis (Luo et al. 2021).
1022 Such studies implied that these patterns may be driven by reductions in the cost of
1023 acquiring nutrients relative to water with increasing pH, which may be exacerbated
1024 in acidic soils.

1025 Consistent with theory (Wright et al. 2003; Prentice et al. 2014), our
1026 results indicate that increasing soil pH was negatively associated with PNUE.

1027 However, there was no effect of soil pH on leaf N content, χ , or leaf N content per
1028 unit χ , most likely because the experimental N additions increased soil N sup-
1029 ply while both increasing (sodium nitrate) and decreasing (ammonium sulfate)
1030 soil pH. These results suggest that soil pH did not play a major role in modify-
1031 ing expected photosynthetic least-cost theory patterns, contrasting findings from
1032 Paillassa et al. (2020) and other gradient studies that note positive effects of in-
1033 creasing soil pH on leaf N content, Rubisco carboxylation, and χ (Viet et al. 2013;
1034 Cornwell et al. 2018; Luo et al. 2021). Instead, null responses to soil pH show
1035 that leaf photosynthetic parameters depend more on soil N availability than pH
1036 per se, and that inferences from gradient studies might be confounding covariation
1037 between N availability and soil acidity.

1038 3.4.3 *Species identity explains a large amount of variation in leaf and whole*
1039 *plant traits*

1040 Species generally explained a larger amount of variation in measured leaf
1041 traits than soil N availability or soil pH. Interspecies variation is an important
1042 factor to consider when deducing mechanisms that drive photosynthetic least-
1043 cost theory, particularly for species that form distinct mycorrhizal associations or
1044 have different photosynthetic pathways, growth forms, or leaf habit (Espelta et al.
1045 2005; Adams et al. 2016; Bialic-Murphy et al. 2021; Scott and Smith 2022). The
1046 need to consider species may also be important when comparing nutrient-water
1047 use tradeoffs in early and late successional species, or in species with different
1048 resource economic strategies (Abrams and Mostoller 1995; Ellsworth and Reich
1049 1996; Wright et al. 2004; Reich 2014; Onoda et al. 2017; Ziegler et al. 2020).

1050 A strength of the study design and sampling effort is that it controls for
1051 many species differences that should modify nitrogen-water use tradeoffs expected
1052 from theory. All tree species measured in this study shared the leaf habit of decid-
1053 uous broadleaves, were growing in forests of similar successional stage, but differed
1054 in mycorrhizal association and consequent resource economic strategies. As stands
1055 tended to be dominated by trees that associate with arbuscular mycorrhizae (*Frax-*
1056 *inus* and both *Acer* species made up 70% of total aboveground biomass across
1057 stands), ecosystem biogeochemical cycle dynamics may be more closely aligned
1058 to the inorganic nutrient economy proposed in Phillips et al. (2013), which may
1059 promote stronger nitrogen-water use tradeoffs in tree species that associate with
1060 arbuscular mycorrhizae. This result was not observed here, as photosynthetic
1061 properties varied as much within as across the two mycorrhizal associations rep-
1062 resented. Given the high variability in measured photosynthetic traits within
1063 and across species, effects of mycorrhizal association likely require more intensive
1064 sampling efforts to detect than were possible here.

1065 3.4.4 *Implications for photosynthetic least-cost theory model development*

1066 In the field, soil nutrient availability is heterogeneous across time and space
1067 (Table S4). Unaccounted within-plot heterogeneity may have contributed to the
1068 low amount of variation explained by soil N availability in our statistical mod-
1069 els, as resin bags are a coarse surrogate for soil N availability. Despite this, we
1070 still observed evidence for nutrient-water use tradeoffs, suggesting that observed
1071 responses reported here may be an underestimate toward the net effect of soil
1072 N availability on these tradeoffs. While we urge caution in the interpretation of

1073 these results, they do provide a promising baseline for future studies investigating
1074 patterns expected from photosynthetic least-cost theory at finer spatiotemporal
1075 resolutions.

1076 The general stronger relationship between leaf N content and photosynthetic parameters versus between leaf N content and soil N availability suggests
1077 that leaf N content is more directly tied to photosynthesis than soil N availability.
1078 While this could be due to the high spatiotemporal heterogeneity of soil N availability,
1079 principles from photosynthetic least-cost theory suggest that leaf N content is the downstream product of leaf nutrient demand to build and maintain
1080 photosynthetic machinery, which is set by aboveground environmental conditions
1081 such as light availability, CO₂, temperature, or vapor pressure deficit (Smith
1082 et al. 2019; Paillassa et al. 2020; Peng et al. 2021; Westerband et al. 2023). The
1083 stronger relationship between leaf N and photosynthetic parameters paired with
1084 the strong negative relationship between leaf N and χ could indicate a relatively
1085 stronger effect of climate on leaf N-photosynthesis relationships than soil resource
1086 availability. However, the short distance between plots and across sites limited
1087 our ability to test this mechanism.

1090 Variation in soil pH affected least cost responses less than variations in
1091 soil N availability, in part because experimental treatments directly increased soil
1092 N and affected soil pH in opposite directions. While soil pH has been shown
1093 to drive nitrogen-water tradeoffs in global gradient analyses (Viet et al. 2013;
1094 Paillassa et al. 2020), these responses may be due to covariations between soil pH
1095 and nutrient cycling rather than a role of pH per se. The direct manipulations
1096 of soil pH and soil N availability in this study allowed us to partly disentangle

1097 these factors and show that variation in N availability matters more for least-cost
1098 tradeoffs than pH alone.

1099 3.4.5 *Conclusions*

1100 Increasing soil N availability generally increased leaf N content (both area-
1101 and mass-based), but did not significantly influence χ . This shift in leaf N led
1102 to a reduction in PNUE, and an increase in leaf N per unit χ with increasing
1103 soil N availability. Despite null effects of soil N availability on χ , we observed a
1104 strong negative relationship between leaf N content and χ . These results provide
1105 empirical support for the nutrient-water use tradeoffs expected from photosyn-
1106 thetic least-cost theory in response to soil nutrient availability, but suggest that
1107 all tenets of the theory may not hold in every environment. These results exper-
1108 imentially test previous work suggesting that leaf water-nitrogen economies vary
1109 across gradients of soil nutrient availability and pH, and show that variations in
1110 nutrient availability matter more for determining variation in leaf photosynthetic
1111 traits than soil pH.

1112

Chapter 4

1113 The relative cost of resource use for photosynthesis drives variance in
1114 leaf nitrogen content across climate and soil resource availability
1115 gradients

1116 4.1 Introduction

1117 Terrestrial biosphere models, which comprise the land surface component of
1118 Earth system models, are sensitive to the formulation of photosynthetic processes
1119 (Knorr 2000; Ziehn et al. 2011; Booth et al. 2012). This is because photosynthe-
1120 sis is the largest carbon flux between the atmosphere and terrestrial biosphere,
1121 and is constrained by ecosystem carbon and nutrient cycles (Hungate et al. 2003;
1122 LeBauer and Treseder 2008; IPCC 2021; Fay et al. 2015). Many terrestrial bio-
1123 sphere models formulate photosynthesis by parameterizing photosynthetic capac-
1124 ity within plant functional groups through empirical linear relationships between
1125 area-based leaf nitrogen content (N_{area}) and the maximum carboxylation rate
1126 of Ribulose-1,5-bisphosphate carboxylase/oxygenase (Kattge et al. 2009; Rogers
1127 2014; Rogers et al. 2017). Models are also beginning to include connected carbon-
1128 nitrogen cycles (Wieder et al. 2015; Shi et al. 2016; Davies-Barnard et al. 2020;
1129 Braghieri et al. 2022), which allows leaf photosynthesis to be predicted directly
1130 through changes in N_{area} and indirectly through changes in soil nitrogen avail-
1131 ability (e.g., LPJ-GUESS, Smith et al., 2014; CLM5.0, Lawrence et al., 2019).
1132 Despite recent model developments, open questions remain regarding the gen-
1133 erality of ecological relationships between soil nitrogen availability, leaf nitrogen
1134 content, and leaf photosynthesis across edaphic and climatic gradients.
1135 Empirical support for positive relationships between soil nitrogen avail-

ability and N_{area} is abundant (Firn et al. 2019; Liang et al. 2020), and is a result often attributed to the high nitrogen cost of building and maintaining Rubisco (Evans 1989; Evans and Seemann 1989; Onoda et al. 2004; Onoda et al. 2017; Dong et al. 2020). Such patterns imply that positive relationships between soil nitrogen availability and N_{area} should cause an increase in leaf photosynthesis and photosynthetic capacity by increasing the maximum rate of Rubisco carboxylation through increased investments to Rubisco construction and maintenance. This integrated N_{area} -photosynthesis response to soil nitrogen availability has been observed both in manipulative experiments and across environmental gradients (Field and Mooney 1986; Evans 1989; Walker et al. 2014; Li et al. 2020), and is thought to be driven by ecosystem nitrogen limitation, which limits its primary productivity globally (LeBauer and Treseder 2008; Fay et al. 2015). However, this response is not consistently observed, as recent studies note variable N_{area} -photosynthesis relationships across soil nitrogen availability gradients (Liang et al. 2020; Luo et al. 2021) and that aboveground growing conditions (e.g., light availability, temperature, vapor pressure deficit) or species identity traits (e.g., photosynthetic pathway, nitrogen acquisition strategy) may be more important for explaining variance in N_{area} and photosynthetic capacity across time and space (Adams et al. 2016; Dong et al. 2017; Dong et al. 2020; Dong et al. 2022; Smith et al. 2019; Peng et al. 2021; Westerband et al. 2023).

1156 4.2 Methods

1157 4.2.1 *Site descriptions and sampling methodology*

1158 We collected leaf and soil samples from 24 open grassland sites across cen-
1159 tral and eastern Texas in summer 2020 and summer 2021 (Fig. 4.1). Twelve
1160 sites were visited between June and July 2020 and 14 sites (11 unique from 2020)
1161 were visited between May and June 2021 (Table 1). We explicitly chose sites
1162 that maximized variability in precipitation and edaphic variability between sites
1163 while minimizing temperature variability across the environmental gradient (Ta-
1164 ble 1). No site with personally communicated or anecdotal evidence of grazing
1165 or disturbance (e.g., mowing, feral hog activity, etc.) were used. We collected
1166 leaf material from three individuals each of the five most abundant species at ran-
1167 dom locations at each site, only selecting species that were broadly classified as
1168 graminoid, forb/herb, shrub, or subshrub growth habits per the USDA PLANTS
1169 database (USDA NRCS 2022). All collected leaves were fully expanded with no
1170 visible herbivory or other external damage and also free from shading by nearby
1171 shrubs or trees. Five soil samples were collected from 0-15cm below the soil sur-
1172 face at each site near the leaf collection sample locations. Soil samples were later
1173 mixed together by hand to create one composite soil sample per site.

1174 4.2.2 *Leaf trait measurements*

1175 Images of each leaf were taken immediately following each site visit using
1176 a flat-bed scanner. Fresh leaf area was determined from each image using the
1177 'LeafArea' R package (Katabuchi 2015), which automates leaf area calculations
1178 using ImageJ software (Schneider et al. 2012). Each leaf was dried at 65°C for at

1179 least 48 hours to a constant mass, weighed, and manually ground in a mortar and
1180 pestle until homogenized. Leaf mass per area (M_{area} ; g m⁻²) was calculated as the
1181 ratio of dry leaf biomass to fresh leaf area. Subsamples of dried and homogenized
1182 leaf tissue were used to measure leaf nitrogen content (N_{mass} ; gN g⁻¹) through el-
1183 emental combustion analysis (Costech-4010, Costech Instruments, Valencia, CA).
1184 Leaf nitrogen content per unit leaf area (N_{area} ; gN m⁻²) was then calculated as
1185 the product of N_{mass} and M_{area} .

1186 Subsamples of dried and homogenized leaf tissue were sent to the University
1187 of California-Davis Stable Isotope Facility to determine leaf $\delta^{13}\text{C}$. Leaf $\delta^{13}\text{C}$ values
1188 were determined using an elemental analyzer (PDZ Europa ANCA-GSL; Sercon
1189 Ltd., Chestshire, UK) interfaced to an isotope ratio mass spectrometer (PDZ
1190 Europa 20-20 Isotope Ratio Mass Spectrometer, Sercon Ltd., Chestshire, UK).
1191 We used leaf $\delta^{13}\text{C}$ values (‰; relative to Vienna Pee Dee Belemnite international
1192 reference standard) to estimate the ratio of intercellular (C_i) to extracellular (C_a)
1193 CO₂ ratio (leaf $C_i:C_a$, χ ; unitless) following the approach of Farquhar et al. (1989)
1194 described in Cernusak et al. (2013). We derived χ as:

$$\chi = \frac{C_i}{C_a} = \frac{\Delta^{13}\text{C} - a}{b - a} \quad (4.1)$$

1195 where $\Delta^{13}\text{C}$ represents the relative difference between leaf $\delta^{13}\text{C}$ (‰) and air $\delta^{13}\text{C}$
1196 (‰), and is calculated as:

$$\Delta^{13}\text{C} = \frac{\delta^{13}\text{C}_{\text{air}} - \delta^{13}\text{C}_{\text{leaf}}}{1 + \delta^{13}\text{C}_{\text{leaf}}} \quad (4.2)$$

1197 $\delta^{13}\text{C}_{\text{air}}$, traditionally assumed to be -8‰ (Keeling et al. 1979; Farquhar et al.

1198 1989), was calculated as a function of calendar year t using an empirical equation
1199 derived in Feng (1999):

$$\delta^{13}C_{air} = -6.429 - 0.006e^{0.0217(t-1740)} \quad (4.3)$$

1200 This calculation resulted in $\delta^{13}C_{air}$ values for 2020 and 2021 as -9.04 and -9.09,
1201 respectively. a represents the fractionation between ^{12}C and ^{13}C due to diffusion
1202 in air, assumed to be 4.4‰, and b represents the fractionation caused by Rubisco
1203 carboxylation, assumed to be 27‰ (Farquhar et al. 1989). For C_4 species, b in
1204 Eqn. 4.1 was set to 6.3‰, and was derived from:

$$b = c + (d \cdot \phi) \quad (4.4)$$

1205 Where c was set to -5.7‰ and d was set to 30‰ (Farquhar et al. 1989). ϕ , which
1206 is the bundle sheath leakiness term, was set to 0.4. All χ values less than 0.2 and
1207 greater than 1.0 were assumed to be incorrect and removed.

1208 We derived the unit cost of resource use (β) using leaf χ and site climate
1209 data with equations first described in Prentice et al. (2014) and simplified in
1210 Lavergne et al. (2020):

$$\beta = 1.6\eta^*D \frac{\chi - (\frac{\Gamma^*}{C_a})^2}{(1 - \chi)^2(K_m + \Gamma^*)} \quad (4.5)$$

1211 where η^* is the viscosity of water relative to 25°C, calculated using elevation and
1212 mean air temperature of the seven days leading up to each site visit following
1213 equations in Huber et al. (2009). D represents vapor pressure deficit (Pa), set

1214 to the mean vapor pressure deficit of the seven days leading up to each site visit,
1215 C_a represents atmospheric CO₂ concentration, arbitrarily set to 420 $\mu\text{mol mol}^{-1}$
1216 CO². K_m (Pa) is the Michaelis-Menten coefficient for Rubisco affinity to CO₂ and
1217 O₂, calculated as:

$$K_m = K_c \cdot \left(1 + \frac{O_i}{K_o}\right) \quad (4.6)$$

1218 where K_c (Pa) and K_o (Pa) are the Michaelis-Menten coefficients for Rubisco
1219 affinity to CO₂ and O₂, respectively, and O_i is the intercellular O₂ concentration.
1220 Γ^* (Pa) is the CO₂ compensation point in the absence of dark respiration. K_c , K_o ,
1221 and Γ^* were determined using equations described in Medlyn et al. (2002) and
1222 derived in Bernacchi et al. (2001), invoking an elevation correction for atmospheric
1223 pressure as explained in Stocker et al. (2020).

Table 4.1. Site locality information, sampling year(s), 2006-2020 mean annual precipitation (MAP; mm), mean annual temperature (MAT; °C), and water holding capacity (WHC; mm)*

Site	Latitude	Longitude	Sampling year	MAP	MAT	WHC
Edwards_2019_17	29.95	-100.36	2020	563.5	19.0	224.7
Uvalde_2020_02	29.59	-100.09	2020, 2021	648.5	19.5	224.7
Menard_2020_01	30.91	-99.59	2020	641.9	18.3	220.2
Kerr_2020_03	30.06	-99.34	2021	672.4	18.3	237.5
Bandera_2020_03	29.85	-99.30	2021	789.4	18.8	235.1
Sansaba_2020_01	31.29	-98.62	2020	733.0	18.8	234.3
Comal_2020_21	29.79	-98.43	2020	878.5	19.9	220.7
Blanco_2019_16	29.99	-98.43	2020	833.0	19.2	222.2
Bexar_2019_13	29.24	-98.43	2020	759.3	21.5	206.0
Burnet_2020_14	30.84	-98.34	2021	763.3	19.5	217.8
Comal_2020_19	30.01	-98.32	2021	845.0	19.3	220.4
Hays_2020_54	29.96	-98.17	2021	861.3	20.0	225.6
Burnet_2020_12	30.82	-98.06	2021	815.1	19.4	245.3
Williamson_2019_09	30.71	-97.86	2020	867.7	19.7	270.2
Williamson_2019_10	30.54	-97.77	2020	819.5	19.9	239.8
Bell_2021_08	31.06	-97.55	2021	937.3	19.6	232.3
Fayette_2021_12	29.86	-97.21	2021	985.7	20.4	165.6
Fayette_2019_04	30.09	-96.78	2020	1017.4	20.6	226.9
Fayette_2020_09	29.86	-96.71	2021	1002.7	20.8	187.6
Washington_2020_08	30.28	-96.41	2021	1077.4	20.4	203.9
Austin_2020_03	29.78	-96.24	2021	1108.7	20.6	253.0
Brazos_2020_16	30.93	-96.23	2021	1078.0	20.1	202.2
Brazos_2020_18	30.52	-96.21	2020, 2021	1099.4	20.4	233.5
Harris_2020_03	29.88	-95.31	2020, 2021	1492.0	21.6	265.6

1224 *Rows are arranged by longitude to visualize precipitation variability across sites

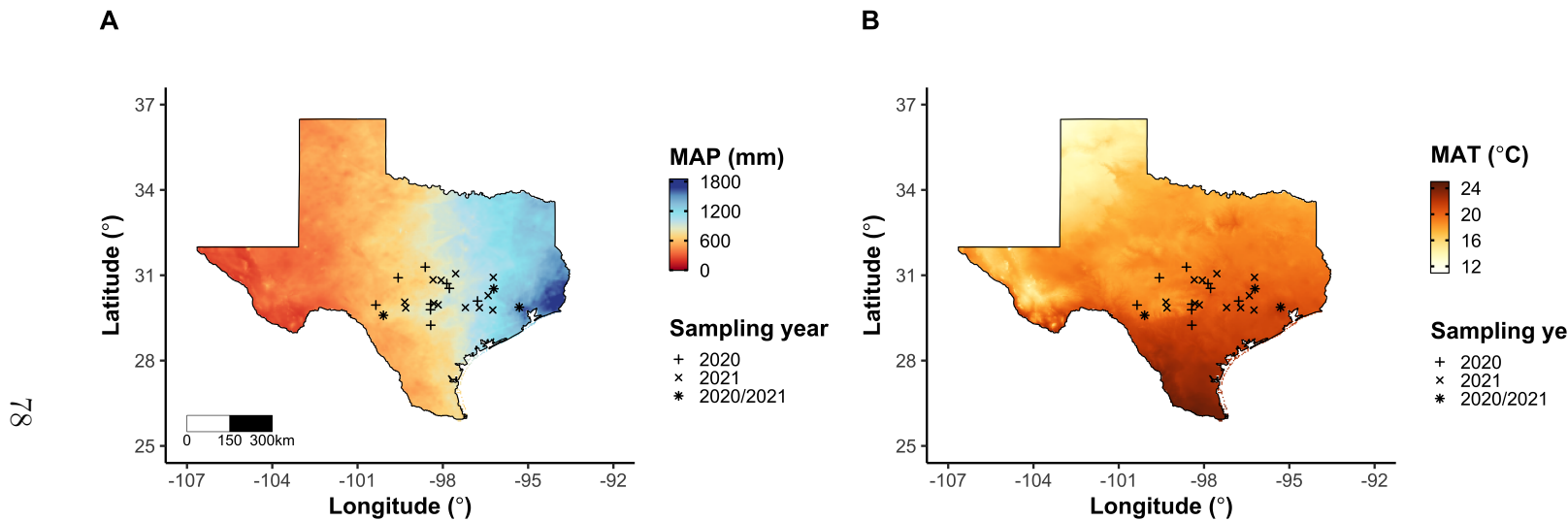


Figure 4.1. Maps that detail site locations along 2006-2020 mean annual precipitation (panel A) and mean annual temperature (panel B) gradients in Texas, USA. Precipitation and temperature data were plotted at a 4-km grid resolution and are masked to include only grid cells that occur in the Texas state boundary in the United States. In both panels, open circles refer to sites visited in 2020, open triangles to sites visited in 2021, and closed circles to sites visited in 2020 and 2021. The scale bar in panel A also applies to panel B.

1225 4.2.3 *Site climate data*

1226 We used the Parameter-elevation Regressions on Independent Slopes Model
1227 (PRISM) (Daly et al. 2008) climate product to access gridded daily temperature
1228 and precipitation data for the coterminous United States at a 4-km grid resolution
1229 between January 1, 2006 and July 31, 2021 (PRISM Climate Group, Oregon State
1230 University, <https://prism.oregonstate.edu>, data created 4 Feb 2014, accessed 24
1231 Mar 2022). Daily mean air temperature, mean VPD, and total precipitation
1232 data were extracted from the grid cell that contained the latitude and longitude
1233 of each property using the ‘extract’ function in the ‘terra’ R package (Hijmans
1234 2022). PRISM data were used in lieu of local weather station data because several
1235 rural sites did not have a local weather station present within a 20-km radius of
1236 the site. Daily site climate data were used to estimate mean annual precipitation
1237 and mean annual temperature for each site between 2006 and 2020 (Table 1). We
1238 then calculated total precipitation and mean daily VPD for the prior 1, 2, 3, 4, 5,
1239 6, 7, 8, 9, 10, 15, 20, 25, 30, 60, and 90 days leading up to each site visit.

1240 4.2.4 *Site edaphic characteristics*

1241 Subsamples of composited soil samples were sent to the Texas A & M
1242 Soil, Water and Forage Laboratory to quantify soil nitrate concentration (NO₃-N;
1243 ppm). Soil NO₃-N was determined by extracting composite soil samples in 1 M
1244 KCl, measuring absorbance values of extracts at 520 nm using the end product of
1245 a NO₃-N to NO₂-N cadmium reduction reaction (Kachurina et al. 2000). Soil tex-
1246 ture data from 0-15cm below the soil surface were accessed using the SoilGrids2.0
1247 data product (Poggio et al. 2021) through the ‘fetchSoilGrids’ function in the

1248 ‘soilDB’ R package (Beaudette et al. 2022). We used SoilGrids2.0 to access soil
1249 texture data in lieu of analyses using the collected composite soil sample due to
1250 a lack of soil material from some sites after sending samples for soil NO₃-N.

1251 Soil moisture was not measured in the field, but was estimated using
1252 the ‘Simple Process-Led Algorithms for Simulating Habitats’ model (‘SPLASH’)
1253 (Davis et al. 2017). This model, derived from the STASH model (Cramer and
1254 Prentice 1988), spins up a bucket model using Priestley-Taylor equations (Priest-
1255 ley and Taylor 1972) to calculate daily soil moisture (W_n ; mm) as a function
1256 of the previous day’s soil moisture (W_{n-1} ; mm), daily precipitation (P_n ; mm),
1257 condensation (C_n ; mm), actual evapotranspiration (E_n^a ; mm), and runoff (RO;
1258 mm):

$$W_n = W_{n-1} + P_n + C_n - E_n^a - RO \quad (4.7)$$

1259 Models were spun up by equilibrating the previous day’s soil moisture using
1260 successive model iterations with daily mean air temperature, daily precipitation
1261 total, the number of daily sunlight hours, and latitude as model inputs (Davis et al.
1262 2017). Daily sunlight hours were estimated for each day at each site using the
1263 ‘getSunlightTimes’ function in the ‘suncalc’ R package, which estimated sunrise
1264 and sunset times of each property using date and site coordinates (Thieurmel and
1265 Elmarhraoui 2019). Water holding capacity (mm), or bucket size, was estimated
1266 as a function of soil texture using pedotransfer equations explained in Saxton and
1267 Rawls (2006), as done in Stocker et al. (2020) and Bloomfield et al. (2022). A
1268 summary of these equations is included in the Supplemental Information.

1269 Daily soil moisture outputs from the SPLASH model for each site were
1270 used to calculate mean daily soil moisture for the prior 1, 2, 3, 4, 5, 6, 7, 8, 9,
1271 10, 15, 20, 25, 30, 60, and 90 days leading up to each site visit. Mean daily
1272 soil moisture values were then expressed as a fraction of water holding capacity
1273 to normalize across sites with different bucket depths, as done in Stocker et al.
1274 (2018).

1275 4.2.5 *Plant functional group assignments*

1276 Plant functional group was assigned to each species and used as the pri-
1277 mary descriptor of species identity. Specifically, we assigned plant functional
1278 groups based on photosynthetic pathway (C_3 , C_4) and ability to form associations
1279 with symbiotic nitrogen-fixing bacteria. The ability to form associations with
1280 symbiotic nitrogen-fixing bacteria was assigned based on whether species were in
1281 the *Fabaceae* family, and photosynthetic pathway of each species was determined
1282 from past literature and confirmed through leaf $\delta^{13}\text{C}$ values. We chose these plant
1283 functional groups based on *a priori* hypotheses regarding the functional role of
1284 nitrogen fixation and photosynthetic pathway on the sensitivity of plant nitrogen
1285 uptake and leaf nitrogen allocation to soil nutrient availability and aboveground
1286 growing conditions. These plant functional group classifications resulted in three
1287 distinct plant functional groups within our dataset: C_3 legumes ($n = 53$), C_3
1288 non-legumes ($n = 350$), and C_4 non-legumes ($n = 117$).

1289 4.2.6 *Data analysis*

1290 All analyses and plotting were conducted in R version 4.1.1 (R Core Team
1291 2021). We constructed a series of separate linear mixed-effects models to inves-
1292 tigate environmental drivers of β , χ , N_{area} , N_{mass} , and M_{area} , followed by a path
1293 analysis using a piecewise structural equation model to investigate direct and
1294 indirect effects of climate and soil resource availability on N_{area} .

1295 To explore environmental drivers of β , we built a linear mixed-effects model
1296 that included soil moisture, soil nitrogen availability, and plant functional group
1297 as fixed effect coefficients. Species were designated as a random intercept term.
1298 Interaction coefficients between all possible combinations of the three fixed effect
1299 coefficients were also included. β was natural log transformed to linearize data.
1300 We used an information-theoretic model selection approach to determine whether
1301 90-, 60-, 30-, 20-, 15-, 10-, 9-, 8-, 7-, 6-, 5-, 4-, 3-, 2-, or 1-day mean daily
1302 soil moisture conferred the best model fit for β . To do this, we constructed 16
1303 separate linear mixed-effects models where log-transformed β was included as the
1304 response variable and each soil moisture timestep was separately included as a
1305 single continuous fixed effect. Species were included as a random intercept term
1306 for all models. We used corrected Akaike Information Criterion (AICc) to select
1307 the soil moisture timescale that conferred the best model fit, indicated by the
1308 model with the lowest AICc score (Table S2; Fig. S2).

1309 To explore environmental drivers of χ , we constructed a second linear mixed
1310 effects model that included VPD, soil moisture, soil nitrogen availability, and plant
1311 functional group as fixed effect coefficients. Two-way interactions between plant
1312 functional group and VPD, soil nitrogen availability, or soil moisture were also

1313 included as fixed effect coefficients, in addition to a three-way interaction between
1314 soil moisture, soil nitrogen availability, and plant functional group. Species were
1315 included as a random intercept term. We used an information-theoretic model
1316 selection approach to determine whether 90-, 60-, 30-, 20-, 15-, 10-, 9-, 8-, 7-, 6-,
1317 5-, 4-, 3-, 2-, or 1-day mean daily VPD conferred the best model fit for χ using
1318 the same approach explained above for the soil moisture effect on β . The soil
1319 moisture timescale was set to the same timescale that conferred the best fit for β .

1320 To explore environmental drivers of N_{area} , N_{mass} , and M_{area} , we constructed
1321 three separate linear mixed effects model that each included χ , soil nitrogen avail-
1322 ability, soil moisture, and plant functional group as fixed effect coefficients. Two-
1323 way interactions between plant functional group and β , χ , soil nitrogen availability,
1324 or soil moisture were included as additional fixed effect coefficients, in addition to
1325 a three-way interaction between soil nitrogen availability, soil moisture, and plant
1326 functional group. Species were included as a random intercept term, with the soil
1327 moisture timescale set to the same timescale that conferred the best fit for β .

1328 In all linear mixed-effects models explained above, including those to select
1329 relevant timescales, we used the 'lmer' function in the 'lme4' R package (Bates
1330 et al. 2015) to fit each model and the 'Anova' function in the 'car' R package (Fox
1331 and Weisberg 2019) to calculate Type II Wald's χ^2 and determine the significance
1332 level ($\alpha = 0.05$) of each fixed effect coefficient. We also used the 'emmeans'
1333 R package (Lenth 2019) to conduct post-hoc comparisons using Tukey's tests,
1334 where degrees of freedom were approximated using the Kenward-Roger approach
1335 (Kenward and Roger 1997). Trendlines and error ribbons for all plots were drawn
1336 using a series of 'emmeans' outputs across the range in plotted x-axis values.

Finally, we conducted a path analysis using a piecewise structural equation model to examine direct and indirect pathways that determined variance in N_{area} . Seven separate linear mixed effects models were loaded into the piecewise structural equation model. Models were constructed per our *a priori* hypotheses following patterns expected from photosynthetic least-cost theory. The first model regressed N_{area} against χ , N_{mass} , and M_{area} . The second model regressed M_{area} against χ . The third model regressed N_{mass} against χ and M_{area} (Dong et al. 2017; Dong et al. 2020). The fourth model regressed χ against β and VPD. The fifth model regressed β against soil nitrogen availability, soil moisture, ability to associate with symbiotic nitrogen-fixing bacteria, and photosynthetic pathway. The sixth model regressed soil nitrogen availability against soil moisture, while the seventh model regressed VPD against soil moisture (Novick et al. 2016; Sulman et al. 2016). All models included the relevant timescale selected in the individual linear mixed effect models explained above (2-day soil moisture, 4-day vapor pressure deficit). Models also included species as a random intercept term, were built using the ‘lme’ function in the ‘nlme’ R package (Pinheiro and Bates 2022), and subsequently loaded into the piecewise structural equation model using the ‘psem’ function in the ‘piecewiseSEM’ R package (Lefcheck 2016).

1355 4.3 Results

1356 4.3.1 Cost to acquire nitrogen relative to water (β)

Model selection indicated that 2-day soil moisture was the timescale that conferred the best model fit for β ($AIC_c = 1227.83$; Table S2; Fig. S1). Increasing soil nitrogen availability generally decreased β ($p < 0.001$; Table 2), a

1360 pattern driven by a negative effect of increasing soil nitrogen availability on β in
1361 C₃ nonlegumes (Tukey: $p < 0.001$) and C₃ legumes (Tukey: $p = 0.004$; Fig. 2a).
1362 C₄ nonlegumes also demonstrated a negative trend in the effect of increasing soil
1363 nitrogen availability on β , but this pattern was not significantly different from
1364 zero (Tukey: $p = 0.307$; Fig. 2a). There was no apparent effect of soil moisture
1365 on β ($p = 0.264$; Table 1; Fig. 2b). A functional group effect ($p < 0.001$; Ta-
1366 ble 1) indicated that C₄ nonlegumes generally had lower β values than both C₃
1367 legumes and C₃ non-legumes when averaged across soil moisture and soil nitrogen
1368 availability values (Tukey: $p < 0.001$ in both cases), while average β values in C₃
1369 legumes did not differ from C₃ nonlegumes (Tukey: $p = 0.691$).

Table 4.2. Effects of soil moisture, soil nitrogen availability, and plant functional group on β

	df	Coefficient	χ^2	p
Intercept	-	3.20E+00	-	-
Soil moisture (SM_2)	1	2.19E-01	1.244	0.265
Soil N (N)	1	-1.70E-02	26.823	<0.001
PFT	2	-	199.617	<0.001
SM_2*N	1	1.77E-03	0.438	0.508
SM_2*PFT	2	-	2.038	0.361
$N*PFT$	2	-	7.668	0.022
$SM_2*N*PFT$	2	-	0.127	0.939

1370 *Significance determined using Type II Wald χ^2 tests ($\alpha = 0.05$). P-values < 0.05

1371 are in bold. Model coefficients are expressed on the natural-log scale and are only

1372 included for continuous fixed effects. Key: df=degrees of freedom, χ^2 =Wald Type

1373 II chi-square test statistic

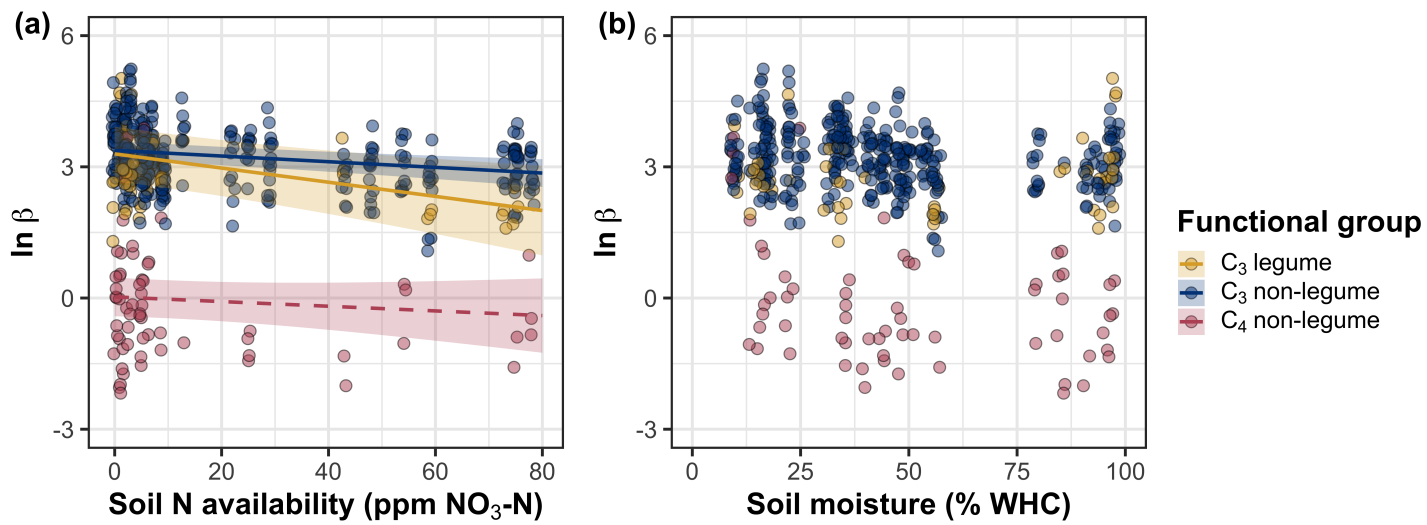


Figure 4.2. Effects of soil nitrogen availability (a) and soil moisture (b) on the unit cost ratio β . In (b), soil moisture is represented as a percent of site water holding capacity. Yellow shading and trendlines indicate C₃ legumes, blue shading and trendlines indicate C₃ non-legumes, and red shading and trendlines indicate C₄ non-legumes. Points are jittered for visibility. Variably colored trendlines are only included if there is an interaction between the x-axis and plant functional group, where solid trendlines indicate slopes that are different from zero ($p < 0.05$) and dashed trendlines indicate slopes that are not different from zero ($p > 0.05$). Error ribbons represent the upper and lower 95% confidence intervals of each fitted trendline.

1374 4.3.2 Leaf $C_i:C_a$ (χ)

1375 Model selection indicated that 4-day daily VPD was the timescale that
1376 conferred the best model fit for χ (AICc = -883.97; Table S1; Fig. S2).

1377 Variance in χ was driven by a series of two-way interactions between func-
1378 tional group and VPD ($p = 0.006$; Table 3), soil moisture ($p = 0.033$, Table 3),
1379 and soil nitrogen availability ($p = 0.022$; Table 3). The interaction between 4-day
1380 VPD and functional group revealed that the general negative effect of increasing
1381 VPD ($p < 0.001$; Table 3) was driven by a negative effect of increasing VPD
1382 on χ in C₃ nonlegumes (Tukey: $p < 0.001$) and marginal negative effect in C₃
1383 legumes (Tukey: $p = 0.074$) paired with a positive trending, but insignificant
1384 effect of increasing VPD in C₄ nonlegumes (Tukey: $p = 0.130$; Fig. 3a). The
1385 interaction between 2-day soil moisture and functional group indicated that the
1386 general negative effect of increasing soil moisture on χ was driven by a positive
1387 effect of increasing soil moisture on χ in C₄ nonlegumes (Tukey: $p = 0.009$) de-
1388 spite a positive trending but insignificant effect of increasing soil moisture on χ
1389 in C₃ legumes (Tukey: $p = 0.116$) and a null effect of soil moisture on χ in C₃
1390 nonlegumes (Tukey: $p = 0.693$; Fig. 3c). The interaction between soil nitrogen
1391 availability and plant functional group revealed a weak negative effect of increas-
1392 ing soil nitrogen availability on χ in C₃ legumes (Tukey: $p = 0.045$), with no
1393 apparent effect in C₃ nonlegumes (Tukey: $p = 0.706$) or C₄ nonlegumes (Tukey:
1394 $p = 0.757$). Finally, an individual effect of functional group ($p < 0.001$; Table 3)
1395 revealed that C₄ nonlegumes generally had lower χ than C₃ legumes and C₃ non-
1396 legumes (Tukey: $p < 0.001$ in both cases), with no apparent difference between
1397 C₃ legumes and C₃ nonlegumes (Tukey: $p = 0.831$).

Table 4.3. Effects of soil moisture, soil nitrogen availability, and plant functional group on χ^*

	df	Coefficient	χ^2	p
Intercept	-	9.33E-01	-	-
Vapor pressure deficit (VPD_4)	1	-1.78E-01	20.792	<0.001
Soil moisture (SM_2)	1	4.53E-02	1.972	0.160
Soil N (N)	1	-1.30E-03	0.168	0.682
PFT	2	-	172.624	<0.001
SM_2^*N	1	7.40E-04	0.849	0.357
VPD_4^*PFT	2	-	10.241	0.006
SM_2^*PFT	2	-	6.806	0.033
N^*PFT	2	-	7.602	0.022
$SM_2^*N^*PFT$	2	-	0.732	0.694

1398 *Significance determined using Type II Wald χ^2 tests ($\alpha = 0.05$). *P*-values less

1399 than 0.05 are in bold and *p*-values where $0.05 < p < 0.1$ are italicized. χ was

1400 not transformed prior to model fitting, so model coefficients are reported on the

1401 response scale. Model coefficients are only included for continuous fixed effects.

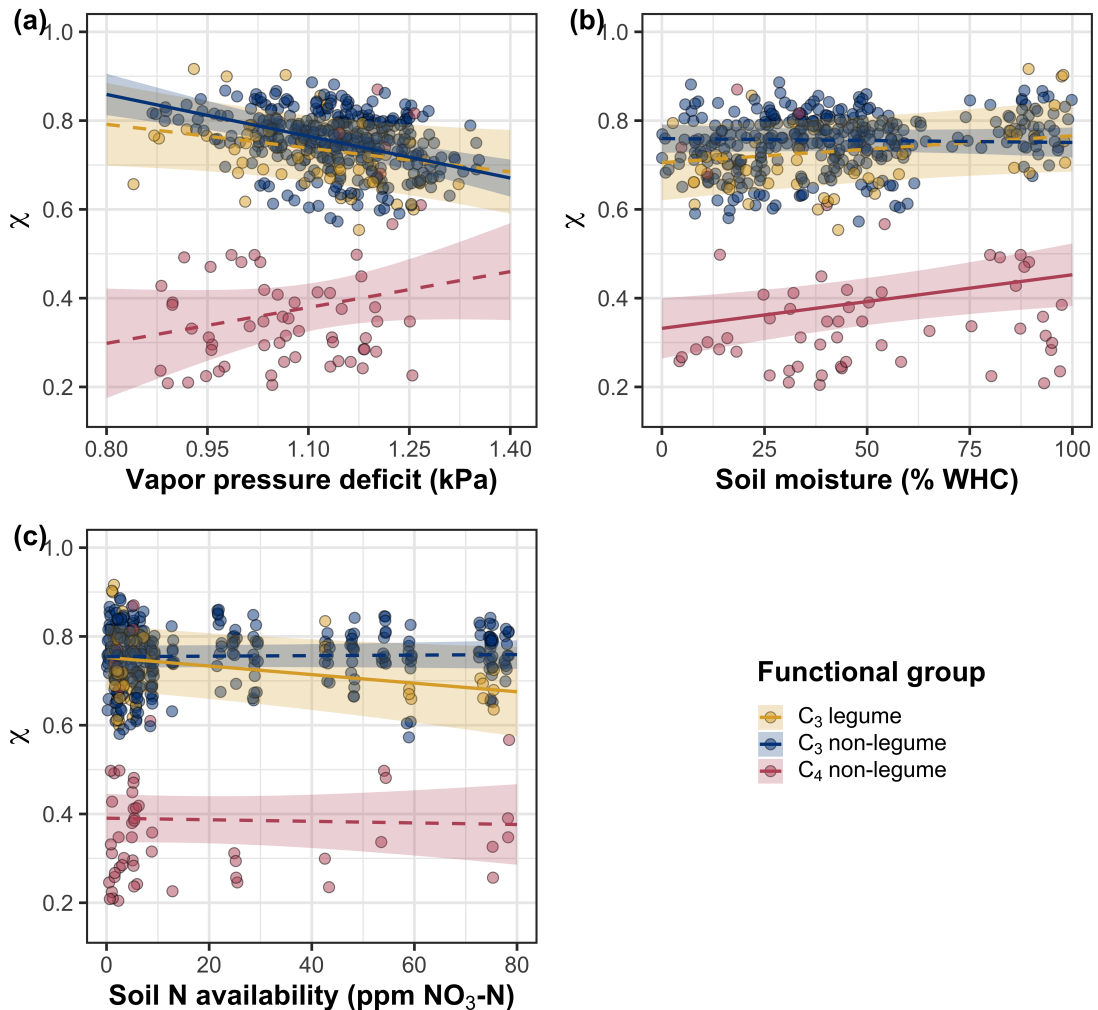


Figure 4.3. Effects of 4-day mean vapor pressure deficit (a), 2-day soil moisture (per water holding capacity; b), and soil nitrogen availability (c) on χ . Shading and trendlines are as explained in Figure 2. Points are jittered for visibility. Variably colored trendlines are only included if there is an interaction between the x-axis and plant functional group, where solid trendlines indicate slopes that are different from zero ($p < 0.05$) and dashed trendlines indicate slopes that are not different from zero ($p > 0.05$). Error ribbons represent the upper and lower 95% confidence intervals of each fitted trendline.

1402 4.3.3 *Leaf nitrogen content*

1403 An interaction between χ and plant functional group ($p < 0.001$; Table
1404 4) revealed that the general negative effect of increasing χ on N_{area} ($p < 0.001$;
1405 Table 4) was driven by a negative effect of increasing χ on N_{area} in C₃ nonlegumes
1406 (Tukey: $p < 0.001$) and C₃ legumes (Tukey: $p = 0.002$) despite a null effect of χ
1407 on N_{area} in C₄ nonlegumes (Tukey: $p = 0.795$; Fig. 4a). An interaction between
1408 soil nitrogen availability and soil moisture ($p = 0.028$; Table 4) indicated that the
1409 marginal positive effect of increasing soil nitrogen availability on N_{area} ($p = 0.091$;
1410 Table 4) decreased with increasing soil moisture, despite no apparent individual
1411 effect of soil moisture on N_{area} ($p = 0.692$; Table 4). Finally, a plant functional
1412 group effect ($p < 0.001$; Table 4) indicated that C₄ nonlegumes had lower N_{area}
1413 values on average compared to C₃ legumes (Tukey: $p < 0.001$) and C₃ nonlegumes
1414 (Tukey: $p = 0.001$), while C₃ legumes had lower average N_{area} values compared
1415 to C₃ nonlegumes (Tukey: $p = 0.012$).

1416 A marginal interaction between χ and plant functional group ($p = 0.088$;
1417 Table 4) revealed that, despite no apparent general effect of χ on N_{mass} ($p = 0.273$;
1418 Table 4), increasing χ decreased N_{mass} in C₃ nonlegumes (Tukey: $p = 0.021$), but
1419 this effect was not apparent in C₄ nonlegumes (Tukey: $p = 0.693$) or C₃ legumes
1420 (Tukey: $p = 0.477$). An interaction between soil nitrogen availability and soil
1421 moisture ($p < 0.001$; Table 4) indicated that the general positive effect of increas-
1422 ing soil nitrogen availability on N_{mass} ($p < 0.001$; Table 4) generally decreased
1423 with increasing soil moisture, despite an apparent general positive effect of in-
1424 creasing soil moisture on N_{mass} ($p < 0.001$; Table 4). This interaction indicated
1425 that the positive effect of increasing soil nitrogen availability on N_{mass} was only

1426 apparent when soil moisture was less than 70% the maximum water holding ca-
1427 pacity (Tukey: $p < 0.05$ in all cases) despite a positive effect of increasing soil
1428 moisture on N_{mass} ($p < 0.001$; Table 4). Finally, a plant functional group effect
1429 ($p < 0.001$; Table 4) indicated that C₄ nonlegumes had lower N_{mass} values on
1430 average compared to C₃ legumes (Tukey: $p = 0.002$) and C₃ nonlegumes (Tukey:
1431 $p = 0.019$), while N_{mass} did not differ between C₃ legumes and C₃ nonlegumes
1432 (Tukey: $p = 0.149$).

1433 An interaction between χ and functional group ($p = 0.005$; Table 4) indi-
1434 cated that the general negative effect of increasing χ on M_{area} ($p < 0.001$; Table
1435 4; Fig. 4c) was driven by a negative effect of increasing χ on M_{area} in C₃ legumes
1436 and C₃ nonlegumes (Tukey: $p < 0.001$ in both cases) despite a nonsignificant
1437 effect of increasing χ on M_{area} in C₄ nonlegumes (Tukey: $p = 0.724$). An in-
1438 teraction between soil nitrogen and soil moisture ($p < 0.001$; Table 4) indicated
1439 that the general negative effect of increasing soil nitrogen availability on M_{area} (p
1440 < 0.001 ; Table 4) decreased with increasing soil moisture, despite an apparent
1441 general negative effect of increasing soil moisture on M_{area} ($p = 0.002$; Table 4).
1442 Specifically, the negative effect of increasing soil nitrogen availability on M_{area} was
1443 only apparent when soil moisture was less than 65% the maximum water holding
1444 capacity (Tukey: $p < 0.05$ in all cases). An additional interaction between soil
1445 nitrogen availability and functional group ($p = 0.034$; Table 4) indicated that the
1446 general negative effect of increasing soil nitrogen availability on M_{area} was driven
1447 by decreases in C₃ nonlegumes (Tukey: $p < 0.001$) and C₄ nonlegumes (Tukey:
1448 $p = 0.003$), with no apparent effect of soil nitrogen availability on M_{area} in C₃
1449 legumes (Tukey: $p = 0.997$).

Table 4.4. Effects of soil nitrogen fertilization, inoculation, and CO₂ treatments on N_{area} , N_{mass} , M_{area} , and Chl_{area}

	N_{area}			N_{mass}			M_{area}			
	df	Coefficient	χ^2	p	Coefficient	χ^2	p	Coefficient	χ^2	p
(Intercept)	-	2.78E+00	-	-	4.42E-01	-	-	6.97E+00	-	-
χ	1	-2.53E+00	15.771	<0.001	4.56E-01	1.201	0.273	-3.10E+00	20.620	<0.001
Soil N (N)	1	1.08E-02	2.855	<i>0.091</i>	1.37E-02	54.531	<0.001	-2.87E-03	29.759	<0.001
Soil moisture (SM ₂)	1	3.61E-01	0.157	<i>0.692</i>	5.04E-01	16.255	<0.001	-1.26E-01	9.282	0.002
PFT	1	-	60.641	<0.001	-	21.539	<0.001	-	11.520	0.003
SM ₂ *N	1	-1.09E-02	4.779	0.029	-1.76E-02	41.784	<0.001	6.35E-03	14.111	<0.001
χ^*PFT	1	-	15.188	<0.001	-	4.864	<i>0.088</i>	-	17.032	0.025
N*PFT	1	-	2.289	<i>0.318</i>	-	0.914	<i>0.633</i>	-	6.760	0.034
SM ₂ *PFT	1	-	0.978	<i>0.613</i>	-	0.128	<i>0.938</i>	-	2.121	0.346
SM ₂ *N*PFT	1	-	1.289	<i>0.525</i>	-	2.180	<i>0.336</i>	-	0.629	0.730

950 *Significance determined using Type II Wald χ^2 tests ($\alpha = 0.05$). P -values less than 0.05 are in bold and p -values
 1451 where $0.05 < p < 0.1$ are italicized. Coefficients are reported on the natural-log scale and are only included for
 1452 continuous fixed effects.

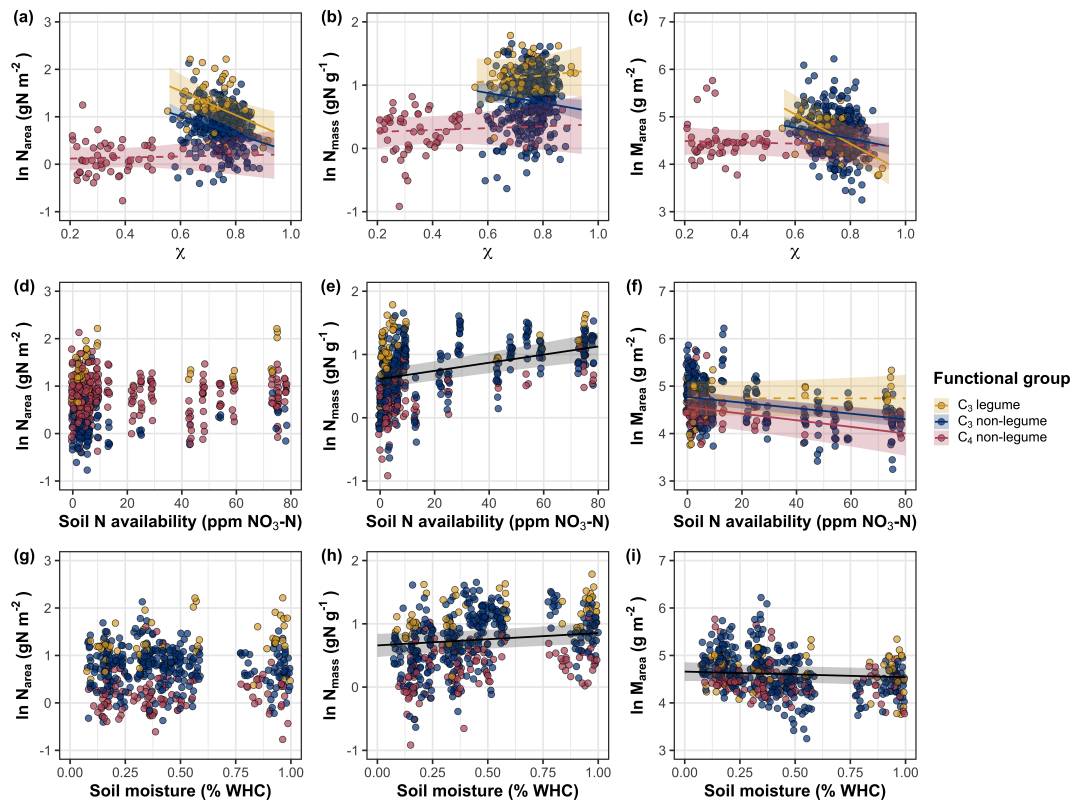


Figure 4.4. Effects of χ (a-c), soil nitrogen availability (d-f), and soil moisture (g-i) on leaf nitrogen content per unit leaf area (a, d, g), leaf nitrogen content per unit leaf biomass (b, e, h), and leaf mass per area (c, f, i). A solid black trendline indicates the bivariate relationship between the fixed effect the x-axis and response variable on the y-axis and is only included when there is no interaction between the x-axis and plant functional group.

1453 4.3.4 *Structural equation model*

1454 The piecewise structural equation model explained 90%, 54%, 80%, 92%,
1455 and 41% of variance in N_{area} , N_{mass} , M_{area} , χ , and β , respectively (Table 5; Fig.
1456 5). Variance in N_{area} was driven by a negative effect of increasing χ ($p < 0.001$;
1457 Table 5) paired with positive effects of increasing N_{mass} and M_{area} ($p < 0.001$ in
1458 both cases; Table 5; Fig. 5). Model results indicated that the negative effect
1459 of χ on N_{area} was driven by a strong reduction in M_{area} with increasing χ ($p <$
1460 0.001; Table 5) paired with no change in χ due to Nmass ($p = 0.150$; Table 5).
1461 However, there was a strong negative effect of increasing M_{area} on N_{mass} ($p <$
1462 0.001; Table 5; Fig. 5). χ generally increased with increasing β ($p < 0.001$; Table
1463 5) and decreased with increasing VPD ($p < 0.001$; Table 5; Fig. 5). Variance in β
1464 was driven by a negative effect of increasing soil nitrogen availability ($p < 0.001$;
1465 Table 5) and was generally higher in C₃ species ($p < 0.001$; Table 5; Fig. 5).
1466 However, β did not change with soil moisture ($p = 0.332$; Table 5) or with ability
1467 to acquire nitrogen via symbiotic nitrogen fixation ($p = 0.546$; Table 5). Finally,
1468 soil nitrogen availability was positively associated with increasing soil moisture (p
1469 < 0.001; Table 5; Fig. 5), while VPD was negatively associated with increasing
1470 soil moisture ($p < 0.001$; Table 5; Fig. 5).

Table 4.5. Structural equation model results investigating direct effects of climatic and soil resource availability on N_{area} , N_{mass} , M_{area} , χ , and β

Predictor	Coefficient	<i>p</i>
$N_{\text{area}} (R^2_c) = 0.90$		
χ	-0.140	<0.001
M_{area}	0.807	<0.001
N_{mass}	0.795	<0.001
$N_{\text{mass}} (R^2_c) = 0.54$		
χ	0.097	<0.001
$M_{\text{area}} (R^2_c) = 0.80$		
χ	-0.372	0.150
M_{area}	-0.303	<0.001
$\chi (R^2_c) = 0.92$		
β	0.261	<0.001
VPD_4	-0.122	<0.001
$\beta (R^2_c) = 0.41$		
Soil N	-0.201	<0.001
SM_2	-0.048	0.332
Photo. pathway	0.490	<0.001
N-fixing ability	-0.053	0.546
Soil N (R^2_c) = 0.39		
SM_2	0.410	<0.001

1471 *Reported coefficients are standardized across the entire structural equation model.

1472 *P*-values less than 0.05 are noted in bold. Positive coefficients for photosyn-

1473 thetic pathway indicate generally larger values in C₃ species, while positive co-

1474 efficients for N-fixing ability indicate generally larger values in N-fixing species.

1475 Key: N_{area} =leaf nitrogen content per unit leaf area, M_{area} =leaf mass per unit leaf

1476 dry biomass, N_{mass} =leaf nitrogen content per unit leaf dry biomass, β =cost of

1477 acquiring nitrogen relative to water, χ =isotope-derived estimate of the leaf Ci:Ca

1478 ratio, VPD_4 = 4-day mean vapor pressure deficit, SM_2 =2-day mean soil moisture,

1479 R^2_c = conditional R² value

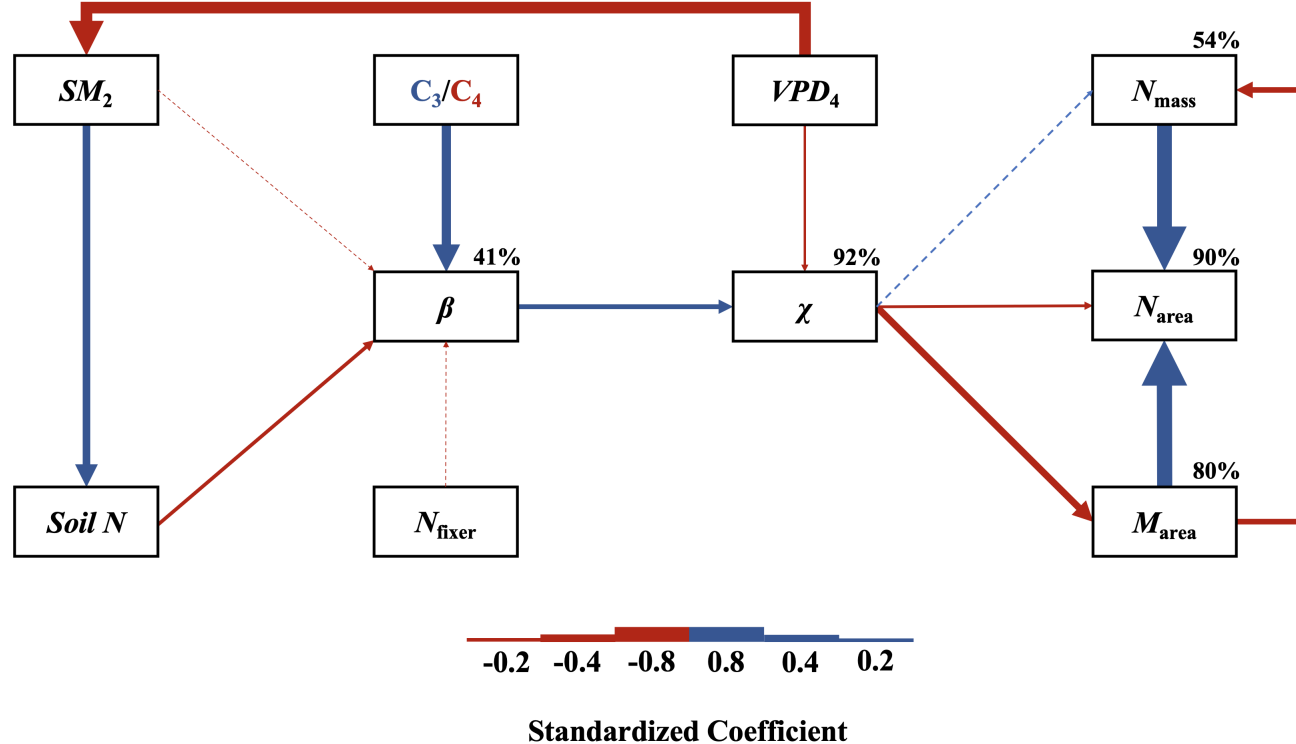


Figure 4.5. Structural equation model results exploring direct and indirect drivers of N_{area} . Boxes indicate measured edaphic factors, climatic factors, and leaf traits. Percentages above boxes indicate conditional R^2 values of each respective leaf trait. Solid arrows indicate bivariate relationships where $p < 0.05$, while dashed arrows indicate bivariate relationships where $p > 0.05$. Positive model coefficients are indicated through blue arrows, while negative model coefficients are indicated through red arrows. Arrow thickness scales with the standardized model coefficient of each bivariate relationship. A positive coefficient for photosynthetic pathway indicates generally larger values in C_3 species, while a positive coefficient for N_{fixer} indicates generally larger values in N-fixing species. Standardized model coefficients and associated p -values are reported in Table 5.

1480 4.4 Discussion

1481

Chapter 5

1482
1483

Optimal resource investment to photosynthetic capacity maximizes nutrient allocation to whole plant growth under elevated CO₂

1484 5.1 Introduction

1485 Terrestrial ecosystems are regulated by complex carbon and nitrogen cy-
1486 cles. As a result, terrestrial biosphere models, which are beginning to include
1487 coupled carbon and nitrogen cycles (Shi et al. 2016; Davies-Barnard et al. 2020;
1488 Braghieri et al. 2022), must accurately represent these cycles under different
1489 environmental scenarios to reliably simulate carbon and nitrogen atmosphere-
1490 biosphere fluxes (Hungate et al. 2003; Prentice et al. 2015). While the inclusion
1491 of coupled carbon and nitrogen cycles tends to reduce model uncertainty (Arora
1492 et al. 2020), large uncertainty in role of soil nitrogen availability and nitrogen ac-
1493 quisition strategy on leaf and whole plant acclimation responses to CO₂ remains
1494 (Smith and Dukes 2013; Terrer et al. 2018; Smith and Keenan 2020). This source
1495 of uncertainty likely contributes to the widespread divergence in future carbon
1496 and nitrogen flux simulations across terrestrial biosphere models (Friedlingstein
1497 et al. 2014; Zaehle et al. 2014; Meyerholt et al. 2020).

1498 Plants grown under elevated CO₂ generally have less leaf nitrogen content
1499 than those grown under ambient CO₂, a response that often corresponds with
1500 reductions in photosynthetic capacity and stomatal conductance at the leaf-level
1501 and biomass stimulation over time at the whole plant level (Curtis 1996; Drake
1502 et al. 1997; Ainsworth et al. 2002; Makino 2003; Morgan et al. 2004; Ainsworth
1503 and Long 2005; Ainsworth and Rogers 2007; Smith and Dukes 2013; Poorter et al.
1504 2022). As net primary productivity is generally limited by nitrogen availability

1505 (Vitousek and Howarth 1991; LeBauer and Treseder 2008; Fay et al. 2015), and
1506 soil nitrogen availability is often positively correlated with leaf nitrogen content
1507 and photosynthetic capacity (Field and Mooney 1986; Evans and Seemann 1989;
1508 Evans 1989; Walker et al. 2014; Firn et al. 2019; Liang et al. 2020), some
1509 have hypothesized that leaf and whole plant acclimation responses to CO₂ are
1510 constrained by soil nitrogen availability. The progressive nitrogen limitation hy-
1511 pothesis predicts that elevated CO₂ will increase plant nitrogen demand, which
1512 will increase plant nitrogen uptake and progressively deplete soil nitrogen if soil
1513 nitrogen supply does not exceed plant nitrogen demand (Luo et al. 2004). The
1514 hypothesis predicts that this response should result in strong acute stimulations in
1515 whole plant growth and primary productivity that diminish over time as nitrogen
1516 becomes more limiting. Assuming a positive relationship between soil nitrogen
1517 availability, leaf nitrogen content, and photosynthetic capacity, this hypothesis
1518 also implies that progressive reductions in soil nitrogen availability should be the
1519 mechanism that drives the downregulation in leaf nitrogen content and photosyn-
1520 thetic capacity under elevated CO₂. This hypothesis has received some support
1521 from free air CO₂ enrichment experiments (Reich et al. 2006; Norby et al. 2010),
1522 although is not consistently observed across experiments (Finzi et al. 2006; Moore
1523 et al. 2006; Liang et al. 2016).

1524 While possible that progressive nitrogen limitation may determine leaf and
1525 whole plant acclimation responses to CO₂, growing evidence indicates that leaf ni-
1526 trogen and photosynthetic capacity are more strongly determined through above-
1527 ground growing conditions than by soil resource availability (Dong et al. 2017;
1528 Dong et al. 2020; Dong et al. 2022; Smith et al. 2019; Smith and Keenan 2020;

1529 Paillassa et al. 2020; Peng et al. 2021; Querejeta et al. 2022; Westerband et al.
1530 2023), and satellite-derived chlorophyll fluorescence data indicate that increasing
1531 atmospheric CO₂ may decrease leaf and canopy demand for nitrogen (Dong et al.
1532 2022). Together, results from these studies suggest that the downregulation in
1533 leaf nitrogen content and photosynthetic capacity due to increasing CO₂ may not
1534 be as tightly linked to progressive nitrogen limitation as previously hypothesized.

1535 A unification of optimal coordination and photosynthetic least-cost the-
1536 ories predicts that leaves acclimate to elevated CO₂ by downregulating nitrogen
1537 allocation to Ribulose-1,5-bisphosphate (RuBP) carboxylase/oxygenase (Rubisco)
1538 to optimize resource use efficiencies at the leaf level, which allows for greater re-
1539 source allocation to whole plant growth (Drake et al. 1997; Wright et al. 2003;
1540 Prentice et al. 2014; Smith et al. 2019). The theory predicts that the downregu-
1541 lation in nitrogen allocation to Rubisco results in a stronger downregulation in the
1542 maximum rate of Rubisco carboxylation (V_{cmax}) than the maximum rate of RuBP
1543 regeneration (J_{max}), which maximizes photosynthetic efficiency by allowing net
1544 photosynthesis rates to be equally co-limited by Rubisco carboxylation and RuBP
1545 regeneration (Chen et al. 1993; Maire et al. 2012). This acclimation response
1546 allows plants to make more efficient use of available light while avoiding overin-
1547 vestment in Rubisco, which has high nitrogen and energetic costs of building and
1548 maintaining (Evans 1989; Evans and Clarke 2019). Instead, additional acquired
1549 resources not needed to optimize leaf photosynthesis are allocated to the mainte-
1550 nance of structures that support whole plant growth (e.g., total leaf area, whole
1551 plant biomass, etc.) or to allocation processes not related to leaf photosynthesis
1552 or growth, such as plant defense mechanisms or leaf structural tissue. Regardless,

1553 optimized resource allocation at the leaf level should allow for greater resource
1554 allocation to whole plant growth. The theory indicates that leaf acclimation re-
1555 sponses to CO₂ should be independent of changes in soil nitrogen availability.
1556 While this leaf acclimation response maximizes nitrogen allocation to structures
1557 that support whole plant growth, the theory suggests that the positive effect of
1558 elevated CO₂ on whole plant growth may be further stimulated by soil nitrogen
1559 availability through a reduction in the cost of acquiring nitrogen (Bae et al. 2015;
1560 Perkowski et al. 2021; Lu et al. 2022).

1561 Plants acquire nitrogen by allocating photosynthetically derived carbon be-
1562 lowground in exchange for nitrogen through different nitrogen acquisition strate-
1563 gies. These nitrogen acquisition strategies can include direct uptake pathways
1564 such as mass flow or diffusion (Barber 1962), symbioses with mycorrhizal fungi or
1565 symbiotic nitrogen-fixing bacteria (Vance and Heichel 1991; Marschner and Dell
1566 1994; Smith and Read 2008; Udvardi and Poole 2013), or through the release
1567 of root exudates that prime free-living soil microbial communities (Phillips et al.
1568 2011; Wen et al. 2022). Plants cannot acquire nitrogen without first allocating
1569 carbon belowground, which implies an inherent carbon cost to the plant for acquir-
1570 ing nitrogen regardless of nitrogen acquisition strategy. Carbon costs to acquire
1571 nitrogen often vary in species with different nitrogen acquisition strategies and
1572 are dependent on external environmental factors such as atmospheric CO₂, light
1573 availability, and soil nitrogen availability (Brzostek et al. 2014; Terrer et al. 2016;
1574 Terrer et al. 2018; Allen et al. 2020; Perkowski et al. 2021; Lu et al. 2022), which
1575 suggests that acquisition strategy may be an important factor in determining ef-
1576 fects of soil nitrogen availability on leaf and whole plant acclimation responses to

1577 elevated CO₂.

1578 A recent meta-analysis using data across 20 grassland and forest CO₂ en-
1579 richment experiments suggested that species which acquire nitrogen from sym-
1580 biotic nitrogen-fixing bacteria had reduced costs of nitrogen acquisition under
1581 elevated CO₂ (Terrer et al. 2018). Findings from this meta-analysis indicated
1582 that reductions in costs of nitrogen acquisition in species that form associations
1583 with symbiotic nitrogen-fixing bacteria under elevated CO₂ may drive stronger
1584 stimulations in whole plant growth and downregulations in V_{cmax} than species that
1585 associate with arbuscular mycorrhizal fungi (Smith and Keenan 2020), which gen-
1586 erally have higher costs of nitrogen acquisition under elevated CO₂ (Terrer et al.
1587 2018). However, plant investments in symbiotic nitrogen fixation generally de-
1588 cline with increasing nitrogen availability (Dovrat et al. 2018; Perkowski et al.
1589 2021), a response that has been previously inferred to be the result of a shift in
1590 the dominant mode of nitrogen acquisition to direct uptake pathways as costs of
1591 direct uptake decrease with increasing soil nitrogen availability (Rastetter et al.
1592 2001; Perkowski et al. 2021). Thus, effects of symbiotic nitrogen fixation on plant
1593 acclimation responses to CO₂ should decline with increasing soil nitrogen avail-
1594 ability, although manipulative experiments that directly test these patterns are
1595 rare.

1596 Here, we conducted a 7-week growth chamber experiment using *Glycine*
1597 *max* L. (Merr.) to examine the effects of soil nitrogen fertilization and inocula-
1598 tion with symbiotic nitrogen-fixing bacteria on leaf and whole plant acclimation
1599 responses to elevated CO₂. Following patterns expected from theory, we hypoth-
1600 esized that individual leaves should acclimate to elevated CO₂ by more strongly

1601 downregulating V_{cmax} relative to J_{max} , allowing leaf photosynthesis to approach
1602 optimal coordination. We expected this response to correspond with a stronger
1603 downregulation in leaf nitrogen content than V_{cmax} and J_{max} , which would in-
1604 crease the fraction of leaf nitrogen content allocated to photosynthesis and photo-
1605 synthetic nitrogen use efficiency. At the whole-plant level, we hypothesized that
1606 plants would acclimate to elevated CO₂ by stimulating whole plant growth and
1607 productivity, a response that would be driven by a strong positive response of
1608 total leaf area and aboveground biomass to elevated CO₂. We predicted that
1609 leaf acclimation responses to elevated CO₂ would be independent of soil nitro-
1610 gen fertilization and inoculation with symbiotic nitrogen-fixing bacteria; however,
1611 we expected that increasing soil nitrogen fertilization would increase the posi-
1612 tive effect of elevated CO₂ on measures of whole plant growth due to a stronger
1613 reduction in the cost of acquiring nitrogen under elevated CO₂ with increasing
1614 fertilization. We also expected stronger stimulations in whole plant growth due
1615 to inoculation, but that this effect would only be apparent under low fertilization
1616 due to a reduction in root nodulation with increasing fertilization.

1617 5.2 Methods

1618 5.2.1 *Seed treatments and experimental design*

1619 *Glycine max* L. (Merr) seeds were planted in 144 6-liter surface sterilized
1620 pots (NS-600, Nursery Supplies, Orange, CA, USA) containing a steam-sterilized
1621 70:30 v:v mix of Sphagnum peat moss (Premier Horticulture, Quakertown, PA,
1622 USA) to sand (Pavestone, subsidiary of Quikrete Companies, Atlanta, GA, USA).
1623 Before planting, all *G. max* seeds were surface sterilized in 2% sodium hypochlorite

1624 for 3 minutes, followed by three separate 3-minute washes with ultrapure water
1625 (MilliQ 7000; MilliporeSigma, Burlington, MA USA). A subset of surface steril-
1626 ized seeds were inoculated with *Bradyrhizobium japonicum* (Verdesian N-Dure™
1627 Soybean, Cary, NC, USA) in a slurry following manufacturer recommendations
1628 (3.12 g inoculant and 241 g deionized water per 1 kg seed).

1629 Seventy-two pots were randomly planted with surface-sterilized seeds inoc-
1630 ulated with *B. japonicum*, while the remaining 72 pots were planted with surface-
1631 sterilized uninoculated seeds. Thirty-six pots within each inoculation treatment
1632 were randomly placed in one of two atmospheric CO₂ treatments (ambient and
1633 1000 μmol mol⁻¹ CO₂). Pots within each unique inoculation-by-CO₂ treatment
1634 combination randomly received one of nine soil nitrogen fertilization treatments
1635 equivalent to 0, 35, 70, 105, 140, 210, 280, 350, or 630 ppm N. Nitrogen fertil-
1636 ization treatments were created using a modified Hoagland solution (Hoagland
1637 and Arnon 1950) designed to keep concentrations of other macronutrients and
1638 micronutrients equivalent across treatments (Table S1). Pots received the same
1639 fertilization treatment throughout the entire duration experiment, which were ap-
1640 plied twice per week in 150 mL doses as topical agents to the soil surface through-
1641 out the duration of the experiment. This experimental design yielded a fully
1642 factorial experiment with four replicates per unique fertilization-by-inoculation-
1643 by-CO₂ combination.

1644 5.2.2 *Growth chamber conditions*

1645 Upon experiment initiation, pots were randomly placed in one of six Per-
1646 cival LED-41L2 growth chambers (Percival Scientific Inc., Perry, IA, USA) over

1647 two experimental iterations due to chamber space limitation. two iterations were
1648 conducted such that one iteration included all elevated CO₂ pots and the second
1649 iteration included all ambient CO₂ pots. Average (\pm SD) CO₂ concentrations
1650 across chambers throughout the experiment were $439 \pm 5 \mu\text{mol mol}^{-1}$ for the
1651 ambient CO₂ treatment and $989 \pm 4 \mu\text{mol mol}^{-1}$ for the elevated CO₂ treatment.

1652 Daytime growing conditions were simulated using a 16-hour photoperiod,
1653 with incoming light radiation set to chamber maximum (mean \pm SD: 1240 ± 32
1654 $\mu\text{mol m}^{-2} \text{s}^{-1}$ across chambers), air temperature set to 25°C, and relative humid-
1655 ity set to 50%. The remaining 8 hours simulated nighttime growing conditions,
1656 with incoming light radiation set to $0 \mu\text{mol m}^{-2} \text{s}^{-1}$, chamber temperature set
1657 to 17°C, and relative humidity set to 50%. Transitions between daytime and
1658 nighttime growing conditions were simulated by ramping incoming light radiation
1659 in 45-minute increments and temperature in 90-minute increments over a 3-hour
1660 period (Table S2).

1661 Including the two, 3-hour ramping periods, pots grew under average (\pm
1662 SD) daytime light intensity of $1049 \pm 27 \mu\text{mol m}^{-2} \text{s}^{-1}$. In the elevated CO₂
1663 iteration, pots grew under $24.0 \pm 0.2^\circ\text{C}$ during the day, $16.4 \pm 0.8^\circ\text{C}$ during the
1664 night, and $51.6 \pm 0.4\%$ relative humidity. In the ambient CO₂ iteration, pots grew
1665 under $23.9 \pm 0.2^\circ\text{C}$ during the day, $16.0 \pm 1.4^\circ\text{C}$ during the night, and $50.3 \pm 0.2\%$
1666 relative humidity. We accounted for climatic differences across the six chambers
1667 by shuffling the same group of pots daily throughout the growth chambers. This
1668 process was done by iteratively moving the group of pots on the top rack of a
1669 chamber to the bottom rack of the same chamber, while simultaneously moving
1670 the group of pots on the bottom rack of a chamber to the top rack of the adjacent

1671 chamber. We moved pots within and across chambers every day throughout the
1672 course of each experiment iteration.

1673 5.2.3 *Leaf gas exchange measurements*

1674 Gas exchange measurements were collected for all individuals on the sev-
1675 enth week of development. All gas exchange measurements were collected on
1676 the center leaf of the most recent fully expanded trifoliate leaf set. Specifi-
1677 cally, we measured net photosynthesis (A_{net} ; $\mu\text{mol m}^{-2} \text{s}^{-1}$), stomatal conduc-
1678 tance (g_{sw} ; $\text{mol m}^{-2} \text{s}^{-1}$), and intercellular CO_2 (C_i ; $\mu\text{mol mol}^{-1}$) concentrations
1679 across a range of atmospheric CO_2 concentrations (i.e., an A_{net}/C_i curve) using the
1680 Dynamic Assimilation Technique™. The Dynamic Assimilation Technique™ has
1681 been shown to correspond well with traditional steady-state CO_2 response curves
1682 in *G. max* (Saathoff and Welles 2021). A_{net}/C_i curves were generated along a
1683 reference CO_2 ramp down from $420 \mu\text{mol mol}^{-1} \text{CO}_2$ to $20 \mu\text{mol mol}^{-1} \text{CO}_2$, fol-
1684 lowed by a ramp up from $420 \mu\text{mol mol}^{-1} \text{CO}_2$ to $1620 \mu\text{mol mol}^{-1} \text{CO}_2$ after
1685 a 90-second wait period at $420 \mu\text{mol mol}^{-1} \text{CO}_2$. The ramp rate for each curve
1686 was set to $200 \mu\text{mol mol}^{-1} \text{min}^{-1}$, logging every five seconds, which generated 96
1687 data points per response curve. All A_{net}/C_i curves were generated after A_{net} and
1688 g_{sw} stabilized in a LI-6800 cuvette set to a 500 mol s^{-1} , 10,000 rpm mixing fan
1689 speed, 1.5 kPa vapor pressure deficit, 25°C leaf temperature, $2000 \mu\text{mol m}^{-2} \text{s}^{-1}$
1690 incoming light radiation, and initial reference CO_2 set to $420 \mu\text{mol mol}^{-1}$.

1691 With the same focal leaf used to generate A_{net}/C_i curves, we measured
1692 dark respiration (R_{d25} ; $\mu\text{mol m}^{-2} \text{s}^{-1}$) following at least a 30-minute period of
1693 darkness. Measurements were collected on a 5-second log interval for 60 seconds

1694 after stabilizing in a LI-6800 cuvette set to a 500 mol s^{-1} , 10,000 rpm mixing fan
1695 speed, 1.5 kPa vapor pressure deficit, 25°C leaf temperature, and $420 \mu\text{mol mol}^{-1}$
1696 reference CO_2 concentration (for both CO_2 concentrations), with incoming light
1697 radiation set to $0 \mu\text{mol m}^{-2} \text{s}^{-1}$. A single dark respiration value was determined
1698 for each focal leaf by calculating the mean dark respiration value (i.e. the absolute
1699 value of A_{net} during the logging period) across the logging interval.

1700 5.2.4 *Leaf trait measurements*

1701 The focal leaf used to generate A_{net}/C_i curves and dark respiration was
1702 harvested immediately following gas exchange measurements. Images of each focal
1703 leaf were curated using a flat-bed scanner to determine wet leaf area using the
1704 'LeafArea' R package (Katabuchi 2015), which automates leaf area calculations
1705 using ImageJ software (Schneider et al. 2012). Each leaf was dried at 65°C for
1706 at least 48 hours, and subsequently weighed and ground until homogenized. Leaf
1707 mass per area (M_{area} ; g m^{-2}) was calculated as the ratio of dry leaf biomass
1708 to fresh leaf area. Using subsamples of ground and homogenized leaf tissue, we
1709 measured leaf nitrogen content (N_{mass} ; gN g^{-1}) through elemental combustion
1710 analysis (Costech-4010, Costech, Inc., Valencia, CA, USA). Leaf nitrogen content
1711 per unit leaf area (N_{area} ; gN m^{-2}) was calculated by multiplying N_{mass} and M_{area} .

1712 We extracted chlorophyll content from a second leaf in the same trifoliolate
1713 leaf set as the focal leaf used to generate A_{net}/C_i curves. Prior to chlorophyll
1714 extraction, we used a cork borer to punch between 3 and 5 0.6 cm^2 disks from
1715 the leaf. Separate images of each punched leaf and set of leaf disks were curated
1716 using a flat-bed scanner to determine wet leaf area, again quantified using the

1717 'LeafArea' R package (Katabuchi 2015). The punched leaf was dried and weighed
1718 after at least 65°C in the drying oven to determine Marea of the chlorophyll leaf.

1719 Leaf disks were shuttled into a test tube containing 10mL dimethyl sul-
1720 foxide, vortexed, and incubated at 65degreeC for 120 minutes (Barnes et al.
1721 1992). Incubated test tubes were vortexed again before loaded in 150 μ L trip-
1722 licate aliquots to a 96-well plate. Dimethyl sulfoxide was also loaded in a 150
1723 μ L triplicate aliquot as a blank. Absorbance measurements at 649.1 nm ($A_{649.1}$)
1724 and 665.1 nm ($A_{665.1}$) were read in each well using a plate reader (Biotek Synergy
1725 H1; Biotek Instruments, Winooski, VT USA) (Wellburn 1994), with triplicates
1726 subsequently averaged and corrected by the mean of the blank absorbance value.
1727 Blank-corrected absorbance values were used to estimate Chl_a (μ g mL $^{-1}$) and
1728 Chl_b (μ g mL $^{-1}$) following equations from Wellburn (1994):

$$Chl_a = 12.47A_{665.1} - 3.62A_{649.1} \quad (5.1)$$

1729 and

$$Chl_b = 25.06A_{665.1} - 6.50A_{649.1} \quad (5.2)$$

1730 Chl_a and Chl_b were converted to mmol mL $^{-1}$ using the molar mass of chlorophyll a
1731 (893.51 g mol $^{-1}$) and the molar mass of chlorophyll b (907.47 g mol $^{-1}$), then added
1732 together to calculate total chlorophyll content in the dimethyl sulfoxide extractant
1733 (mmol mL $^{-1}$). Total chlorophyll content was multiplied by the volume of the
1734 dimethyl sulfoxide extractant (10 mL) and converted to area-based chlorophyll
1735 content by dividing by the total area of the leaf disks (Chl_{area} ; mmol m $^{-2}$). Mass-
1736 based chlorophyll content (Chl_{mass} ; mmol g $^{-1}$) was calculated by dividing Chl_{area}

1737 by the leaf mass per area of the punched leaf.

1738 5.2.5 *A/C_i curve fitting and parameter estimation*

1739 We fit A_{net}/C_i curves of each individual using the ‘fitaci’ function in the
1740 ‘plantecophys’ R package (Duursma 2015). This function estimates the maximum
1741 rate of Rubisco carboxylation V_{cmax} ; $\mu\text{mol m}^{-2} \text{s}^{-1}$) and maximum rate of electron
1742 transport for RuBP regeneration (J_{max} ; $\mu\text{mol m}^{-2} \text{s}^{-1}$) based on the Farquhar bio-
1743 chemical model of C₃ photosynthesis (Farquhar et al. 1980). Triose phosphate
1744 utilization (TPU) limitation was included in all curve fits, and all curve fits in-
1745 cluded measured dark respiration values. As A_{net}/C_i curves were generated using
1746 a common leaf temperature, curves were fit using Michaelis-Menton coefficients
1747 for Rubisco affinity to CO₂ (K_c ; $\mu\text{mol mol}^{-1}$) and O₂ (K_o ; $\mu\text{mol mol}^{-1}$), and the
1748 CO₂ compensation point (Γ^* ; $\mu\text{mol mol}^{-1}$) reported in Bernacchi et al. (2001).
1749 Specifically, K_c was set to 404.9 $\mu\text{mol mol}^{-1}$, K_o was set to 278.4 $\mu\text{mol mol}^{-1}$, and
1750 Γ^* was set to 42.75 $\mu\text{mol mol}^{-1}$. The use of a common leaf temperature across
1751 curves and dark respiration measurements also eliminated the need to manually
1752 standardize rate estimates. For clarity, we reference V_{cmax} , J_{max} , and
1753 R_d estimates throughout the rest of the paper as $V_{\text{cmax}25}$, $J_{\text{max}25}$, and R_{d25} .

1754 5.2.6 Stomatal limitation

1755 We quantified the extent by which stomatal conductance limited photo-
1756 synthesis (l; unitless) following equations originally described in Farquhar and
1757 Sharkey (1982). Stomatal limitation was calculated as:

$$l = 1 - \frac{A_{net}}{A_{mod}} \quad (5.3)$$

1758 where A_{mod} represents the photosynthetic rate where $C_i = C_a$. A_{mod} was calcu-

1759 lated as:

$$A_{mod} = V_{cmax25} - \frac{420 - \Gamma^*}{420 + K_m} - R_{d25} \quad (5.4)$$

1760 K_m is the Michaelis-Menten coefficient for Rubisco-limited photosynthesis, calcu-

1761 lated as:

$$K_m = K_c \cdot \left(1 + \frac{O_i}{K_o}\right) \quad (5.5)$$

1762 where O_i refers to leaf intercellular O_2 concentrations, set to $210 \mu\text{mol mol}^{-1}$.

1763 5.2.7 *Proportion of leaf nitrogen allocated to photosynthesis and structure*

1764 We used equations from Niinemets and Tenhunen (1997) to estimate the

1765 proportion of leaf N content allocated to Rubisco bioenergetics, and light harvest-

1766 ing proteins. The proportion of leaf N allocated to Rubisco (ρ_{rub} ; gN gN^{-1}) was

1767 calculated as a function of V_{cmax25} and N_{area} :

$$\rho_{rubisco} = \frac{V_{cmax25} N_r}{V_{cr} N_{area}} \quad (5.6)$$

1768 where N_r is the amount of nitrogen in Rubisco, set to $0.16 \text{ gN (gN in Rubisco)}^{-1}$

1769 and V_{cr} is the maximum rate of RuBP carboxylation per unit Rubisco protein,

1770 set to $20.5 \mu\text{mol CO}_2 (\text{g Rubisco})^{-1}$. The proportion of leaf nitrogen allocated to

1771 bioenergetics (ρ_{bioe} ; gN gN^{-1}) was similarly calculated as a function of J_{max25} and

1772 N_{area} :

$$\rho_{\text{bioe}} = \frac{J_{\text{max}25} N_b}{J_{\text{mc}} N_{\text{area}}} \quad (5.7)$$

1773 where N_b is the amount of nitrogen in cytochrome f, set to 0.12407 gN (μmol

1774 cytochrome f) $^{-1}$ assuming a constant 1: 1: 1.2 cytochrome f: ferredoxin NADP

1775 reductase: coupling factor molar ratio (Evans and Seemann 1989; Niinemets and

1776 Tenhunen 1997), and J_{mc} is the capacity of electron transport per cytochrome f,

1777 set to 156 μmol electron (μmol cytochrome f) $^{-1}\text{s}^{-1}$.

1778 The proportion of leaf nitrogen allocated to light harvesting proteins was

1779 calculated as a function of Chl_{mass} and N_{mass} :

$$\rho_{\text{light}} = \frac{Chl_{\text{mass}}}{N_{\text{mass}} c_b} \quad (5.8)$$

1780 where c_b is the stoichiometry of the light-harvesting chlorophyll complexes of

1781 photosystem II, set to 2.75 mmol chlorophyll (gN in chlorophyll) $^{-1}$. We used the

1782 N_{mass} value of the focal leaf used to generate A_{net}/C_i curves instead of the leaf

1783 used to extract chlorophyll content, as the two leaves are from the same trifoliolate

1784 leaf set and are highly correlated with each other (Figure SX).

1785 The proportion of leaf nitrogen content allocated to photosynthetic tissue

1786 (ρ_{photo} ; gN gN $^{-1}$) was estimated as the sum of ρ_{rubisco} , ρ_{bioe} , and ρ_{light} .

1787 Finally, the proportion of leaf N content allocated to structural tissue (ρ_{str} ;

1788 gN gN $^{-1}$) was estimated as:

$$\rho_{\text{structure}} = \frac{N_{\text{cw}}}{N_{\text{area}}} \quad (5.9)$$

1789 where N_{cw} is the leaf N content allocated to cell walls (gN m^{-2}), calculated as a
1790 function of M_{area} using an empirical equation from Onoda et al. (2017):

$$N_{cw} = 0.000355 * M_{area}^{1.39} \quad (5.10)$$

1791 5.2.8 *Whole plant traits*

1792 Seven weeks after experiment initiation and immediately following gas ex-
1793 change measurements, we harvested all experimental individuals and separated
1794 biomass of each experimental individual into major organ types (leaves, stems,
1795 roots, and nodules when present). Fresh leaf area of all harvested leaves was mea-
1796 sured using an LI-3100C (Li-COR Biosciences, Lincoln, Nebraska, USA). Total
1797 fresh leaf area (cm^2) was calculated as the sum of all leaf areas, including the focal
1798 leaf used to collect gas exchange data and the focal leaf used to extract chlorophyll
1799 content. All harvested material was dried in an oven set to 65°C for at least 48
1800 hours, weighed, and ground to homogeneity. Leaves and nodules were manually
1801 ground either with a mortar and pestle, while stems and roots were ground using
1802 a Wiley mill (E3300 Mini Mill; Eberbach Corp., MI, USA). Total dry biomass (g)
1803 was calculated as the sum of dry leaf (including focal leaf for both the A_{net}/C_i
1804 curve and leaf used to extract chlorophyll content), stem, root, and root nodule
1805 biomass. We also quantified carbon and nitrogen content of each respective organ
1806 type through elemental combustion (Costech-4010, Costech, Inc., Valencia, CA,
1807 USA) using subsamples of ground and homogenized organ tissue.

1808 Following the approach explained in Perkowski et al. (2021), we calcu-
1809 lated structural carbon costs to acquire nitrogen as the ratio of total belowground

1810 carbon biomass to whole plant nitrogen biomass (N_{cost} ; gC gN⁻¹). Belowground
 1811 carbon biomass (C_{bg} ; gC) was calculated as the sum of root carbon biomass
 1812 and root nodule carbon biomass. Root carbon biomass and root nodule carbon
 1813 biomass was calculated as the product of the organ biomass and the respective
 1814 organ carbon content. Whole plant nitrogen biomass (N_{wp} ; gN) was similarly
 1815 calculated as the sum of total leaf, stem, root, and root nodule nitrogen biomass,
 1816 including the focal leaf used for A_{net}/C_i curve and chlorophyll extractions. Leaf,
 1817 stem, root, and root nodule nitrogen biomass was calculated as the product of
 1818 the organ biomass and the respective organ nitrogen content. This calculation
 1819 only quantifies plant structural carbon costs to acquire nitrogen and does not
 1820 include any additional costs of nitrogen acquisition associated with respiration,
 1821 root exudation, or root turnover. An explicit explanation of the limitations for
 1822 interpreting this calculation can be found in Perkowski et al. (2021) and Terrer
 1823 et al. (2018).

1824 Finally, plant investments in nitrogen fixation were calculated as the ratio
 1825 of root nodule biomass to root biomass, where increasing values indicate an in-
 1826 crease in plant investments to nitrogen fixation (Dovrat et al. 2018; Dovrat et al.
 1827 2020; Perkowski et al. 2021). We also calculated the percent of leaf nitrogen
 1828 acquired from the atmosphere (% N_{dfa}) using leaf δ¹⁵N and the following equation
 1829 from Andrews et al. (2011):

$$\%N_{\text{dfa}} = \frac{\delta^{15}N_{\text{reference}} - \delta^{15}N_{\text{sample}}}{\delta^{15}N_{\text{reference}} - B} \quad (5.11)$$

1830 where δ¹⁵N_{reference} refers to a reference plant that exclusively acquires nitrogen via

1831 direct uptake, $\delta^{15}\text{N}_{\text{sample}}$ refers to an individual's leaf $\delta^{15}\text{N}$, and B refers to individuals
1832 that are entirely reliant on nitrogen fixation. Within each unique nitrogen
1833 fertilization treatment-by-CO₂ treatment combination, we calculated the mean
1834 leaf $\delta^{15}\text{N}$ for individuals growing in the non-inoculated treatment for $\delta^{15}\text{N}_{\text{reference}}$.
1835 Any individuals with visual confirmation of root nodule formation or nodule initia-
1836 tion were omitted from the calculation of $\delta^{15}\text{N}_{\text{reference}}$. Following recommendations
1837 from Andrews et al. (2011) we calculated B within each CO₂ treatment using the
1838 mean leaf $\delta^{15}\text{N}$ of inoculated individuals that received 0 ppm N. We did not calcu-
1839 late B within each unique soil nitrogen x CO₂ treatment combination, as previous
1840 studies suggest decreased reliance on nitrogen fixation with increasing soil nitro-
1841 gen availability (Perkowski et al. 2021). This approach for estimating nitrogen
1842 fixation standardizes values such that approaching 1 indicates increasing reliance
1843 on nitrogen fixation.

1844 5.2.9 *Statistical analyses*

1845 Any uninoculated pots that had substantial root nodule formation (nodule
1846 biomass: root biomass values greater than 0.05 g g⁻¹) were removed from our
1847 analyses. This was because they were assumed to have been colonized by symbiotic
1848 nitrogen-fixing bacteria from outside sources. This decision resulted in the removal
1849 of sixteen pots from our analysis: two pots in the elevated CO₂ treatment that
1850 received 35 ppm N, three pots in the elevated CO₂ treatment that received 70
1851 ppm N, one pot in the elevated CO₂ treatment that received 210 ppm N, two pots
1852 in the elevated CO₂ treatment that received 280 ppm N, two pots in the ambient
1853 CO₂ treatment that received 0 ppm N, three pots in the ambient CO₂ treatment

1854 that received 70 ppm N, two pots in the ambient CO₂ treatment that received
1855 105 ppm N, and one pot in the ambient CO₂ treatment that received 280 ppm N.

1856 We built a series of linear mixed effects models to investigate the impacts of
1857 CO₂ concentration, soil nitrogen fertilization, and inoculation with *B. japonicum*
1858 on *G. max* gas exchange, tradeoffs between nitrogen and water use, whole plant
1859 growth, and investment in nitrogen fixation. All models included CO₂ treatment
1860 as a categorical fixed effect, inoculation treatment as a categorical fixed effect,
1861 soil nitrogen fertilization as a continuous fixed effect, with interaction terms be-
1862 tween all three fixed effects. All models also accounted for climatic difference
1863 between chambers across experiment iterations by including a random intercept
1864 term that nested starting chamber rack by CO₂ treatment. Models with this
1865 independent variable structure were created for each of the following dependent
1866 variables: N_{area} , M_{area} , N_{mass} , Chl_{area} , V_{cmax25} , J_{max25} , $J_{\text{max25}}:V_{\text{cmax25}}$, R_{d25} , g_{sw} ,
1867 stomatal limitation, ρ_{rubisco} , ρ_{bioe} , ρ_{light} , ρ_{photo} , $\rho_{\text{structure}}$, N_{cost} , C_{bg} , N_{wp} , total
1868 biomass, total leaf area, nodule biomass, and the ratio of nodule biomass to root
1869 biomass.

1870 We used Shapiro-Wilk tests of normality to determine whether linear mixed
1871 effects models satisfied residual normality assumptions. If residual normality as-
1872 sumptions were not met (Shapiro-Wilk: $p < 0.05$), then models were fit using
1873 dependent variables that were natural log transformed. All residual normality
1874 assumptions that did not originally satisfy residual normality assumptions were
1875 met with either a natural log or square root data transformation (Shapiro-Wilk:
1876 $p > 0.05$ in all cases). Specifically, models for N_{area} , N_{mass} , Chl_{area} , V_{cmax25} ,
1877 J_{max25} , $J_{\text{max25}}:V_{\text{cmax25}}$, g_{sw} , stomatal limitation, ρ_{rubisco} , ρ_{bioe} , ρ_{light} , ρ_{photo} , and to-

1878 tal leaf area satisfied residual normality assumptions without data transformation.
1879 Models for M_{area} , $\rho_{\text{structure}}$, N_{cost} , C_{bg} , N_{wp} , and total biomass satisfied residual
1880 normality assumptions with a natural log data transformation, while models for
1881 nodule biomass and nodule biomass: root biomass satisfied residual normality
1882 assumptions with a square root data transformation.

1883 In all statistical models, we used the 'lmer' function in the 'lme4' R package
1884 (Bates et al. 2015) to fit each model and the 'Anova' function in the 'car' R
1885 package (Fox and Weisberg 2019) to calculate Type II Wald's χ^2 and determine the
1886 significance ($\alpha = 0.05$) of each fixed effect coefficient. We then used the 'emmeans'
1887 R package (Lenth 2019) to conduct post-hoc comparisons using Tukey's tests,
1888 where degrees of freedom were approximated using the Kenward-Roger approach
1889 (Kenward and Roger 1997). All analyses and plots were conducted in R version
1890 4.2.0 (R Core Team 2021).

1891 5.3 Results

1892 5.3.1 *Leaf nitrogen content, chlorophyll content, and mass per area*

1893 Elevated CO₂ reduced N_{area} , N_{mass} , and Chl_{area} by 29%, 50%, and 31%,
1894 respectively, and stimulated M_{area} by 44% ($p < 0.001$ in all cases; Table 1). An in-
1895 teraction between fertilization and CO₂ (CO₂-by-fertilization interaction: $p_{N_{\text{area}}} =$
1896 0.017, $p_{N_{\text{mass}}} < 0.001$, $p_{M_{\text{area}}} = 0.006$, $p_{Chl_{\text{area}}} = 0.083$; Table 1) indicated that the
1897 general positive effect of increasing fertilization on N_{area} , N_{mass} , and Chl_{area} ($p <$
1898 0.001 in all cases; Table 1) was generally stronger under ambient CO₂ (Tukey _{N_{area}} :
1899 $p = 0.026$; Tukey _{N_{mass}} : $p < 0.001$; Tukey _{M_{area}} : $p = 0.009$; Tukey _{Chl_{area}} : $p = 0.065$;
1900 Table 1; Figs. 1a-d). This pattern resulted in a stronger reduction in N_{area} , N_{mass} ,

1901 and Chl_{area} as well as a stronger stimulation in M_{area} under elevated CO₂ with
1902 increasing fertilization. An additional interaction between inoculation and CO₂
1903 on N_{area} (CO₂-by-inoculation interaction: $p = 0.030$; Table 1) indicated that the
1904 general positive effect of inoculation on N_{area} ($p < 0.001$; Table 1) was stronger
1905 under elevated CO₂ (45% increase; Tukey: $p < 0.001$) than under ambient CO₂
1906 (18% increase; Tukey: $p < 0.001$), a result that increased the reduction in N_{area}
1907 in inoculated pots under elevated CO₂. Inoculation treatment did not modify the
1908 downregulation in N_{mass} (CO₂-by-inoculation interaction: $p = 0.148$; Table 1) and
1909 Chl_{area} ($p = 0.147$; Table 1) or the stimulation in M_{area} ($p = 0.866$; Table 1) un-
1910 der elevated CO₂. However, interactions between fertilization and inoculation on
1911 N_{area} (fertilization-by-inoculation interaction: $p < 0.001$; Table 1; Fig. 1a), N_{mass}
1912 ($p = 0.001$; Table 1; Fig. 1b), M_{area} ($p = 0.025$; Table 1; Fig. 1c), and Chl_{area} (p
1913 < 0.001 ; Table 1; Fig. 1d) indicated that the general positive effect of increasing
1914 fertilization on each trait was stronger in uninoculated pots (Tukey _{N_{area}} : $p <$
1915 0.001; Tukey _{N_{mass}} : $p = 0.001$; Tukey _{M_{area}} : $p = 0.031$; Tukey _{Chl_{area}} : $p < 0.001$).

Table 5.1. Effects of soil nitrogen fertilization, inoculation, and CO₂ treatments on N_{area} , N_{mass} , M_{area} , and Chl_{area}

	N_{area}			N_{mass}			M_{area}^a			
	df	Coefficient	χ^2	p	Coefficient	χ^2	p	Coefficient	χ^2	p
(Intercept)	-	1.10E+00	-	-	3.05E-02	-	-	3.64E+00	-	-
CO ₂	1	-5.67E-01	155.908	<0.001	-1.80E-02	272.362	<0.001	3.04E-01	151.319	<0.001
Inoculation (I)	1	6.21E-01	86.029	<0.001	7.54E-03	15.576	<0.001	1.81E-01	19.158	<0.001
Fertilization (N)	1	3.06E-03	316.408	<0.001	5.78E-05	106.659	<0.001	3.10E-04	21.440	<0.001
CO ₂ *I	1	2.63E-01	4.729	0.030	3.96E-03	2.025	0.155	-3.37E-02	0.029	0.866
CO ₂ *N	1	-3.68E-04	5.723	0.017	-2.85E-05	22.542	<0.001	2.80E-04	7.619	0.006
I*N	1	-1.36E-03	43.381	<0.001	-2.00E-05	11.137	0.001	-3.36E-04	5.022	0.025
CO ₂ *I*N	1	-3.23E-04	0.489	0.484	-2.59E-06	0.041	0.839	1.15E-04	0.208	0.649

	Chl_{area}			
	df	Coefficient	χ^2	p
(Intercept)	-	2.13E-02	-	-
CO ₂	1	-1.33E-02	69.233	<0.001
Inoculation (I)	1	1.24E-01	136.341	<0.001
Fertilization (N)	1	3.35E-04	163.111	<0.001
CO ₂ *I	1	-3.18E-02	2.102	0.147
CO ₂ *N	1	-8.79E-05	2.999	0.083
I*N	1	-2.65E-04	75.769	<0.001
CO ₂ *I*N	1	7.68E-05	2.144	0.147

*Significance determined using Type II Wald χ^2 tests ($\alpha = 0.05$). P-values < 0.05 are in bold, while p-values between 0.05 and 0.1 are italicized. A superscript “a” is included after trait labels to indicate if models were fit with natural log transformed response variables. Key: df = degrees of freedom, N_{area} = leaf nitrogen content per unit leaf area, N_{mass} = leaf nitrogen content, M_{area} = leaf mass per unit leaf area.

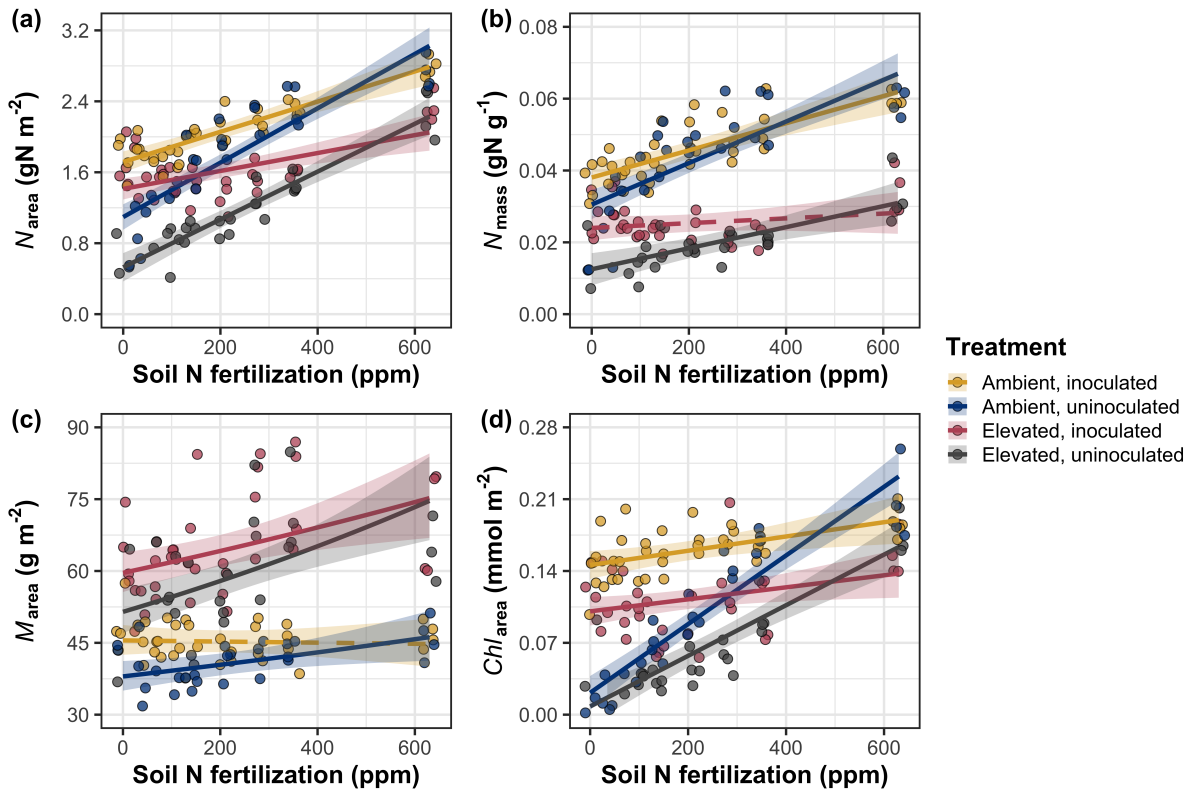


Figure 5.1. Effects of CO_2 , fertilization, and inoculation on leaf nitrogen per unit leaf area (a), leaf nitrogen content (b), leaf mass per unit leaf area (c), and chlorophyll content per unit leaf area (d). Soil nitrogen fertilization is represented on the x-axis in all panels. Yellow points and trendlines indicate inoculated individuals grown under ambient CO_2 , blue points and trendlines indicate uninoculated individuals grown under ambient CO_2 , red points and trendlines indicate inoculated individuals grown under elevated CO_2 , and grey points indicate uninoculated individuals grown under elevated CO_2 . Solid trendlines indicate regression slopes that are different from zero ($p < 0.05$), while dashed trendlines indicate slopes that are not distinguishable from zero ($p > 0.05$).

1916 5.3.2 *Leaf biochemistry and stomatal conductance*

1917 Elevated CO₂ resulted in plants with 16% lower V_{cmax25} ($p < 0.001$; Table
1918 2) and 10% lower J_{max25} ($p = 0.014$; Table 2) as compared to those grown un-
1919 der ambient CO₂, but did not influence R_{d25} ($p = 0.613$; Table 2). A relatively
1920 stronger downregulation in V_{cmax25} than J_{max25} resulted in an 8% stimulation in
1921 $J_{max25}:V_{cmax25}$ under elevated CO₂ ($p < 0.001$; Table 2; Fig. 2E). The downregu-
1922 latory effect of CO₂ on V_{cmax25} and J_{max25} was not modified across the fertilization
1923 gradient (CO₂-by-fertilization interaction: $p = 0.185$, $p = 0.389$ for V_{cmax25} and
1924 J_{max25} , respectively; Table 2; Fig. 2A, 2C) or between inoculation treatments
1925 (CO₂-by-inoculation interaction: $p = 0.799$ and $p = 0.714$ for V_{cmax25} and J_{max25} ,
1926 respectively; Table 2). However, a strong interaction between fertilization and
1927 inoculation (fertilization-by-inoculation interaction: $p \leq 0.001$ in all cases; Table
1928 2) indicated that the general positive effect of increasing fertilization on V_{cmax25} ($p
1929 < 0.001$; Table 2), J_{max25} ($p < 0.001$; Table 2), and R_{d25} ($p = 0.015$; Table 2) was
1930 only observed in uninoculated pots (Tukey: $p \leq 0.001$ in all cases), as there was
1931 no apparent effect of fertilization on V_{cmax25} (Tukey: $p = 0.456$), J_{max25} (Tukey: $p
1932 = 0.180$), or R_{d25} (Tukey: $p = 0.443$) in inoculated pots (Figs. 2B, 2D, 2F, 2H). A
1933 relatively stronger positive effect of increasing fertilization on V_{cmax25} than J_{max25}
1934 resulted in a general reduction in $J_{max25}:V_{cmax25}$ with increasing fertilization ($p <
1935 0.001$), though this pattern was only seen in uninoculated pots (Tukey: $p = 0.003$)
1936 and not inoculated plants (Tukey: $p > 0.05$).

1937 Elevated CO₂ reduced stomatal conductance by 20% ($p < 0.001$; Table 2)
1938 compared to ambient CO₂, but this downregulation did not influence stomatal
1939 limitation of photosynthesis ($p = 0.355$; Table 2). As with V_{cmax25} and J_{max25} , the

1940 downregulation of stomatal conductance due to elevated CO₂ was not modified
1941 across the fertilization gradient (CO₂-by-fertilization interaction: $p = 0.141$; Table
1942 2) or between inoculation treatments (CO₂-by-inoculation interaction: $p = 0.179$;
1943 Table 2). Fertilization also did not modify the general null effect of CO₂ on stom-
1944 atal limitation (CO₂-by-fertilization interaction: $p = 0.554$; Table 2), although
1945 an interaction between CO₂ and inoculation (CO₂-by-inoculation interaction: p
1946 = 0.043; Table 2) indicated that inoculation increased stomatal limitation un-
1947 der ambient CO₂ (Tukey: $p = 0.021$), but not under elevated CO₂ (Tukey: p
1948 > 0.999). An interaction between inoculation and fertilization on stomatal con-
1949 ductance (fertilization-by-inoculation interaction: $p < 0.001$; Table 2) indicated
1950 that increasing fertilization increased stomatal conductance in uninoculated pots
1951 (Tukey: $p = 0.003$) but decreased stomatal conductance in inoculated pots (Tukey:
1952 $p = 0.021$). The similar in magnitude, but opposite direction, trend in the effect of
1953 increasing fertilization on stomatal conductance between inoculation treatments
1954 likely drove a null general response of stomatal conductance to increasing fertil-
1955 ization ($p = 0.642$; Table 2).

Table 5.2. Effects of soil nitrogen fertilization, inoculation, and CO₂ on leaf biochemistry

	<i>V</i> _{cmax25}			<i>J</i> _{max25}			<i>R</i> _{d25}			
	df	Coefficient	χ^2	p	Coefficient	χ^2	p	Coefficient	χ^2	p
(Intercept)	-	4.36E+01	-	-	8.30E+01	-	-	1.69E+00	-	-
CO ₂	1	-7.05E+00	18.039	<0.001	-9.11E+00	6.042	0.014	4.53E-01	0.256	0.613
Inoculation (I)	1	5.87E+01	98.579	<0.001	9.62E+01	85.064	<0.001	1.04E+00	3.094	0.079
Fertilization (N)	1	1.32E-01	37.053	<0.001	2.09E-01	25.356	<0.001	2.86E-03	5.965	0.015
CO ₂ *I	1	-4.65E+00	0.065	0.799	7.84E-01	0.667	0.414	-5.71E-01	2.563	0.109
CO ₂ *N	1	-3.58E-02	1.758	0.185	-4.33E-02	0.742	0.389	-1.55E-03	2.675	0.102
I*N	1	-1.35E-01	60.394	<0.001	-2.30E-01	57.410	<0.001	-2.84E-03	12.083	0.001
CO ₂ *I*N	1	2.73E-02	0.748	0.387	3.46E-02	0.377	0.539	7.21E-04	0.244	0.622

123

	<i>J</i> _{max25} : <i>V</i> _{cmax25}			<i>g</i> _{sw}			Stomatal limitation			
	df	Coefficient	χ^2	p	Coefficient	χ^2	p	Coefficient	χ^2	p
(Intercept)	-	1.92E+00	-	-	1.95E-01	-	-	2.12E-01	-	-
CO ₂	1	5.71E-02	92.010	<0.001	-6.23E-02	9.718	0.002	3.91E-02	0.856	0.355
Inoculation (I)	1	-1.79E-01	27.768	<0.001	1.30E-01	22.351	<0.001	7.87E-02	4.582	0.032
Fertilization (N)	1	-4.61E-04	28.147	<0.001	2.50E-04	0.066	0.797	2.60E-04	32.218	<0.001
CO ₂ *I	1	8.94E-02	2.916	0.088	6.69E-02	1.810	0.179	-7.84E-02	4.093	0.043
CO ₂ *N	1	2.35E-04	3.210	0.073	-8.50E-05	2.165	0.141	-1.24E-04	0.350	0.554
I*N	1	3.27E-04	9.607	0.002	-3.09E-04	14.696	<0.001	-1.67E-04	2.547	0.110
CO ₂ *I*N	1	-1.66E-04	1.102	0.294	-8.89E-05	0.234	0.629	1.67E-04	2.231	0.135

*Significance determined using Type II Wald χ^2 tests ($\alpha = 0.05$). P-values < 0.05 are in bold, while p-values between 0.05 and 0.1 are italicized. Key: *V*_{cmax25} – maximum rate of Rubisco carboxylation at 25°C; *J*_{max25} – maximum rate of electron transport for RuBP regeneration at 25°C, *R*_{d25} - dark respiration at 25°C; *J*_{max25}:*V*_{cmax25} – the ratio of *J*_{max25} to *V*_{cmax25}; *g*_{sw} - stomatal conductance.

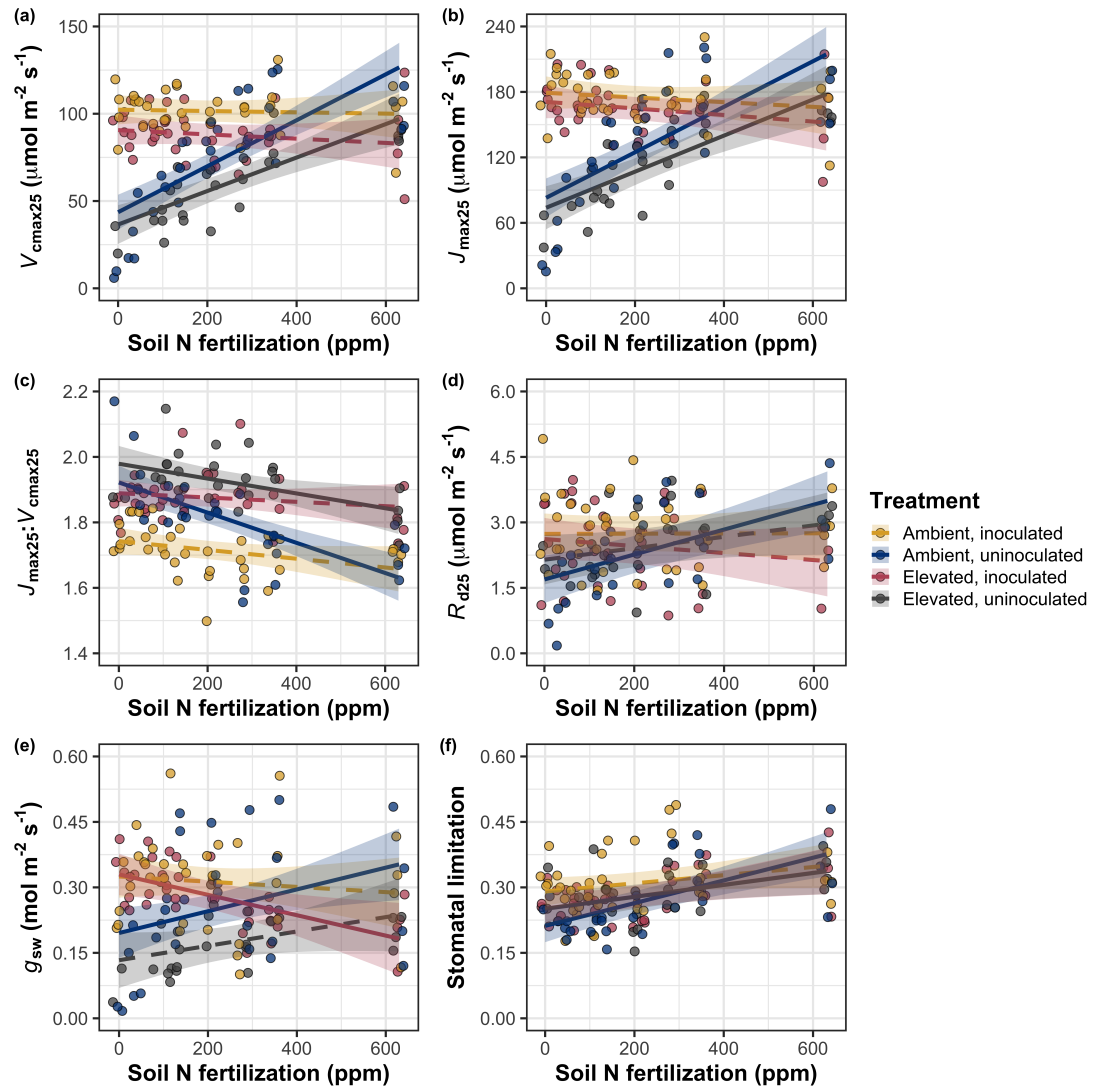


Figure 5.2. Effects of CO₂, fertilization, and inoculation on maximum rate of Rubisco carboxylation (a), the maximum rate of RuBP regeneration (b), and the ratio of the maximum rate of RuBP regeneration to the maximum rate of Rubisco carboxylation leaf mass per unit leaf area (c), dark respiration (d), stomatal conductance (e), and stomatal limitation (f). Soil nitrogen fertilization is represented on the x-axis in all panels. Colored points and trendlines are as explained in Figure 1.

1956 5.3.3 *Leaf nitrogen allocation*

1957 A relatively stronger downregulation in N_{area} than $V_{\text{cmax}25}$ or $J_{\text{max}25}$ resulted
1958 in an 20% and 29% respective stimulation in ρ_{rubisco} and ρ_{bioe} under elevated CO₂
1959 ($p < 0.001$ in both cases; Table 3). There was no apparent CO₂ effect on ρ_{light}
1960 ($p = 0.700$; Table 3), but the strong stimulation in ρ_{rubisco} and ρ_{bioe} resulted
1961 in a 21% stimulation of ρ_{photo} under elevated CO₂ ($p < 0.001$; Table 3; Fig.
1962 3A). The stimulation of ρ_{rubisco} , ρ_{bioe} , and ρ_{photo} due to elevated CO₂ was not
1963 modified across the fertilization gradient (CO₂-by-fertilization interaction: p_{rubisco}
1964 = 0.269, $p_{\text{bioe}} = 0.298$, $p_{\text{photo}} = 0.281$; Table 3). A marginal interaction between
1965 inoculation and CO₂ on ρ_{rubisco} and ρ_{photo} (CO₂-by-inoculation interaction: p_{rubisco}
1966 = 0.057, $p_{\text{photo}} = 0.057$; Table 3) indicated that the general positive effect of
1967 inoculation on ρ_{rubisco} and ρ_{photo} ($p < 0.001$ in both cases; Table 3) was only
1968 apparent under ambient CO₂ (Tukey: $p < 0.001$ in both cases), with no apparent
1969 effect of inoculation under elevated CO₂ (Tukey_{rubisco}: $p = 0.200$; Tukey_{photo}: p
1970 = 0.147). Inoculation did not modify the stimulation of ρ_{bioe} under elevated CO₂
1971 (CO₂-by-inoculation interaction: $p = 0.122$; Table 3) or the null effect of CO₂ on
1972 ρ_{bioe} (CO₂-by-inoculation interaction: $p = 0.298$; Table 3). Strong interactions
1973 between fertilization and inoculation on ρ_{rubisco} , ρ_{bioe} , and ρ_{photo} (fertilization-
1974 by-inoculation interaction: $p < 0.001$ in all cases; Table 3) indicated that the
1975 general negative effect of increasing fertilization ($p < 0.001$ in all cases; Table
1976 3) was only observed in inoculated pots (Tukey: $p < 0.001$ in all cases), with
1977 no apparent effect of fertilization on ρ_{rubisco} (Tukey: $p = 0.612$), ρ_{bioe} (Tukey:
1978 $p = 0.544$), or ρ_{photo} (Tukey: $p = 0.521$; Fig 3B) in uninoculated pots. An
1979 additional interaction between fertilization and inoculation on ρ_{light} (fertilization-

1980 by-inoculation interaction: $p < 0.001$; Table 3) indicated a negative effect of
1981 increasing fertilization on ρ_{light} in inoculated pots (Tukey: $p = 0.041$), but a
1982 positive effect of increasing fertilization in uninoculated pots (Tukey: $p < 0.001$).

1983 The stimulation in M_{area} resulted in an 133% stimulation of $\rho_{\text{structure}}$ under
1984 elevated CO₂ ($p < 0.001$; Table 3; Fig 3C). An interaction between fertilization
1985 and CO₂ (CO₂-by-fertilization interaction: $p = 0.039$; Table 3) indicated that the
1986 general negative effect of increasing fertilization ($p < 0.001$; Table 3) on $\rho_{\text{structure}}$
1987 was marginally stronger under ambient CO₂ (Tukey: $p = 0.055$), resulting in a
1988 stronger stimulation in $\rho_{\text{structure}}$ under elevated CO₂ with increasing fertilization.
1989 A marginal interaction between inoculation and CO₂ (CO₂-by-inoculation inter-
1990 action: $p = 0.057$; Table 3) indicated that the general positive effect of inoculation
1991 on $\rho_{\text{structure}}$ ($p < 0.001$; Table 3) was only observed under elevated CO₂ (Tukey:
1992 $p < 0.001$), with no apparent inoculation effect observed under ambient CO₂
1993 (Tukey: $p = 0.513$). Finally, an interaction between fertilization and inoculation
1994 (fertilization-by-inoculation interaction: $p < 0.001$; Table 3; Fig. 3D) indicated
1995 that, while increasing fertilization generally increased $\rho_{\text{structure}}$ ($p < 0.001$; Table
1996 3), this response was generally stronger in uninoculated pots (Tukey: $p = 0.001$).

Table 5.3. Effects of soil N availability, soil pH, species, and N_{area} on leaf nitrogen allocation

	ρ_{rubisco}			ρ_{bioe}			ρ_{light}			
	df	Coefficient	χ^2	p	Coefficient	χ^2	p	Coefficient	χ^2	p
(Intercept)	-	2.70E-01	-	-	5.26E-02	-	-	8.48E-03	-	-
CO ₂	1	1.42E-01	23.510	<0.001	3.00E-02	53.899	<0.001	2.03E-03	0.149	0.700
Inoculation (I)	1	1.83E-01	23.475	<0.001	2.80E-02	13.860	<0.001	2.04E-02	147.234	<0.001
Fertilization (N)	1	1.35E-04	16.609	<0.001	1.22E-05	26.827	<0.001	3.22E-05	19.378	<0.001
CO ₂ *I	1	-1.07E-01	3.629	<i>0.057</i>	-1.67E-02	2.390	0.122	-5.33E-03	0.684	0.408
CO ₂ *N	1	-2.16E-04	1.223	<i>0.269</i>	-3.59E-05	1.085	0.298	-7.01E-06	0.351	0.553
I*N	1	-4.26E-04	20.045	<0.001	-6.87E-05	15.458	<0.001	-4.37E-05	64.042	<0.001
CO ₂ *I*N	1	2.50E-04	3.327	<i>0.068</i>	4.08E-05	2.651	0.103	1.74E-05	3.735	<i>0.053</i>

	ρ_{photo}			$\rho_{\text{structure}}^a$			
	df	Coefficient	χ^2	p	Coefficient	χ^2	p
(Intercept)	-	3.32E-01	-	-	-2.93E+00	-	-
CO ₂	1	1.81E-01	27.651	<0.001	8.77E-01	229.571	<0.001
Inoculation (I)	1	2.31E-01	26.238	<0.001	-2.55E-01	13.872	<0.001
Fertilization (N)	1	1.76E-04	15.899	<0.001	-1.51E-03	38.128	<0.001
CO ₂ *I	1	-1.36E-01	3.671	<i>0.055</i>	-2.99E-01	3.622	<i>0.057</i>
CO ₂ *N	1	-2.72E-04	1.163	<i>0.281</i>	3.14E-04	4.266	0.039
I*N	1	-5.37E-04	21.355	<0.001	7.00E-04	11.025	0.001
CO ₂ *I*N	1	3.29E-04	4.009	0.045	4.52E-04	0.669	0.413

*Significance determined using Type II Wald χ^2 tests ($\alpha = 0.05$). P-values < 0.05 are in bold, while p-values between 0.05 and 0.1 are italicized. A superscript “a” is included after trait labels to indicate if models were fit with natural log transformed response variables. Key: df=degrees of freedom, ρ_{rubisco} = proportion of leaf N allocated to photosynthesis, ρ_{bioe} = proportion of leaf N allocated to bioenergetics, ρ_{light} =proportion of leaf N allocated to light harvesting proteins, ρ_{photo} =proportion of leaf N allocated to photosynthesis, $\rho_{\text{structure}}$ =proportion of leaf N allocated to cell wall structural tissue

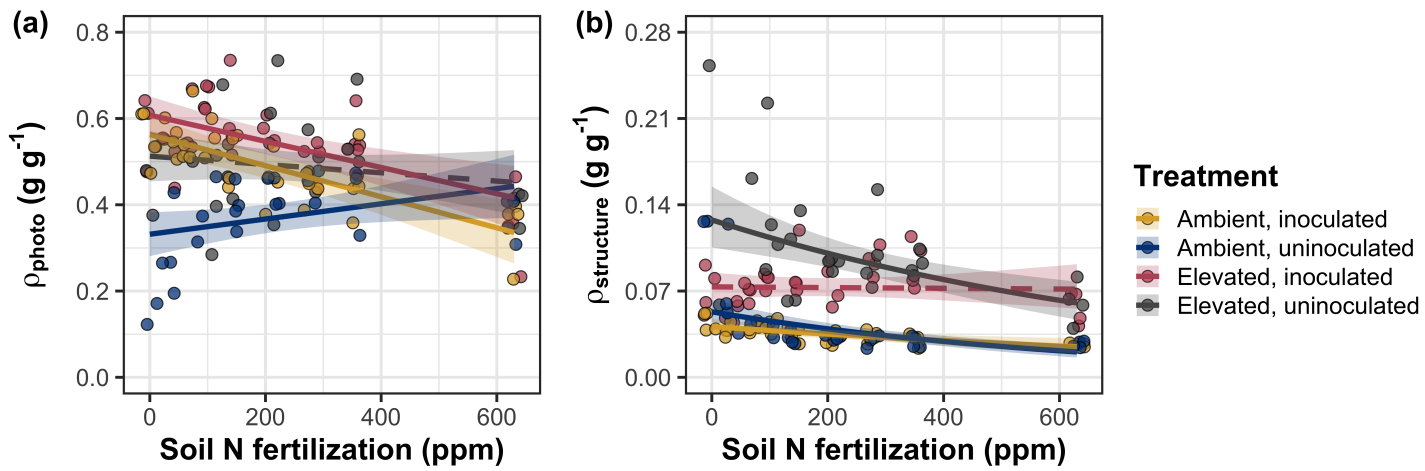


Figure 5.3. Effects of CO_2 , fertilization, and inoculation on the relative fraction of leaf nitrogen allocated to photosynthesis (a) and the fraction of leaf nitrogen allocated to structure (b). Soil nitrogen fertilization is represented on the x-axis in both panels. Colored points and trendlines are as explained in Figure 1.

1997 5.3.4 *Whole plant growth and total leaf area*

1998 Total leaf area was 51% greater and total biomass was 102% greater under elevated CO₂ ($p < 0.001$ in both cases; Table 4), a pattern that was enhanced by fertilization (CO₂-by-fertilization interaction: $p < 0.001$ in both cases; Table 4; Fig. 4a-b) but was not modified across inoculation treatments (CO₂-by-inoculation interaction: $p_{total_leaf_area} = 0.151$, $p_{total_biomass} = 0.472$; Table 4). Specifically, the general positive effect of increasing fertilization on total leaf area and whole plant biomass ($p < 0.001$ in both cases; Table 4) was stronger under elevated CO₂ (Tukey: $p < 0.001$ in both cases). The general positive effect of increasing fertilization on total leaf area was modified by inoculation treatment (fertilization-by-inoculation interaction: $p < 0.001$ in both cases; Table 4), indicating a stronger positive effect of increasing fertilization in uninoculated pots (Tukey: $p_{total_leaf_area} = 0.002$, $p_{total_biomass} = 0.001$).

2010 5.3.5 *Carbon costs to acquire nitrogen*

2011 A general 62% stimulation in N_{cost} under elevated CO₂ was modified through a strong three-way interaction between CO₂, fertilization, and inoculation (CO₂-by-inoculation-by-fertilization interaction: $p < 0.001$; Table 4). This interaction revealed a general negative effect of increasing fertilization on N_{cost} ($p < 0.001$; Table 4) that was observed in all treatment combinations (Tukey: $p < 0.001$ in all cases) except for inoculated pots grown under elevated CO₂ (Tukey: $p = 0.779$; Fig. 5c). This response also resulted in generally stronger negative effects of increasing fertilization on N_{cost} in uninoculated pots grown under elevated CO₂ than uninoculated pots grown under ambient CO₂ (Tukey: $p = 0.001$) and

2020 inoculated pots grown under either ambient CO₂ (Tukey: $p < 0.001$) or elevated
2021 CO₂ (Tukey: $p < 0.001$), while uninoculated pots grown under ambient CO₂ had
2022 generally stronger negative effects of increasing fertilization on N_{cost} than inocu-
2023 lated pots grown under elevated CO₂ (Tukey: $p = 0.002$), but not inoculated pots
2024 grown under ambient CO₂ (Tukey: $p = 0.216$). The general reduction in N_{cost}
2025 with increasing fertilization and in uninoculated pots were driven by a stronger
2026 positive effect of increasing fertilization on N_{wp} (denominator of N_{cost}) than C_{bg}
2027 (numerator of N_{cost}), while the general stimulation in N_{cost} under elevated CO₂
2028 was driven by a stronger positive effect of elevated CO₂ on C_{bg} than N_{wp} (Table
2029 4).

Table 5.4. Effects of soil N availability, soil pH, species, and N_{area} on total leaf area, whole plant biomass, and costs of nitrogen acquisition

	Total leaf area			Total biomass			N_{cost}			
	df	Coefficient	χ^2	p	Coefficient	χ^2	p	Coefficient	χ^2	p
(Intercept)	-	8.78E+01	-	-	9.96E-01	-	-	8.67E+00	-	-
CO_2	1	3.36E+01	69.291	<0.001	5.07E-01	131.477	<0.001	8.75E+00	88.189	<0.001
Inoculation (I)	1	1.88E+02	35.715	<0.001	7.96E-01	34.264	<0.001	-1.68E+00	136.343	<0.001
Fertilization (N)	1	9.35E-01	274.199	<0.001	3.14E-03	269.046	<0.001	-8.50E-03	80.501	<0.001
$\text{CO}_2 * \text{I}$	1	6.44E+01	2.064	0.151	-7.69E-02	0.518	0.472	-8.38E+00	85.237	<0.001
$\text{CO}_2 * \text{N}$	1	5.05E-01	18.655	<0.001	1.61E-03	16.877	<0.001	-9.17E-03	1.050	0.306
$\text{I} * \text{N}$	1	-3.84E-01	10.804	0.001	-1.45E-03	15.779	<0.001	4.20E-03	46.489	<0.001
$\text{CO}_2 * \text{I} * \text{N}$	1	-2.97E-03	<0.001	0.990	-1.14E-04	0.023	0.880	1.32E-02	18.125	<0.001

	C_{bg}			N_{wp}			
	df	Coefficient	χ^2	p	Coefficient	χ^2	p
(Intercept)	-	-1.70E+00	-	-	1.24E-01	-	-
CO_2	1	9.21E-01	84.134	<0.001	-3.41E-03	23.890	<0.001
Inoculation (I)	1	1.18E+00	41.030	<0.001	1.68E-01	134.460	<0.001
N fertilization (N)	1	3.38E-03	152.248	<0.001	6.69E-04	529.021	<0.001
$\text{CO}_2 * \text{I}$	1	-6.18E-01	8.965	0.003	3.68E-02	1.190	0.275
$\text{CO}_2 * \text{N}$	1	-3.66E-05	1.188	0.276	1.58E-04	5.915	0.015
$\text{I} * \text{N}$	1	-2.22E-03	22.648	<0.001	-3.20E-04	55.562	<0.001
$\text{CO}_2 * \text{I} * \text{N}$	1	8.09E-04	1.109	0.292	-7.54E-05	0.620	0.431

*Significance determined using Type II Wald χ^2 tests ($\alpha = 0.05$). P-values < 0.05 are in bold, while p-values between 0.05 and 0.1 are italicized. A superscript “a” after trait labels indicates if models were fit using natural log transformed response variables, while a superscript “b” indicates if models were fit using square root transformed variables. Key: df=degrees of freedom

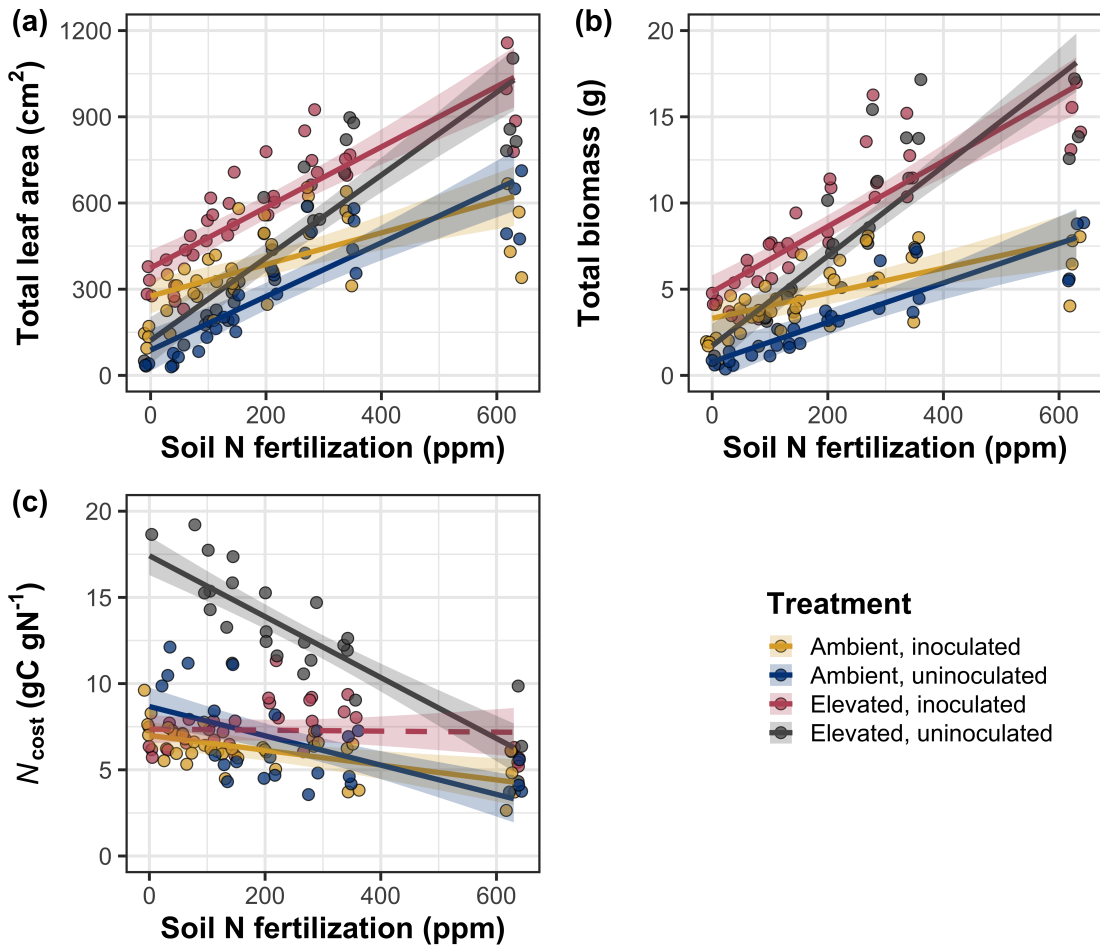


Figure 5.4. Effects of CO₂, fertilization, and inoculation on total leaf area (a), total biomass (b), and structural carbon costs to acquire nitrogen (c). Soil nitrogen fertilization is represented continuously on the x-axis in all panels. Colored points and trendlines are as explained in Figure 1.

2030 5.3.6 *Nitrogen fixation*

2031 Nodule biomass was stimulated by 30% under elevated CO₂ ($p < 0.001$;
2032 Table 5), a pattern that was modified across the fertilization gradient (CO₂-by-
2033 fertilization interaction: $p = 0.479$; Table 5), but not between inoculation treat-
2034 ments (CO₂-by-inoculation interaction: $p = 0.404$; Table 5). Specifically, the
2035 general negative effect of increasing fertilization on nodule biomass ($p < 0.001$;
2036 Table 5) was stronger under elevated CO₂ than ambient CO₂ (Tukey: $p < 0.001$;
2037 Fig. 5a), which reduced the stimulation in nodule biomass under elevated CO₂
2038 with increasing fertilization. A strong interaction between fertilization and inocu-
2039 lation (fertilization-by-inoculation interaction: $p < 0.001$; Table 5) was driven by
2040 a stronger negative effect of increasing fertilization in inoculated pots (Tukey: p
2041 < 0.001 ; Fig. 5a).

2042 There was no effect of CO₂ on nodule: root biomass ($p = 0.767$; Table 5),
2043 although an interaction between CO₂ and inoculation (CO₂-by-inoculation inter-
2044 action: $p < 0.001$; Table 5) indicated that the general positive effect of inoculation
2045 on nodule: root biomass ($p < 0.001$; Table 5) was stronger under ambient CO₂
2046 (3129% increase; Tukey: $p < 0.001$) than elevated CO₂ (379% increase; Tukey:
2047 $p < 0.001$; Fig. 5b). The null effect of CO₂ on nodule: root biomass was con-
2048 sistently observed across the fertilization gradient ($p = 0.183$; Table 5; Fig. 5b).
2049 An interaction between fertilization and inoculation (fertilization-by-inoculation
2050 interaction: $p < 0.001$; Table 5) indicated that the general negative effect of in-
2051 creasing fertilization on nodule: root biomass ($p < 0.001$; Table 5) was stronger
2052 in inoculated pots (Tukey: $p < 0.001$; Fig. 5b).

2053 There was no effect of CO₂ on %N_{dfa} ($p = 0.472$; Table 5), a pattern

2054 that was not modified by inoculation (CO_2 -by-inoculation interaction: $p = 0.156$;
2055 Table 5) or fertilization (CO_2 -by-fertilization interaction: $p = 0.099$; Table 5).
2056 An interaction between fertilization and inoculation (fertilization-by-inoculation
2057 interaction: $p < 0.001$; Table 5) indicated that the general negative effect of
2058 increasing fertilization on $\%N_{\text{dfa}}$ ($p < 0.001$; Table 5) was only observed in inoc-
2059 ulated pots (Tukey: $p < 0.001$), with no apparent effect of fertilization on $\%N_{\text{dfa}}$
2060 in uninoculated pots (Tukey: $p = 0.651$; Table 5; Fig. 5c).

Table 5.5. Effects of soil N availability, soil pH, species, and N_{area} on leaf biochemistry

	df	Root nodule biomass ^b			Root nodule: root biomass ^b			% N_{dfa}^b		
		Coefficient	χ^2	p	Coefficient	χ^2	p	Coefficient	χ^2	p
(Intercept)	-	9.41E-03	-	-	1.33E-02	-	-	7.48E-01	-	-
CO ₂	1	1.20E-01	19.258	<0.001	9.94E-02	0.087	0.768	-1.00E-01	0.518	0.472
Inoculation (I)	1	5.74E-01	755.020	<0.001	5.40E-01	903.691	<0.001	9.01E+00	955.570	<0.001
Fertilization (N)	1	7.71E-06	84.376	<0.001	-5.99E-06	258.099	<0.001	3.64E-04	292.938	<0.001
CO ₂ *I	1	-4.68E-02	0.950	0.330	-1.38E-01	20.614	<0.001	-1.44E-01	2.010	0.156
CO ₂ *N	1	-1.59E-04	2.106	0.147	-1.73E-04	1.773	0.183	-6.21E-05	2.716	0.099
I*N	1	-5.82E-04	44.622	<0.001	-7.45E-04	133.918	<0.001	-1.58E-02	231.290	<0.001
CO ₂ *I*N	1	7.26E-05	0.196	0.658	1.76E-04	2.359	0.125	2.77E-03	2.119	0.145

*Significance determined using Type II Wald χ^2 tests ($\alpha = 0.05$). P-values < 0.05 are in bold, while p-values between 0.05 and 0.1 are italicized. Superscript letters indicate model coefficients fit to square-root (^b) transformed data. Key: % N_{dfa} =percent nitrogen fixed from the atmosphere.

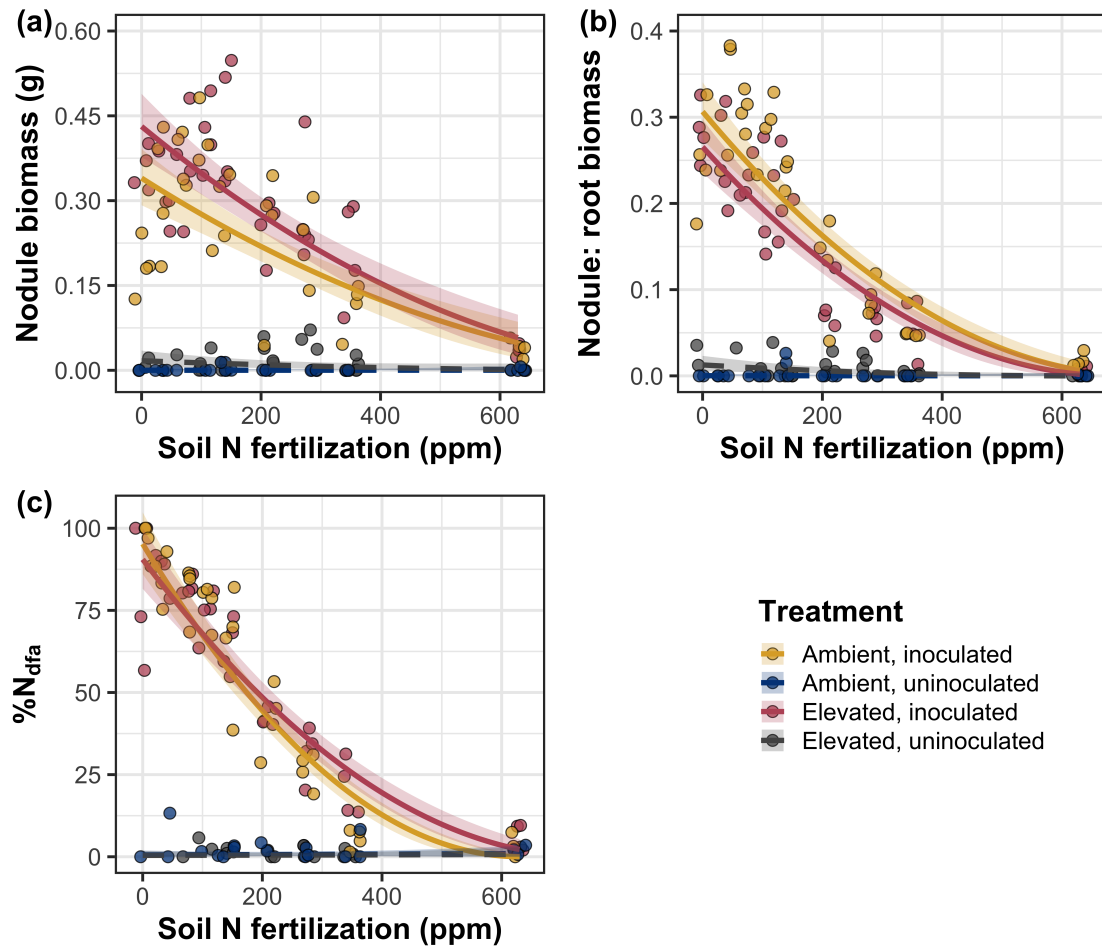


Figure 5.5. Effects of CO_2 , fertilization, and inoculation on nodule biomass (a), nodule: root biomass (b), and percent nitrogen fixed from the atmosphere (c). Soil nitrogen fertilization is represented on the x-axis. Yellow points and trendlines indicate inoculated individuals grown under ambient CO_2 , blue points and trendlines indicate uninoculated individuals grown under ambient CO_2 , red points and trendlines indicate inoculated individuals grown under elevated CO_2 , and grey points indicate uninoculated individuals grown under elevated CO_2 . Solid trendlines indicate slopes that are different from zero ($p < 0.05$), while dashed trendlines indicate slopes that are not different from zero ($p > 0.05$). Curvilinear trendlines occur as a result of back-transforming models where response variables received either a natural log or square root transformation prior to fitting.

2061 5.4 Discussion

2062 In this study, we determined leaf and whole plant acclimation responses of
2063 7-week *G. max* seedlings grown under two CO₂ concentrations, two inoculation
2064 treatments, and nine soil nitrogen fertilization treatments in a full-factorial growth
2065 chamber experiment. In support of our hypotheses and patterns expected from
2066 theory, elevated CO₂ reduced N_{area} , V_{cmax25} , and J_{max25} . The relatively stronger
2067 downregulation in V_{cmax25} than J_{max25} under elevated CO₂ resulted in a stimu-
2068 lation in $J_{\text{max25}}:V_{\text{cmax25}}$ under elevated CO₂. The downregulation of V_{cmax25} and
2069 J_{max25} under elevated CO₂ was similar across fertilization and inoculation treat-
2070 ments, indicating that the CO₂ responses were not due to nitrogen limitation.
2071 Interestingly, our results indicate that elevated CO₂ increased the fraction of leaf
2072 nitrogen allocated to photosynthesis and structure, leading to a stimulation in
2073 nitrogen use efficiency under elevated CO₂ despite the apparent downregulation
2074 in N_{area} , V_{cmax25} , and J_{max25} . The downregulation in leaf photosynthetic processes
2075 under elevated CO₂ also corresponded with a strong stimulation in total leaf area
2076 and total biomass. Strong stimulations in whole plant growth due to elevated CO₂
2077 were generally enhanced with increasing fertilization and were negatively related
2078 to structural carbon costs to acquire nitrogen. Inoculation generally did not mod-
2079 ify whole plant responses to elevated CO₂ across the fertilization gradient, likely
2080 due to a strong reduction in root nodulation with increasing fertilization. However,
2081 strong positive effects of inoculation on whole plant growth were observed under
2082 low fertilization, consistent with our hypothesis. Overall, observed leaf and whole
2083 plant acclimation responses to CO₂ support our hypotheses and patterns expected
2084 from photosynthetic least-cost theory, showing that leaf acclimation responses to

2085 CO₂ were decoupled from soil nitrogen availability and ability to acquire nitro-
2086 gen via symbiotic nitrogen fixation. Instead, leaf and whole plant acclimation
2087 responses to CO₂ were driven by optimal resource investment to photosynthetic
2088 capacity, where optimal resource investment at the leaf level maximized nitrogen
2089 allocation to structures that support whole plant growth.

2090 5.4.1 *Soil nitrogen fertilization has divergent effects on leaf and whole plant
2091 acclimation responses to CO₂*

2092 Elevated CO₂ reduced N_{area} , V_{cmax25} , J_{max25} , and stomatal conductance by
2093 29%, 16%, 10%, and 20%, respectively (Table 5.2). The larger downregulation in
2094 V_{cmax25} than J_{max25} led to an 8% stimulation in $J_{\text{max25}}:V_{\text{cmax25}}$ (Table 5.2), while
2095 the larger downregulation in N_{area} than V_{cmax25} resulted in a 21% stimulation
2096 in the fraction of leaf nitrogen allocated to photosynthesis under elevated CO₂.
2097 These acclimation responses are directionally consistent with previous studies that
2098 have investigated or reviewed leaf acclimation responses to CO₂ (Drake et al.
2099 1997; Makino et al. 1997; Ainsworth et al. 2002; Ainsworth and Long 2005;
2100 Ainsworth and Rogers 2007; Smith and Dukes 2013; Smith and Keenan 2020;
2101 Poorter et al. 2022), and follow patterns expected from photosynthetic least-cost
2102 theory (Wright et al. 2003; Prentice et al. 2014; Smith et al. 2019; Smith and
2103 Keenan 2020). Together, the stimulation in $J_{\text{max25}}:V_{\text{cmax25}}$ and the fraction of leaf
2104 nitrogen allocated to photosynthesis, and nitrogen use efficiency under elevated
2105 CO₂ provide strong support for the idea that leaves were downregulating V_{cmax25}
2106 in response to elevated CO₂ in order to optimally coordinate photosynthesis such
2107 that net photosynthesis rates approached becoming equally co-limited by Rubisco

2108 carboxylation and RuBP regeneration (Chen et al. 1993; Maire et al. 2012).

2109 Increasing fertilization and inoculation induced strong positive effects on
2110 N_{area} (Fig. 1a), $V_{\text{cmax}25}$ (Fig. 5.2a), $J_{\text{max}25}$ (Fig. 5.2b). The general positive
2111 response of N_{area} to increasing fertilization and in inoculated pots was enhanced
2112 under ambient CO₂, which, paired with the general downregulation in N_{area} un-
2113 der elevated CO₂, resulted in a stronger downregulation of N_{area} under elevated
2114 CO₂ with increasing fertilization and in inoculated pots (Fig. 5.1a). These pat-
2115 terns suggest that N_{area} responses to CO₂ were at least partially dependent on
2116 soil nitrogen fertilization and nitrogen acquisition strategy. However, the general
2117 stimulation in the fraction of leaf nitrogen allocated to Rubisco, bioenergetics,
2118 or photosynthesis under elevated CO₂ was not modified across the fertilization
2119 gradient and was only marginally enhanced in inoculated pots. These patterns
2120 suggest that the increased downregulation of Narea under elevated CO₂ with in-
2121 creasing fertilization was not associated with a change in relative investment to
2122 photosynthetic tissue. Instead, a stronger downregulation in the fraction of leaf
2123 nitrogen allocated to structure under ambient CO₂ resulted in a stronger stim-
2124 ulation in $\rho_{\text{structure}}$ under elevated CO₂ with increasing fertilization (Fig. 5.3b),
2125 indicating that fertilization shifted relative investment in leaf structural tissue un-
2126 der elevated CO₂. These results, combined with a stimulation in PNUE (Fig. SX)
2127 and iWUE (Fig. SX) under elevated CO₂ that was independent of fertilization
2128 or inoculation treatment, provide additional support for the hypothesis that leaf
2129 acclimation photosynthetic responses to CO₂ were independent of fertilization;
2130 though fertilization may contribute to changes in leaf morphology under elevated
2131 CO₂ through shifts in M_{area} (Onoda et al. 2017; Wang et al. 2017; Dong et al.

2132 2022).

2133 The downregulation in N_{area} , V_{cmax25} , and J_{max25} under elevated CO₂ cor-
2134 responded with a respective 62% and 100% stimulation in total leaf area (Fig.
2135 5.4a) and total biomass (Fig. 5.4b). The stimulation in total leaf area and total
2136 biomass under elevated CO₂ also corresponded with generally higher structural
2137 carbon costs to acquire nitrogen (Fig. 5.4c), a pattern driven by a stimulation
2138 in belowground carbon biomass and reduction in whole plant nitrogen biomass.
2139 Alone, this result suggests that elevated CO₂ reduces plant nitrogen uptake effi-
2140 ciency, which does not explain why plants grown under elevated CO₂ generally had
2141 higher biomass and total leaf area. However, a strong negative effect of increasing
2142 fertilization on structural carbon costs to acquire nitrogen, which were generally
2143 similar between CO₂ concentrations, was driven by a stronger increase in whole
2144 plant nitrogen biomass than belowground carbon biomass. Thus, increases in the
2145 positive response of whole plant growth and total leaf area under elevated CO₂
2146 with increasing fertilization were likely driven by an increase in nitrogen uptake
2147 efficiency, allowing plants to satisfy any increase in whole plant nitrogen demand
2148 associated with increased CO₂.

2149 Interestingly, our results indicate that the general stimulation in total leaf
2150 area and whole plant growth under elevated CO₂ was not modified by inoculation
2151 despite an apparent general negative effect of inoculation on N_{cost} . This response
2152 could have been due to strong negative effect of increasing fertilization on nodu-
2153 lation (Fig. 5.5), which may have caused the strong increase in the positive effect
2154 of elevated CO₂ on whole plant growth with increasing fertilization to mask any
2155 increase in the positive effect of elevated CO₂ on whole plant growth due to in-

2156 inoculation. Reductions in nodulation with increasing fertilization are commonly
2157 observed patterns that have been inferred to be a response that allows species
2158 optimize nitrogen uptake efficiency as costs to acquire nitrogen via direct uptake
2159 become more similar (Fig. 5.4c) (Gibson and Harper 1985; Rastetter et al. 2001).
2160 In this study, pairwise comparisons indicated strong positive effects of inocula-
2161 tion on total leaf area and total biomass (158% increase in total leaf area, 119%
2162 increase in total biomass) under elevated CO₂ at 0 ppm N, but no observable
2163 inoculation effect on total leaf area or total biomass under elevated CO₂ at 350
2164 ppm N or 630 ppm N. While these responses did not generally differ from those
2165 observed under ambient CO₂, they do confirm our hypothesis that positive effects
2166 of inoculation on whole plant growth responses to elevated CO₂ would decrease
2167 with increasing fertilization.

2168 Combined, results reported here suggest that soil nitrogen availability has
2169 a divergent role in modifying leaf and whole plant acclimation responses to CO₂.
2170 Leaf acclimation responses were generally decoupled from fertilization, while whole
2171 plant acclimation responses relied heavily on an increase in nitrogen uptake ef-
2172 ficiency and consequent reduction in costs of acquiring nitrogen associated with
2173 increasing fertilization. However, whole plant responses to CO₂ indicated that fer-
2174 tilization may play a more important role in determining whole plant acclimation
2175 responses to CO₂ than nitrogen acquisition strategy, although these patterns were
2176 likely driven by reductions in nodulation with increasing fertilization. Our results
2177 suggest that plants acclimate to CO₂ in nitrogen-limited systems by minimizing
2178 the number of optimally coordinated leaves, and that the downregulation in leaf
2179 nitrogen content under elevated CO₂ is not a direct response to changes in soil

2180 nitrogen availability as previously implied.

2181 5.4.2 *Implications for future model development*

2182 Many terrestrial biosphere models predict photosynthetic capacity through
2183 plant functional group-specific linear regressions between N_{area} and V_{cmax} (Rogers
2184 2014; Rogers et al. 2017), which assumes that leaf nitrogen-photosynthesis rela-
2185 tionships are constant across growing environments. Our results build on previ-
2186 ous work suggesting that leaf nitrogen-photosynthesis relationships dynamically
2187 change across growing environments (Luo et al. 2021; Dong et al. 2022). Specif-
2188 ically, results from this experiment indicate that CO_2 concentration increased
2189 the fraction of leaf nitrogen content allocated to photosynthesis, while a general
2190 negative effect of increasing fertilization on the fraction of leaf nitrogen content
2191 allocated to photosynthesis was dependent on inoculation treatment. Similar in-
2192 creases in N_{area} , $V_{\text{cmax}25}$, and $J_{\text{max}25}$ with increasing fertilization resulted in no
2193 change in the fraction of leaf nitrogen allocated to photosynthesis in uninoculated
2194 pots, while larger increases in N_{area} than $V_{\text{cmax}25}$ and $J_{\text{max}25}$ with increasing fertil-
2195 ization decreased the fraction of leaf nitrogen allocated to photosynthesis in inoc-
2196 ulated pots (Fig. 5.3a). As inoculated pots were able to access less finite supply of
2197 nitrogen across the fertilization gradient, these patterns suggest that constant leaf
2198 nitrogen-photosynthesis relationships may only apply in environments where ni-
2199 trogen is limiting and will likely change with increasing CO_2 concentrations. Thus,
2200 terrestrial biosphere models that parameterize photosynthetic capacity through
2201 linear relationships between N_{area} and V_{cmax} (Rogers 2014; Rogers et al. 2017)
2202 may be overestimating photosynthetic capacity in systems where nitrogen is not

2203 as limiting and may contribute to erroneous model simulations under future CO₂
2204 concentrations.

2205 Our results also demonstrate that optimal resource investment to photo-
2206 synthetic capacity defines leaf acclimation responses to elevated CO₂, and that
2207 these responses were independent of fertilization or inoculation treatment. Cur-
2208 rent approaches for simulating photosynthetic responses to CO₂ generally invoke
2209 patterns expected from progressive nitrogen limitation, where the downregulation
2210 in N_{area} , and therefore photosynthetic capacity, due to elevated CO₂ are commonly
2211 a function of progressive reductions in soil nitrogen availability. Our results con-
2212 tradict this formulation, suggesting that the leaf acclimation response is driven
2213 by optimal resource investment to photosynthetic capacity and is independent
2214 of soil resource supply. Optimality models that leverage principles from optimal
2215 coordination and photosynthetic least-cost theories (Wang et al. 2017; Stocker
2216 et al. 2020; Scott and Smith 2022) are capable of capturing such acclimation re-
2217 sponses to CO₂ (Smith and Keenan 2020), suggesting that the implementation of
2218 these models may improve the simulation of photosynthetic processes in terrestrial
2219 biosphere models under increasing CO₂ concentrations.

2220 5.4.3 *Study limitations and future directions*

2221 There are two study limitations that must be addressed to contextualize
2222 patterns observed in this study. First, restricting the volume of belowground
2223 substrate via a potted experiment does not adequately replicate belowground en-
2224 vironments of natural systems, and therefore may modify effects of soil resource
2225 availability and inoculation on plant nitrogen uptake, particularly if pot size limits

2226 whole plant growth (Poorter et al. 2012). We attempted to minimize the extent
2227 of pot size limitation experienced in Perkowski et al. (2021) and account for the
2228 expected stimulation in whole plant growth under elevated CO₂ by using 6-liter
2229 pots. Despite attempts to minimize growth limitation imposed by pot volume, fer-
2230 tilization and CO₂ treatments increased the biomass: pot volume ratio such that
2231 all treatment combinations to exceed 1 g L⁻¹ biomass: pot volume under high
2232 fertilization. The 1 g L⁻¹ biomass: pot volume recommendation from Poorter
2233 et al. (2012) was designated to avoid growth limitation imposed by pot volume.
2234 However, if pot size limitation indeed limited whole plant growth, then structural
2235 carbon costs to acquire nitrogen, belowground carbon biomass, whole plant ni-
2236 trogen biomass, and whole plant biomass should each exhibit strong saturation
2237 points with increasing fertilization, which was not observed here. Additionally,
2238 a second set of photosynthetic measurements from one week prior to the harvest
2239 (6 weeks post-germination) revealed ... As pot limitation is expected to de-
2240 crease net photosynthesis, and focal leaves were of similar ages between the sixth
2241 and seventh week, one might expect growth limitation induced by constricted
2242 pot volume to result in a dampened effect of inoculation and fertilization on net
2243 photosynthesis, V_{cmax} , and J_{max25} . Analyses from the sixth week of development
2244 revealed ... Additionally, analyses revealed a stronger/weaker downregulation in
2245 V_{cmax25} and J_{max25} on week 7, though disentangling the causality of this response
2246 (i.e. whether due to pot size limitation or simply a stronger acclimation response)
2247 would be difficult.

2248 Second, this study evaluated leaf and whole plant responses to CO₂ in 7-
2249 week seedlings. Given the long-term scale of the progressive nitrogen limitation

2250 hypothesis, patterns observed here should be validated in longer-term nitrogen
2251 manipulation experiments. Previous work in free air CO₂ enrichment experiments
2252 show some support for patterns expected from the progressive nitrogen limitation
2253 hypothesis (Reich et al. 2006; Norby et al. 2010), although results are not consis-
2254 tent across experimental sites (Finzi et al. 2006; Moore et al. 2006; Liang et al.
2255 2016). We found some support for patterns expected by the progressive nitrogen
2256 limitation hypothesis, namely an increase in plant nitrogen uptake under elevated
2257 CO₂ (Luo et al. 2004), though leaf acclimation responses to CO₂ were strongly
2258 indicative of optimal resource investment to photosynthetic capacity as expected
2259 from photosynthetic least-cost theory (Prentice et al. 2014; Smith et al. 2019;
2260 Smith and Keenan 2020).

2261 5.4.4 *Conclusions*

2262 This study provides strong evidence suggesting that leaf acclimation re-
2263 sponds to elevated CO₂ did not vary with soil nitrogen fertilization or ability
2264 to acquire nitrogen through symbiotic nitrogen fixation. However, whole plant
2265 acclimation responses to CO₂ were dependent on fertilization, where increasing
2266 fertilization increased the positive effect of whole plant growth under elevated
2267 CO₂. Results also indicate that fertilization played a relatively more important
2268 role in modifying whole plant responses to CO₂, perhaps due to a reduction in
2269 nodulation across the fertilization gradient. These patterns strongly support the
2270 hypothesis that leaf and whole plant acclimation responses are driven by opti-
2271 mal resource investment to photosynthetic capacity, and that leaf acclimation
2272 responses to CO₂ were not modified by changes in soil nitrogen availability. Ad-

2273 ditionally, strong interactions between fertilization and inoculation on leaf and
2274 whole plant traits indicated positive effects of fertilization on leaf and whole plant
2275 traits in uninoculated pots, but null effects of fertilization on leaf and whole plant
2276 traits in inoculated pots. These results build on previous work suggesting that
2277 constant leaf nitrogen-photosynthesis relationships are dynamic and change across
2278 growing environments, calling the use of constant relationships by terrestrial bio-
2279 sphere models into question.

2280

Chapter 6

2281

Conclusions

2282 Experiments included in this dissertation leverage patterns expected from
2283 photosynthetic least-cost theory to investigate effects of soil resource availability
2284 and aboveground climate on costs of nitrogen acquisition, leaf nitrogen-water use
2285 tradeoffs, and plant acclimation responses to elevated CO₂. Photosynthetic least-
2286 cost theory provides a contemporary framework for understanding impacts of
2287 climatic and edaphic characteristics on plant ecophysiological processes, namely
2288 leaf nitrogen allocation and photosynthetic capacity. When I began planning
2289 experiments for this dissertation in August 2018,, empirical tests of the theory
2290 were sparse and model development was just beginning with a goal of eventually
2291 implementing the theory in terrestrial biosphere models. At the time, it was
2292 critical that experimentation be done to test underlying assumptions of the theory
2293 and validate its suitability for implementing in terrestrial biosphere models.

2294 Early iterations of model development held the unit cost of acquiring ni-
2295 trogen relative to water constant (Wang et al. 2017), in part because limited data
2296 existed to evaluate how this parameter changes across spatiotemporal scales and
2297 different environmental gradients. However, the Fixation and Uptake of Nitrogen
2298 model (Fisher et al. 2010; Brzostek et al. 2014) indicates that costs of nitro-
2299 gen acquisition decreased with increasing soil nitrogen availability and varies in
2300 species with different nitrogen acquisition strategies, suggesting that the unit cost
2301 of acquiring nitrogen relative to water should change across nitrogen availability
2302 gradients. Additionally,

2303 All experimental chapters in this dissertation provide strong and consist-
2304 ent support for patterns expected from the theory across different experimental
2305 approaches, spatiotemporal scales, and different plant functional groups. In this
2306 chapter, I first summarize experimental approaches and primary findings of each
2307 experimental chapter. Then, I use findings from the four experimental chapters
2308 to synthesize recommendations for future photosynthetic least-cost theory model
2309 development, and propose experiments that will allow for further understanding
2310 of mechanisms that drive patterns expected from photosynthetic least-cost theory
2311 across environmental gradients.

2312

References

- 2313** Abrams, M. D. and S. A. Mostoller (1995). Gas exchange, leaf structure and
2314 nitrogen in contrasting successional tree species growing in open and under-
2315 story sites during a drought. *Tree Physiology* 15(6), 361–370.
- 2316** Adams, M. A., T. L. Turnbull, J. I. Sprent, and N. Buchmann (2016). Legumes
2317 are different: Leaf nitrogen, photosynthesis, and water use efficiency. *Pro-
2318 ceedings of the National Academy of Sciences of the United States of Amer-
2319 ica* 113(15), 4098–4103.
- 2320** Ainsworth, E. A., P. A. Davey, C. J. Bernacchi, O. C. Dermody, E. A. Heaton,
2321 D. J. Moore, P. B. Morgan, S. L. Naidu, H. S. Y. Ra, X. G. Zhu, P. S. Curtis,
2322 and S. P. Long (2002). A meta-analysis of elevated [CO₂] effects on soybean
2323 (*Glycine max*) physiology, growth and yield. *Global Change Biology* 8(8),
2324 695–709.
- 2325** Ainsworth, E. A. and S. P. Long (2005). What have we learned from 15 years of
2326 free-air CO₂ enrichment (FACE)? A meta-analytic review of the responses
2327 of photosynthesis, canopy properties and plant production to rising CO₂.
2328 *New Phytologist* 165(2), 351–372.
- 2329** Ainsworth, E. A. and A. Rogers (2007). The response of photosynthesis and
2330 stomatal conductance to rising [CO₂]: mechanisms and environmental in-
2331 teractions. *Plant, Cell and Environment* 30(3), 258–270.
- 2332** Allen, K., J. B. Fisher, R. P. Phillips, J. S. Powers, and E. R. Brzostek (2020).
2333 Modeling the carbon cost of plant nitrogen and phosphorus uptake across
2334 temperate and tropical forests. *Frontiers in Forests and Global Change* 3,

- 2335 1–12.
- 2336 Allison, S. D., C. I. Czimczik, and K. K. Treseder (2008). Microbial activity
2337 and soil respiration under nitrogen addition in Alaskan boreal forest. *Global
2338 Change Biology* 14(5), 1156–1168.
- 2339 Andersen, M. K., H. Hauggaard-Nielsen, P. Ambus, and E. S. Jensen (2005).
2340 Biomass production, symbiotic nitrogen fixation and inorganic N use in dual
2341 and tri-component annual intercrops. *Plant and Soil* 266(1-2), 273–287.
- 2342 Andrews, M., E. K. James, J. I. Sprent, R. M. Boddey, E. Gross, and F. B. dos
2343 Reis (2011). Nitrogen fixation in legumes and actinorhizal plants in natural
2344 ecosystems: Values obtained using ^{15}N natural abundance. *Plant Ecology
2345 and Diversity* 4(2-3), 117–130.
- 2346 Arndal, M. F., A. Tolver, K. S. Larsen, C. Beier, and I. K. Schmidt (2018). Fine
2347 root growth and vertical distribution in response to elevated CO₂, warming
2348 and drought in a mixed heathland–grassland. *Ecosystems* 21(1), 15–30.
- 2349 Arnone, J. A. (1997). Indices of plant N availability in an alpine grassland under
2350 elevated atmospheric CO₂. *Plant and Soil* 190(1), 61–66.
- 2351 Arora, V. K., A. Katavouta, R. G. Williams, C. D. Jones, V. Brovkin,
2352 P. Friedlingstein, J. Schwinger, L. Bopp, O. Boucher, P. Cadule, M. A.
2353 Chamberlain, J. R. Christian, C. Delire, R. A. Fisher, T. Hajima, T. Ilyina,
2354 E. Joetzjer, M. Kawamiya, C. D. Koven, J. P. Krasting, R. M. Law, D. M.
2355 Lawrence, A. Lenton, K. Lindsay, J. Pongratz, T. Raddatz, R. Séférian,
2356 K. Tachiiri, J. F. Tjiputra, A. Wiltshire, T. Wu, and T. Ziehn (2020).
2357 Carbon-concentration and carbon-climate feedbacks in CMIP6 models and
2358 their comparison to CMIP5 models. *Biogeosciences* 17(16), 4173–4222.

- 2359 Bae, K., T. J. Fahey, R. D. Yanai, and M. Fisk (2015). Soil nitrogen availabil-
2360 ity affects belowground carbon allocation and soil respiration in northern
2361 hardwood forests of New Hampshire. *Ecosystems* 18(7), 1179–1191.
- 2362 Barber, S. A. (1962). A diffusion and mass-flow concept of soil nutrient avail-
2363 ability. *Soil Science* 93(1), 39–49.
- 2364 Barnes, J. D., L. Balaguer, E. Manrique, S. Elvira, and A. W. Davison (1992).
2365 A reappraisal of the use of DMSO for the extraction and determination
2366 of chlorophylls a and b in lichens and higher plants. *Environmental and*
2367 *Experimental Botany* 32(2), 85–100.
- 2368 Bates, D., M. Mächler, B. Bolker, and S. Walker (2015). Fitting linear mixed-
2369 effects models using lme4. *Journal of Statistical Software* 67(1), 1–48.
- 2370 Beaudette, D., J. Skovlin, S. Roeker, and A. Brown (2022). soilDB: Soil
2371 Database Interface.
- 2372 Bengtson, P., J. Barker, and S. J. Grayston (2012). Evidence of a strong cou-
2373 pling between root exudation, C and N availability, and stimulated SOM
2374 decomposition caused by rhizosphere priming effects. *Ecology and Evolu-*
2375 *tion* 93(8), 1843–1852.
- 2376 Bernacchi, C. J., E. L. Singsaas, C. Pimentel, A. R. Portis, and S. P. Long
2377 (2001). Improved temperature response functions for models of Rubisco-
2378 limited photosynthesis. *Plant, Cell and Environment* 24(2), 253–259.
- 2379 Bialic-Murphy, L., N. G. Smith, P. Voothuluru, R. M. McElderry, M. D.
2380 Roche, S. T. Cassidy, S. N. Kivlin, and S. Kalisz (2021). Invasion-induced
2381 root–fungal disruptions alter plant water and nitrogen economies. *Ecology*

- 2382** *Letters* 24(6), 1145–1156.
- 2383** Bloom, A. J., F. S. Chapin, and H. A. Mooney (1985). Resource limitation
- 2384** in plants - an economic analogy. *Annual Review of Ecology and Systemat-*
- 2385** *ics* 16(1), 363–392.
- 2386** Bloomfield, K. J., B. D. Stocker, T. F. Keenan, and I. C. Prentice (2022).
- 2387** Environmental controls on the light use efficiency of terrestrial gross primary
- 2388** production. *Global Change Biology*, 0–2.
- 2389** Bonan, G. B., M. D. Hartman, W. J. Parton, and W. R. Wieder (2013). Evaluat-
- 2390** ing litter decomposition in earth system models with long-term litterbag ex-
- 2391** periments: an example using the Community Land Model version 4 (CLM4).
- 2392** *Global Change Biology* 19(3), 957–974.
- 2393** Bonan, G. B., P. J. Lawrence, K. W. Oleson, S. Levis, M. Jung, M. Reich-
- 2394** stein, D. M. Lawrence, and S. C. Swenson (2011). Improving canopy pro-
- 2395** cesses in the Community Land Model version 4 (CLM4) using global flux
- 2396** fields empirically inferred from FLUXNET data. *Journal of Geophysical Re-*
- 2397** *search* 116(G2), G02014.
- 2398** Booth, B. B. B., C. D. Jones, M. Collins, I. J. Totterdell, P. M. Cox, S. Sitch,
- 2399** C. Huntingford, R. A. Betts, G. R. Harris, and J. Lloyd (2012). High sen-
- 2400** sitivity of future global warming to land carbon cycle processes. *Environ-*
- 2401** *mental Research Letters* 7(2), 024002.
- 2402** Borer, E. T., W. S. Harpole, P. B. Adler, E. M. Lind, J. L. Orrock, E. W.
- 2403** Seabloom, and M. D. Smith (2014). Finding generality in ecology: A model
- 2404** for globally distributed experiments. *Methods in Ecology and Evolution* 5(1),
- 2405** 65–73.

- 2406** Braghieri, R. K., J. B. Fisher, K. Allen, E. Brzostek, M. Shi, X. Yang, D. M.
- 2407** Ricciuto, R. A. Fisher, Q. Zhu, and R. P. Phillips (2022). Modeling global
- 2408** carbon costs of plant nitrogen and phosphorus acquisition. *Journal of Ad-*
- 2409** *vances in Modeling Earth Systems* 14(8), 1–23.
- 2410** Brix, H. (1971). Effects of nitrogen fertilization on photosynthesis and respi-
- 2411** ration in Douglas-fir. *Forest Science* 17(4), 407–414.
- 2412** Brzostek, E. R., J. B. Fisher, and R. P. Phillips (2014). Modeling the carbon
- 2413** cost of plant nitrogen acquisition: Mycorrhizal trade-offs and multipath
- 2414** resistance uptake improve predictions of retranslocation. *Journal of Geo-*
- 2415** *physical Research: Biogeosciences* 119, 1684–1697.
- 2416** Bubier, J. L., R. Smith, S. Juutinen, T. R. Moore, R. Minocha, S. Long, and
- 2417** S. Minocha (2011). Effects of nutrient addition on leaf chemistry, morphol-
- 2418** ogy, and photosynthetic capacity of three bog shrubs. *Oecologia* 167(2),
- 2419** 355–368.
- 2420** Cernusak, L. A., N. Ubierna, K. Winter, J. A. M. Holtum, J. D. Marshall, and
- 2421** G. D. Farquhar (2013). Environmental and physiological determinants of
- 2422** carbon isotope discrimination in terrestrial plants. *New Phytologist* 200(4),
- 2423** 950–965.
- 2424** Chen, J.-L., J. F. Reynolds, P. C. Harley, and J. D. Tenhunen (1993). Coor-
- 2425** dination theory of leaf nitrogen distribution in a canopy. *Oecologia* 93(1),
- 2426** 63–69.
- 2427** Clark, D. B., L. M. Mercado, S. Sitch, C. D. Jones, N. Gedney, M. J. Best,
- 2428** M. Pryor, G. G. Rooney, R. L. H. Essery, E. Blyth, O. Boucher, R. J.
- 2429** Harding, C. Huntingford, and P. M. Cox (2011). The Joint UK Land Envi-

- 2430** ronment Simulator (JULES), model description. Part 2: Carbon fluxes and
2431 vegetation dynamics. *Geoscientific Model Development* 4(3), 701–722.
- 2432** Cornwell, W. K., J. H. C. Cornelissen, K. Amatangelo, E. Dorrepaal, V. T.
2433 Eviner, O. Godoy, S. E. Hobbie, B. Hoorens, H. Kurokawa, N. Pérez-
2434 Harguindeguy, H. M. Quested, L. S. Santiago, D. A. Wardle, I. J. Wright,
2435 R. Aerts, S. D. Allison, P. van Bodegom, V. Brovkin, A. Chatain, T. V.
2436 Callaghan, S. Díaz, E. Garnier, D. E. Gurvich, E. Kazakou, J. A. Klein,
2437 J. Read, P. B. Reich, N. A. Soudzilovskaia, M. V. Vaieretti, and M. Westoby
2438 (2008). Plant species traits are the predominant control on litter decompo-
2439 sition rates within biomes worldwide. *Ecology Letters* 11(10), 1065–1071.
- 2440** Cornwell, W. K., I. J. Wright, J. Turner, V. Maire, M. M. Barbour, L. A.
2441 Cernusak, T. E. Dawson, D. S. Ellsworth, G. D. Farquhar, H. Griffiths,
2442 C. Keitel, A. Knohl, P. B. Reich, D. G. Williams, R. Bhaskar, J. H. C. Cor-
2443 nelissen, A. Richards, S. Schmidt, F. Valladares, C. Körner, E.-D. Schulze,
2444 N. Buchmann, and L. S. Santiago (2018). Climate and soils together regulate
2445 photosynthetic carbon isotope discrimination within C₃ plants worldwide.
2446 *Global Ecology and Biogeography* 27(9), 1056–1067.
- 2447** Cramer, W. and I. C. Prentice (1988). Simulation of regional soil moisture
2448 deficits on a European scale. *Norsk Geografisk Tidsskrift - Norwegian Jour-
2449 nal of Geography* 42(2-3), 149–151.
- 2450** Curtis, P. S. (1996). A meta-analysis of leaf gas exchange and nitrogen in trees
2451 grown under elevated carbon dioxide. *Plant, Cell and Environment* 19(2),
2452 127–137.
- 2453** Daly, C., M. Halbleib, J. I. Smith, W. P. Gibson, M. K. Doggett, G. H. Taylor,

- 2454** J. Curtis, and P. P. Pasteris (2008). Physiographically sensitive mapping
2455 of climatological temperature and precipitation across the conterminous
2456 United States. *International Journal of Climatology* 28(15), 2031–2064.
- 2457** Davies-Barnard, T., J. Meyerholt, S. Zaehle, P. Friedlingstein, V. Brovkin,
2458 Y. Fan, R. A. Fisher, C. D. Jones, H. Lee, D. Peano, B. Smith, D. Wårlind,
2459 and A. J. Wiltshire (2020). Nitrogen cycling in CMIP6 land surface models:
2460 progress and limitations. *Biogeosciences* 17(20), 5129–5148.
- 2461** Davis, T. W., I. C. Prentice, B. D. Stocker, R. T. Thomas, R. J. Whitley,
2462 H. Wang, B. J. Evans, A. V. Gallego-Sala, M. T. Sykes, and W. Cramer
2463 (2017). Simple process-led algorithms for simulating habitats (SPLASH
2464 v.1.0): robust indices of radiation, evapotranspiration and plant-available
2465 moisture. *Geoscientific Model Development* 10, 689–708.
- 2466** Delaire, M., E. Frak, M. Sigogne, B. Adam, F. Beaujard, and X. Le Roux
2467 (2005). Sudden increase in atmospheric CO₂ concentration reveals strong
2468 coupling between shoot carbon uptake and root nutrient uptake in young
2469 walnut trees. *Tree Physiology* 25(2), 229–235.
- 2470** Doane, T. A. and W. R. Horwáth (2003). Spectrophotometric determination of
2471 nitrate with a single reagent. *Analytical Letters* 36(12), 2713–2722.
- 2472** Dong, N., I. C. Prentice, B. J. Evans, S. Caddy-Retalic, A. J. Lowe, and I. J.
2473 Wright (2017). Leaf nitrogen from first principles: field evidence for adaptive
2474 variation with climate. *Biogeosciences* 14(2), 481–495.
- 2475** Dong, N., I. C. Prentice, I. J. Wright, B. J. Evans, H. F. Togashi, S. Caddy-
2476 Retalic, F. A. McInerney, B. Sparrow, E. Leitch, and A. J. Lowe (2020).
2477 Components of leaf-trait variation along environmental gradients. *New Phy-*

- 2478** *tologist* 228(1), 82–94.
- 2479** Dong, N., I. C. Prentice, I. J. Wright, H. Wang, O. K. Atkin, K. J. Bloomfield,
2480 T. F. Domingues, S. M. Gleason, V. Maire, Y. Onoda, H. Poorter, and N. G.
2481 Smith (2022). Leaf nitrogen from the perspective of optimal plant function.
2482 *Journal of Ecology* 110(11), 2585–2602.
- 2483** Dong, N., I. J. Wright, J. M. Chen, X. Luo, H. Wang, T. F. Keenan, N. G.
2484 Smith, and I. C. Prentice (2022). Rising CO₂ and warming reduce global
2485 canopy demand for nitrogen. *New Phytologist* 235(5), 1692–1700.
- 2486** Dovrat, G., H. Bakhshian, T. Masci, and E. Sheffer (2020). The nitrogen eco-
2487 nomic spectrum of legume stoichiometry and fixation strategy. *New Phytol-
ogist* 227(2), 365–375.
- 2489** Dovrat, G., T. Masci, H. Bakhshian, E. Mayzlish Gati, S. Golan, and E. Shef-
2490 fer (2018). Drought-adapted plants dramatically downregulate dinitrogen
2491 fixation: Evidences from Mediterranean legume shrubs. *Journal of Ecol-
ogy* 106(4), 1534–1544.
- 2493** Drake, B. G., M. A. González-Meler, and S. P. Long (1997). More efficient
2494 plants: a consequence of rising atmospheric CO₂? *Annual Review of Plant
Biology* 48, 609–639.
- 2496** Duursma, R. A. (2015). Plantecophys - An R Package for Analysing and Mod-
2497 elling Leaf Gas Exchange Data. *PLOS ONE* 10(11), e0143346.
- 2498** Eastman, B. A., M. B. Adams, E. R. Brzostek, M. B. Burnham, J. E. Carrara,
2499 C. Kelly, B. E. McNeil, C. A. Walter, and W. T. Peterjohn (2021). Altered
2500 plant carbon partitioning enhanced forest ecosystem carbon storage after 25

- 2501 years of nitrogen additions. *New Phytologist* 230(4), 1435–1448.
- 2502 Ellsworth, D. S. and P. B. Reich (1996). Photosynthesis and leaf nitrogen in five
- 2503 Amazonian tree species during early secondary succession. *Ecology* 77(2),
- 2504 581–594.
- 2505 Espelta, J. M., P. Cortés, M. Mangirón, and J. Retana (2005). Differences in
- 2506 biomass partitioning, leaf nitrogen content, and water use efficiency d13C
- 2507 result in similar performance of seedlings of two Mediterranean oaks with
- 2508 contrasting leaf habit. *Ecoscience* 12(4), 447–454.
- 2509 Evans, J. R. (1989). Photosynthesis and nitrogen relationships in leaves of C₃
- 2510 plants. *Oecologia* 78(1), 9–19.
- 2511 Evans, J. R. and V. C. Clarke (2019). The nitrogen cost of photosynthesis.
- 2512 *Journal of Experimental Botany* 70(1), 7–15.
- 2513 Evans, J. R. and H. Poorter (2001). Photosynthetic acclimation of plants to
- 2514 growth irradiance: the relative importance of specific leaf area and nitrogen
- 2515 partitioning in maximizing carbon gain. *Plant, Cell and Environment* 24(8),
- 2516 755–767.
- 2517 Evans, J. R. and J. R. Seemann (1989). The allocation of protein nitrogen in
- 2518 the photosynthetic apparatus: costs, consequences, and control. *Photosyn-*
- 2519 *thesis* 8, 183–205.
- 2520 Exbrayat, J.-F., A. A. Bloom, P. Falloon, A. Ito, T. L. Smallman, and
- 2521 M. Williams (2018). Reliability ensemble averaging of 21st century projec-
- 2522 tions of terrestrial net primary productivity reduces global and regional
- 2523 uncertainties. *Earth System Dynamics* 9(1), 153–165.

- 2524 Farquhar, G. D., J. R. Ehleringer, and K. T. Hubick (1989). Carbon Isotope
2525 Discrimination and Photosynthesis. *Annual Review of Plant Physiology and*
2526 *Plant Molecular Biology* 40(1), 503–537.
- 2527 Farquhar, G. D. and T. D. Sharkey (1982). Stomatal conductance and photo-
2528 synthesis. *Annual Review of Plant Physiology* 33(1), 317–345.
- 2529 Farquhar, G. D., S. von Caemmerer, and J. A. Berry (1980). A biochemical
2530 model of photosynthetic CO₂ assimilation in leaves of C₃ species.
2531 *Planta* 149(1), 78–90.
- 2532 Fay, P. A., S. M. Prober, W. S. Harpole, J. M. H. Knops, J. D. Bakker, E. T.
2533 Borer, E. M. Lind, A. S. MacDougall, E. W. Seabloom, P. D. Wragg, P. B.
2534 Adler, D. M. Blumenthal, Y. M. Buckley, C. Chu, E. E. Cleland, S. L.
2535 Collins, K. F. Davies, G. Du, X. Feng, J. Firn, D. S. Gruner, N. Hagenah,
2536 Y. Hautier, R. W. Heckman, V. L. Jin, K. P. Kirkman, J. A. Klein, L. M.
2537 Ladwig, Q. Li, R. L. McCulley, B. A. Melbourne, C. E. Mitchell, J. L. Moore,
2538 J. W. Morgan, A. C. Risch, M. Schütz, C. J. Stevens, D. A. Wedin, and
2539 L. H. Yang (2015). Grassland productivity limited by multiple nutrients.
2540 *Nature Plants* 1(7), 15080.
- 2541 Feng, X. (1999). Trends in intrinsic water-use efficiency of natural trees for the
2542 past 100-200 years: A response to atmospheric CO₂ concentration. *Geochim-
2543 ica et Cosmochimica Acta* 63(13-14), 1891–1903.
- 2544 Field, C. B. and H. A. Mooney (1986). The photosynthesis-nitrogen relationship
2545 in wild plants. In T. J. Givnish (Ed.), *On the Economy of Plant Form and*
2546 *Function*, pp. 25–55. Cambridge: Cambridge University Press.
- 2547 Finzi, A. C., D. J. P. Moore, E. H. DeLucia, J. Lichter, K. S. Hofmockel, R. B.

- 2548 Jackson, H. S. Kim, R. Matamala, H. R. McCarthy, R. Oren, J. S. Pippen,
2549 and W. H. Schlesinger (2006). Progressive nitrogen limitation of ecosystem
2550 processes under elevated CO₂ in a warm-temperate forest. *Ecology* 87(1),
2551 15–25.
- 2552 Firn, J., J. M. McGree, E. Harvey, H. Flores Moreno, M. Schutz, Y. M. Buckley,
2553 E. T. Borer, E. W. Seabloom, K. J. La Pierre, A. M. MacDougall, S. M.
2554 Prober, C. J. Stevens, L. L. Sullivan, E. Porter, E. Ladouceur, C. Allen,
2555 K. H. Moromizato, J. W. Morgan, W. S. Harpole, Y. Hautier, N. Eisen-
2556 hauer, J. P. Wright, P. B. Adler, C. A. Arnillas, J. D. Bakker, L. Biederman,
2557 A. A. D. Broadbent, C. S. Brown, M. N. Bugalho, M. C. Caldeira, E. E. Cle-
2558 land, A. Ebeling, P. A. Fay, N. Hagenah, A. R. Kleinhesselink, R. Mitchell,
2559 J. L. Moore, C. Nogueira, P. L. Peri, C. Roscher, M. D. Smith, P. D. Wragg,
2560 and A. C. Risch (2019). Leaf nutrients, not specific leaf area, are consistent
2561 indicators of elevated nutrient inputs. *Nature Ecology and Evolution* 3(3),
2562 400–406.
- 2563 Fisher, J. B., S. Sitch, Y. Malhi, R. A. Fisher, C. Huntingford, and S.-Y. Tan
2564 (2010). Carbon cost of plant nitrogen acquisition: A mechanistic, globally
2565 applicable model of plant nitrogen uptake, retranslocation, and fixation.
2566 *Global Biogeochemical Cycles* 24(1), 1–17.
- 2567 Fox, J. and S. Weisberg (2019). *An R companion to applied regression* (Third
2568 edit ed.). Thousand Oaks, California: Sage.
- 2569 Franklin, O., R. E. McMurtrie, C. M. Iversen, K. Y. Crous, A. C. Finzi, D. Tis-
2570 sue, D. S. Ellsworth, R. Oren, and R. J. Norby (2009). Forest fine-root
2571 production and nitrogen use under elevated CO₂: contrasting responses

- 2572 in evergreen and deciduous trees explained by a common principle. *Global*
2573 *Change Biology* 15(1), 132–144.
- 2574 Friedlingstein, P., M. Meinshausen, V. K. Arora, C. D. Jones, A. Anav, S. K.
2575 Liddicoat, and R. Knutti (2014). Uncertainties in CMIP5 climate projections
2576 due to carbon cycle feedbacks. *Journal of Climate* 27(2), 511–526.
- 2577 Friel, C. A. and M. L. Friesen (2019). Legumes modulate allocation to rhizobial
2578 nitrogen fixation in response to factorial light and nitrogen manipulation.
2579 *Frontiers in Plant Science* 10, 1316.
- 2580 Fujikake, H., A. Yamazaki, N. Ohtake, K. Sueoshi, S. Matsuhashi, T. Ito,
2581 C. Mizuniwa, T. Kume, S. Hoshimoto, N.-S. Ishioka, S. Watanabe, A. Osa,
2582 T. Sekine, H. Uchida, A. Tsuji, and T. Ohyama (2003). Quick and reversible
2583 inhibition of soybean root nodule growth by nitrate involves a decrease in
2584 sucrose supply to nodules. *Journal of Experimental Botany* 54(386), 1379–
2585 1388.
- 2586 Ghimire, B., W. J. Riley, C. D. Koven, J. Kattge, A. Rogers, P. B. Reich, and
2587 I. J. Wright (2017). A global trait-based approach to estimate leaf nitro-
2588 gen functional allocation from observations:. *Ecological Applications* 27(5),
2589 1421–1434.
- 2590 Giardina, C. P., M. D. Coleman, J. E. Hancock, J. S. King, E. A. Lilleskov,
2591 W. M. Loya, K. S. Pregitzer, M. G. Ryan, and C. C. Trettin (2005). The
2592 response of belowground carbon allocation in forests to global change. In
2593 D. Binkley and O. Manyailo (Eds.), *Tree Species Effects on Soils: Implica-*
2594 *tions for Global Change* (Volume 55 ed.), Chapter Chapter 7, pp. 119–154.
2595 Berlin/Heidelberg: Springer-Verlag.

- 2596 Gibson, A. H. and J. E. Harper (1985). Nitrate effect on nodulation of soybean
2597 by *Bradyrhizobium japonicum*. *Crop Science* 25(3), 497–501.
- 2598 Gill, A. L. and A. C. Finzi (2016). Belowground carbon flux links biogeochemical
2599 cycles and resource-use efficiency at the global scale. *Ecology Letters* 19(12),
2600 1419–1428.
- 2601 Goll, D. S., V. Brovkin, B. R. Parida, C. H. Reick, J. Kattge, P. B. Reich, P. M.
2602 van Bodegom, and Ü. Niinemets (2012). Nutrient limitation reduces land
2603 carbon uptake in simulations with a model of combined carbon, nitrogen
2604 and phosphorus cycling. *Biogeosciences Discussions* 9(3), 3173–3232.
- 2605 Gregory, L. M., A. M. McClain, D. M. Kramer, J. D. Pardo, K. E. Smith, O. L.
2606 Tessmer, B. J. Walker, L. G. Ziccardi, and T. D. Sharkey (2021, oct). The
2607 triose phosphate utilization limitation of photosynthetic rate: Out of global
2608 models but important for leaf models. *Plant, Cell and Environment* 44(10),
2609 3223–3226.
- 2610 Guerrieri, R., M. Mencuccini, L. J. Sheppard, M. Saurer, M. P. Perks, P. Levy,
2611 M. A. Sutton, M. Borghetti, and J. Grace (2011). The legacy of enhanced
2612 N and S deposition as revealed by the combined analysis of $\delta^{13}\text{C}$, $\delta^{18}\text{O}$ and
2613 $\delta^{15}\text{N}$ in tree rings. *Global Change Biology* 17(5), 1946–1962.
- 2614 Gulmon, S. L. and C. C. Chu (1981). The effects of light and nitrogen on pho-
2615 tosynthesis, leaf characteristics, and dry matter allocation in the chaparral
2616 shrub, <i>Diplacus aurantiacus</i>. *Oecologia* 49(2), 207–212.
- 2617 Gutschick, V. P. (1981). Evolved strategies in nitrogen acquisition by plants.
2618 *The American Naturalist* 118(5), 607–637.

- 2619** Hallik, L., Ü. Niinemets, and I. J. Wright (2009). Are species shade and drought
2620 tolerance reflected in leaf-level structural and functional differentiation in
2621 Northern Hemisphere temperate woody flora? *New Phytologist* 184(1), 257–
2622 274.
- 2623** Harrison, M. T., E. J. Edwards, G. D. Farquhar, A. B. Nicotra, and J. R.
2624 Evans (2009). Nitrogen in cell walls of sclerophyllous leaves accounts for
2625 little of the variation in photosynthetic nitrogen-use efficiency. *Plant, Cell
and Environment* 32(3), 259–270.
- 2627** Harrison, S. P., W. Cramer, O. Franklin, I. C. Prentice, H. Wang,
2628 Å. Bränström, H. de Boer, U. Dieckmann, J. Joshi, T. F. Keenan,
2629 A. Lavergne, S. Manzoni, G. Mengoli, C. Morfopoulos, J. Peñuelas,
2630 S. Pietsch, K. T. Rebel, Y. Ryu, N. G. Smith, B. D. Stocker, and I. J.
2631 Wright (2021). Eco-evolutionary optimality as a means to improve vegeta-
2632 tion and land-surface models. *New Phytologist* 231(6), 2125–2141.
- 2633** Henneron, L., P. Kardol, D. A. Wardle, C. Cros, and S. Fontaine (2020). Rhizo-
2634 sphere control of soil nitrogen cycling: a key component of plant economic
2635 strategies. *New Phytologist* 228(4), 1269–1282.
- 2636** Hijmans, R. J. (2022). terra: Spatial Data Analysis.
- 2637** Hikosaka, K. and A. Shigeno (2009). The role of Rubisco and cell walls in the
2638 interspecific variation in photosynthetic capacity. *Oecologia* 160(3), 443–
2639 451.
- 2640** Hoagland, D. R. and D. I. Arnon (1950). The water culture method for growing
2641 plants without soil. *California Agricultural Experiment Station: 347* 347(2),
2642 1–32.

- 2643** Hobbie, E. A. (2006). Carbon allocation to ectomycorrhizal fungi correlates
2644 with belowground allocation in culture studies. *Ecology* 87(3), 563–569.
- 2645** Hobbie, E. A. and J. E. Hobbie (2008). Natural abundance of ^{15}N in nitrogen-
2646 limited forests and tundra can estimate nitrogen cycling through mycorrhizal
2647 fungi: a review. *Ecosystems* 11(5), 815–830.
- 2648** Hoek, T. A., K. Axelrod, T. Biancalani, E. A. Yurtsev, J. Liu, and J. Gore
2649 (2016). Resource availability modulates the cooperative and competitive na-
2650 nature of a microbial cross-feeding mutualism. *PLOS Biology* 14(8), e1002540.
- 2651** Höglberg, M. N., M. J. I. Briones, S. G. Keel, D. B. Metcalfe, C. Campbell, A. J.
2652 Midwood, B. Thornton, V. Hurry, S. Linder, T. Näsholm, and P. Höglberg
2653 (2010). Quantification of effects of season and nitrogen supply on tree below-
2654 ground carbon transfer to ectomycorrhizal fungi and other soil organisms in
2655 a boreal pine forest. *New Phytologist* 187(2), 485–493.
- 2656** Höglberg, P., M. N. Höglberg, S. G. Göttlicher, N. R. Betson, S. G. Keel, D. B.
2657 Metcalfe, C. Campbell, A. Schindlbacher, V. Hurry, T. Lundmark, S. Linder,
2658 and T. Näsholm (2008). High temporal resolution tracing of photosynthate
2659 carbon from the tree canopy to forest soil microorganisms. *New Phytolo-*
2660 *gist* 177(1), 220–228.
- 2661** Houlton, B. Z., Y.-P. Wang, P. M. Vitousek, and C. B. Field (2008). A uni-
2662 fying framework for dinitrogen fixation in the terrestrial biosphere. *Nature*
2663 454(7202), 327–330.
- 2664** Huber, M. L., R. A. Perkins, A. Laesecke, D. G. Friend, J. V. Sengers, M. J.
2665 Assael, I. N. Metaxa, E. Vogel, R. Mareš, and K. Miyagawa (2009). New
2666 international formulation for the viscosity of H₂O. *Journal of Physical and*

- 2667** *Chemical Reference Data* 38(2), 101–125.
- 2668** Hungate, B. A., J. S. Dukes, M. R. Shaw, Y. Luo, and C. B. Field (2003).
- 2669** Nitrogen and climate change. *Science* 302(5650), 1512–1513.
- 2670** IPCC (2021). *Climate Change 2021: The Physical Science Basis. Contribution of Working Group I to the Sixth Assessment Report of the Intergovernmental Panel on Climate Change*. Cambridge University Press.
- 2673** Johnson, N. C., J. H. Graham, and F. A. Smith (1997). Functioning of mycorrhizal associations along the mutualism-parasitism continuum. *New Phytologist* 135(4), 575–585.
- 2674**
- 2675**
- 2676** Kachurina, O. M., H. Zhang, W. R. Raun, and E. G. Krenzer (2000). Simultaneous determination of soil aluminum, ammonium- and nitrate- nitrogen using 1 M potassium chloride. *Communications in Soil Science and Plant Analysis* 31(7-8), 893–903.
- 2677**
- 2678**
- 2679**
- 2680** Kaiser, C., M. R. Kilburn, P. L. Clode, L. Fuchslueger, M. Koranda, J. B. Cliff, Z. M. Solaiman, and D. V. Murphy (2015). Exploring the transfer of recent plant photosynthates to soil microbes: mycorrhizal pathway vs direct root exudation. *New Phytologist* 205(4), 1537–1551.
- 2684** Katabuchi, M. (2015). LeafArea: An R package for rapid digital analysis of leaf area. *Ecological Research* 30(6), 1073–1077.
- 2685**
- 2686** Kattge, J. and W. Knorr (2007). Temperature acclimation in a biochemical model of photosynthesis: a reanalysis of data from 36 species. *Plant, Cell and Environment* 30(9), 1176–1190.
- 2688**
- 2689** Kattge, J., W. Knorr, T. Raddatz, and C. Wirth (2009). Quantifying photosyn-

- 2690 thetic capacity and its relationship to leaf nitrogen content for global-scale
2691 terrestrial biosphere models. *Global Change Biology* 15(4), 976–991.
- 2692 Kayler, Z., A. Gessler, and N. Buchmann (2010). What is the speed of link
2693 between aboveground and belowground processes? *New Phytologist* 187(4),
2694 885–888.
- 2695 Kayler, Z., C. Keitel, K. Jansen, and A. Gessler (2017). Experimental evi-
2696 dence of two mechanisms coupling leaf-level C assimilation to rhizosphere
2697 CO₂ release. *Environmental and Experimental Botany* 135,
2698 21–26.
- 2699 Keeling, C. D., W. G. Mook, and P. P. Tans (1979, jan). Recent trends in the
2700 ¹³C/¹²C ratio of atmospheric carbon dioxide.
2701 *Nature* 277(5692), 121–123.
- 2702 Kenward, M. G. and J. H. Roger (1997). Small sample inference for fixed effects
2703 from restricted maximum likelihood. *Biometrics* 53(3), 983.
- 2704 Knapp, A. K., M. L. Avolio, C. Beier, C. J. W. Carroll, S. L. Collins, J. S.
2705 Dukes, L. H. Fraser, R. J. Griffin-Nolan, D. L. Hoover, A. Jentsch, M. E.
2706 Loik, R. P. Phillips, A. K. Post, O. E. Sala, I. J. Slette, L. Yahdjian, and
2707 M. D. Smith (2017). Pushing precipitation to the extremes in distributed
2708 experiments: recommendations for simulating wet and dry years. *Global
2709 Change Biology* 23(5), 1774–1782.
- 2710 Knorr, W. (2000). Annual and interannual CO₂ exchanges of the
2711 terrestrial biosphere: process-based simulations and uncertainties. *Global
2712 Ecology and Biogeography* 9(3), 225–252.

- 2713 Knorr, W. and M. Heimann (2001). Uncertainties in global terrestrial biosphere
2714 modeling: 1. A comprehensive sensitivity analysis with a new photosynthesis
2715 and energy balance scheme. *Global Biogeochemical Cycles* 15(1), 207–225.
- 2716 Kulmatiski, A., P. B. Adler, J. M. Stark, and A. T. Tredennick (2017). Water
2717 and nitrogen uptake are better associated with resource availability than
2718 root biomass. *Ecosphere* 8(3), e01738.
- 2719 Lavergne, A., D. Sandoval, V. J. Hare, H. Graven, and I. C. Prentice (2020).
2720 Impacts of soil water stress on the acclimated stomatal limitation of pho-
2721 tosynthesis: Insights from stable carbon isotope data. *Global Change Biol-*
2722 *ogy* 26(12), 7158–7172.
- 2723 Lawrence, D. M., R. A. Fisher, C. D. Koven, K. W. Oleson, S. C. Swen-
2724 son, G. B. Bonan, N. Collier, B. Ghimire, L. Kamphout, D. Kennedy,
2725 E. Kluzeck, P. J. Lawrence, F. Li, H. Li, D. L. Lombardozzi, W. J. Riley,
2726 W. J. Sacks, M. Shi, M. Vertenstein, W. R. Wieder, C. Xu, A. A. Ali,
2727 A. M. Badger, G. Bisht, M. Broeke, M. A. Brunke, S. P. Burns, J. Buzan,
2728 M. Clark, A. Craig, K. M. Dahlin, B. Drewniak, J. B. Fisher, M. Flanner,
2729 A. M. Fox, P. Gentine, F. M. Hoffman, G. Keppel-Aleks, R. Knox, S. Ku-
2730 mar, J. Lenaerts, L. R. Leung, W. H. Lipscomb, Y. Lu, A. Pandey, J. D.
2731 Pelletier, J. Perket, J. T. Randerson, D. M. Ricciuto, B. M. Sanderson,
2732 A. Slater, Z. M. Subin, J. Tang, R. Q. Thomas, M. Val Martin, and X. Zeng
2733 (2019). The Community Land Model Version 5: description of new features,
2734 benchmarking, and impact of forcing uncertainty. *Journal of Advances in*
2735 *Modeling Earth Systems* 11(12), 4245–4287.
- 2736 LeBauer, D. S. and K. K. Treseder (2008). Nitrogen limitation of net primary

- 2737 productivity. *Ecology* 89(2), 371–379.
- 2738 Lefcheck, J. S. (2016). piecewiseSEM: Piecewise structural equation modelling
2739 in r for ecology, evolution, and systematics. *Methods in Ecology and Evolution*
2740 7(5), 573–579.
- 2741 Lenth, R. (2019). emmeans: estimated marginal means, aka least-squares
2742 means.
- 2743 Li, W., H. Zhang, G. Huang, R. Liu, H. Wu, C. Zhao, and N. G. McDowell
2744 (2020). Effects of nitrogen enrichment on tree carbon allocation: A global
2745 synthesis. *Global Ecology and Biogeography* 29(3), 573–589.
- 2746 Liang, J., X. Qi, L. Souza, and Y. Luo (2016). Processes regulating progressive
2747 nitrogen limitation under elevated carbon dioxide: a meta-analysis. *Biogeosciences*
2748 13(9), 2689–2699.
- 2749 Liang, X., T. Zhang, X. Lu, D. S. Ellsworth, H. BassiriRad, C. You, D. Wang,
2750 P. He, Q. Deng, H. Liu, J. Mo, and Q. Ye (2020). Global response patterns of
2751 plant photosynthesis to nitrogen addition: A meta-analysis. *Global Change
2752 Biology* 26(6), 3585–3600.
- 2753 Lu, J., J. Yang, C. Keitel, L. Yin, P. Wang, W. Cheng, and F. A. Dijkstra
2754 (2022). Belowground Carbon Efficiency for Nitrogen and Phosphorus Ac-
2755 quisition Varies Between *Lolium perenne* and *Trifolium repens* and Depends
2756 on Phosphorus Fertilization. *Frontiers in Plant Science* 13, 1–9.
- 2757 Luo, X., T. F. Keenan, J. M. Chen, H. Croft, I. C. Prentice, N. G. Smith,
2758 A. P. Walker, H. Wang, R. Wang, C. Xu, and Y. Zhang (2021). Global
2759 variation in the fraction of leaf nitrogen allocated to photosynthesis. *Nature*

- 2760** *Communications* 12(1), 4866.
- 2761** Luo, Y., W. S. Currie, J. S. Dukes, A. C. Finzi, U. A. Hartwig, B. A. Hungate,
- 2762** R. E. McMurtrie, R. Oren, W. J. Parton, D. E. Pataki, R. M. Shaw, D. R.
- 2763** Zak, and C. B. Field (2004). Progressive nitrogen limitation of ecosystem
- 2764** responses to rising atmospheric carbon dioxide. *BioScience* 54(8), 731–739.
- 2765** Maire, V., P. Martre, J. Kattge, F. Gastal, G. Esser, S. Fontaine, and J.-F.
- 2766** Soussana (2012). The coordination of leaf photosynthesis links C and N
- 2767** fluxes in C₃ plant species. *PLoS ONE* 7(6), e38345.
- 2768** Makino, A. (2003). Rubisco and nitrogen relationships in rice: leaf photosyn-
- 2769** thesis and plant growth. *Soil Science and Plant Nutrition* 49(3), 319–327.
- 2770** Makino, A., M. Harada, T. Sato, H. Nakano, and T. Mae (1997). Growth and N
- 2771** Allocation in Rice Plants under CO₂ Enrichment. *Plant Physiology* 115(1),
- 2772** 199–203.
- 2773** Markham, J. H. and C. Zekveld (2007). Nitrogen fixation makes biomass al-
- 2774** location to roots independent of soil nitrogen supply. *Canadian Journal of*
- 2775** *Botany* (9), 787–793.
- 2776** Marschner, H. and B. Dell (1994). Nutrient uptake in mycorrhizal symbiosis.
- 2777** *Plant and Soil* 159(1), 89–102.
- 2778** Matamala, R. and W. H. Schlesinger (2000). Effects of elevated atmospheric
- 2779** CO₂ on fine root production and activity in an intact tem-
- 2780** perate forest ecosystem. *Global Change Biology* 6(8), 967–979.
- 2781** Medlyn, B. E., E. Dreyer, D. S. Ellsworth, M. Forstreuter, P. C. Harley,
- 2782** M. U. F. Kirschbaum, X. Le Roux, P. Montpied, J. Strassmeyer, A. Wal-

- 2783 croft, K. Wang, and D. Loustau (2002). Temperature response of parameters
2784 of a biochemically based model of photosynthesis. II. A review of experimen-
2785 tal data. *Plant, Cell and Environment* 25(9), 1167–1179.
- 2786 Menge, D. N. L., S. A. Levin, and L. O. Hedin (2008). Evolutionary tradeoffs can
2787 select against nitrogen fixation and thereby maintain nitrogen limitation.
2788 *Proceedings of the National Academy of Sciences* 105(5), 1573–1578.
- 2789 Menne, M. J., I. Durre, R. S. Vose, B. E. Gleason, and T. G. Houston (2012).
2790 An overview of the global historical climatology network-daily database.
2791 *Journal of Atmospheric and Oceanic Technology* 29(7), 897–910.
- 2792 Meyerholt, J., K. Sickel, and S. Zaehle (2020). Ensemble projections elucidate
2793 effects of uncertainty in terrestrial nitrogen limitation on future carbon up-
2794 take. *Global Change Biology* 26(7), 3978–3996.
- 2795 Meyerholt, J., S. Zaehle, and M. J. Smith (2016). Variability of pro-
2796 jected terrestrial biosphere responses to elevated levels of atmospheric
2797 CO₂ due to uncertainty in biological nitrogen fixation. *Bio-*
2798 *geosciences* 13(5), 1491–1518.
- 2799 Minocha, R., S. Long, A. H. Magill, J. D. Aber, and W. H. McDowell (2000).
2800 Foliar free polyamine and inorganic ion content in relation to soil and soil
2801 solution chemistry in two fertilized forest stands at the Harvard Forest,
2802 Massachusetts. *Plant and Soil* 222(1-2), 119–137.
- 2803 Moore, D. J., S. Aref, R. M. Ho, J. S. Pippen, J. G. Hamilton, and E. H. De
2804 Lucia (2006). Annual basal area increment and growth duration of *Pinus*
2805 *taeda* in response to eight years of free-air carbon dioxide enrichment. *Global*
2806 *Change Biology* 12(8), 1367–1377.

- 2807 Morgan, J. A., D. E. Pataki, C. Körner, H. Clark, S. J. Del Grosso, J. M.
2808 Grünzweig, A. K. Knapp, A. R. Mosier, P. C. D. Newton, P. A. Niklaus,
2809 J. B. Nippert, R. S. Nowak, W. J. Parton, H. W. Polley, and M. R. Shaw
2810 (2004). Water relations in grassland and desert ecosystems exposed to ele-
2811 vated atmospheric CO₂. *Oecologia* 140(1), 11–25.
- 2812 Muñoz, N., X. Qi, M. W. Li, M. Xie, Y. Gao, M. Y. Cheung, F. L. Wong, and
2813 H.-M. Lam (2016). Improvement in nitrogen fixation capacity could be part
2814 of the domestication process in soybean. *Heredity* 117(2), 84–93.
- 2815 Nadelhoffer, K. J. and J. W. Raich (1992). Fine root production estimates and
2816 belowground carbon allocation in forest ecosystems. *Ecology* 73(4), 1139–
2817 1147.
- 2818 Niinemets, Ü. and J. D. Tenhunen (1997). A model separating leaf struc-
2819 tural and physiological effects on carbon gain along light gradients for the
2820 shade-tolerant species <i>Acer saccharum</i>. *Plant, Cell and Environ-
2821 ment* 20(7), 845–866.
- 2822 Norby, R. J., J. Ledford, C. D. Reilly, N. E. Miller, and E. G. O'Neill
2823 (2004). Fine-root production dominates response of a deciduous forest to
2824 atmospheric CO₂ enrichment. *Proceedings of the National Academy of Sci-
2825 ences* 101(26), 9689–9693.
- 2826 Norby, R. J., J. M. Warren, C. M. Iversen, B. E. Medlyn, and R. E. Mc-
2827 Murtrie (2010). CO₂ enhancement of forest productivity constrained by
2828 limited nitrogen availability. *Proceedings of the National Academy of Sci-
2829 ences* 107(45), 19368–19373.
- 2830 Novick, K. A., D. L. Ficklin, P. C. Stoy, C. A. Williams, G. Bohrer, A. C.

- 2831** Oishi, S. A. Papuga, P. D. Blanken, A. Noormets, B. N. Sulman, R. L.
2832 Scott, L. Wang, and R. P. Phillips (2016). The increasing importance of
2833 atmospheric demand for ecosystem water and carbon fluxes. *Nature Climate
Change* 6(11), 1023–1027.
- 2835** Noyce, G. L., M. L. Kirwan, R. L. Rich, and J. P. Megonigal (2019). Asyn-
2836 chronous nitrogen supply and demand produce nonlinear plant allocation
2837 responses to warming and elevated CO₂. *Proceedings of the
2838 National Academy of Sciences* 116(43), 21623–21628.
- 2839** Onoda, Y., K. Hikosaka, and T. Hirose (2004). Allocation of nitrogen to
2840 cell walls decreases photosynthetic nitrogen-use efficiency. *Functional Ecol-
ogy* 18(3), 419–425.
- 2842** Onoda, Y., I. J. Wright, J. R. Evans, K. Hikosaka, K. Kitajima, Ü. Niinemets,
2843 H. Poorter, T. Tosens, and M. Westoby (2017). Physiological and structural
2844 tradeoffs underlying the leaf economics spectrum. *New Phytologist* 214(4),
2845 1447–1463.
- 2846** Oreskes, N., K. Shrader-Frechette, and K. Belitz (1994). Verification, vali-
2847 dation, and confirmation of numerical models in the Earth sciences. *Sci-
2848 ence* 263(5147), 641–646.
- 2849** Paillassa, J., I. J. Wright, I. C. Prentice, S. Pepin, N. G. Smith, G. Ethier,
2850 A. C. Westerband, L. J. Lamarque, H. Wang, W. K. Cornwell, and V. Maire
2851 (2020). When and where soil is important to modify the carbon and water
2852 economy of leaves. *New Phytologist* 228(1), 121–135.
- 2853** Parvin, S., S. Uddin, S. Tausz Posch, R. Armstrong, and M. Tausz (2020). Car-
2854 bon sink strength of nodules but not other organs modulates photosynthesis

- 2855 of faba bean (*i>Vicia faba</i>) grown under elevated [CO₂] and different
2856 water supply. *New Phytologist* 227(1), 132–145.*
- 2857 Peng, Y., K. J. Bloomfield, L. A. Cernusak, T. F. Domingues, and I. C. Prentice (2021). Global climate and nutrient controls of photosynthetic capacity.
2858 *Communications Biology* 4(1), 462.
- 2860 Perkowski, E. A., E. F. Waring, and N. G. Smith (2021). Root mass carbon
2861 costs to acquire nitrogen are determined by nitrogen and light availability
2862 in two species with different nitrogen acquisition strategies. *Journal of*
2863 *Experimental Botany* 72(15), 5766–5776.
- 2864 Phillips, R. P., E. R. Brzostek, and M. G. Midgley (2013). The mycorrhizal-
2865 associated nutrient economy: a new framework for predicting carbon-
2866 nutrient couplings in temperate forests. *New Phytologist* 199(1), 41–51.
- 2867 Phillips, R. P., A. C. Finzi, and E. S. Bernhardt (2011). Enhanced root ex-
2868 udation induces microbial feedbacks to N cycling in a pine forest under
2869 long-term CO₂ fumigation. *Ecology Letters* 14(2), 187–194.
- 2870 Pinheiro, J. and D. Bates (2022). nlme: linear and nonlinear mixed effects
2871 models.
- 2872 Poggio, L., L. M. De Sousa, N. H. Batjes, G. B. M. Heuvelink, B. Kempen,
2873 E. Ribeiro, and D. Rossiter (2021). SoilGrids 2.0: Producing soil information
2874 for the globe with quantified spatial uncertainty. *Soil* 7(1), 217–240.
- 2875 Pons, T. L. and R. W. Pearcy (1994). Nitrogen reallocation and photosynthetic
2876 acclimation in response to partial shading in soybean plants. *Physiologia*
2877 *Plantarum* 92(4), 636–644.

- 2878** Poorter, H., J. Bühler, D. Van Dusschoten, J. Climent, and J. A. Postma (2012).
- 2879** Pot size matters: A meta-analysis of the effects of rooting volume on plant
- 2880** growth. *Functional Plant Biology* 39(11), 839–850.
- 2881** Poorter, H., O. Knopf, I. J. Wright, A. A. Temme, S. W. Hogewoning, A. Graf,
- 2882** L. A. Cernusak, and T. L. Pons (2022). A meta-analysis of responses of C₃
- 2883** plants to atmospheric CO₂: dose-response curves for 85 traits ranging from
- 2884** the molecular to the whole-plant level. *New Phytologist* 233(4), 1560–1596.
- 2885** Prentice, I. C., N. Dong, S. M. Gleason, V. Maire, and I. J. Wright (2014).
- 2886** Balancing the costs of carbon gain and water transport: testing a new theo-
- 2887** retical framework for plant functional ecology. *Ecology Letters* 17(1), 82–91.
- 2888** Prentice, I. C., X. Liang, B. E. Medlyn, and Y.-P. Wang (2015). Reliable, ro-
- 2889** bust and realistic: The three R's of next-generation land-surface modelling.
- 2890** *Atmospheric Chemistry and Physics* 15, 5987–6005.
- 2891** Priestley, C. H. B. and R. J. Taylor (1972). On the Assessment of Surface
- 2892** Heat Flux and Evaporation Using Large-Scale Parameters. *Monthly Weather*
- 2893** *Review* 100(2), 81–92.
- 2894** Querejeta, J. I., I. Prieto, C. Armas, F. Casanoves, J. S. Diémé, M. Diouf,
- 2895** H. Yossi, B. Kaya, F. I. Pugnaire, and G. M. Rusch (2022). Higher leaf
- 2896** nitrogen content is linked to tighter stomatal regulation of transpiration
- 2897** and more efficient water use across dryland trees. *New Phytologist* 235(4),
- 2898** 1351–1364.
- 2899** R Core Team (2021). R: A language and environment for statistical computing.
- 2900** Raich, J. W., D. A. Clark, L. Schwendenmann, and T. E. Wood (2014). Above-

- 2901 ground tree growth varies with belowground carbon allocation in a tropical
2902 rainforest environment. *PLoS ONE* 9(6), e100275.
- 2903 Rastetter, E. B., P. M. Vitousek, C. B. Field, G. R. Shaver, D. Herbert, and
2904 G. I. Ågren (2001). Resource optimization and symbiotic nitrogen fixation.
2905 *Ecosystems* 4(4), 369–388.
- 2906 Reich, P. B. (2014). The world-wide 'fast-slow' plant economics spectrum: a
2907 traits manifesto. *Journal of Ecology* 102(2), 275–301.
- 2908 Reich, P. B., S. E. Hobbie, T. Lee, D. S. Ellsworth, J. B. West, D. Tilman,
2909 J. M. H. Knops, S. Naeem, and J. Trost (2006). Nitrogen limitation con-
2910 strains sustainability of ecosystem response to CO₂. *Nature* 440(7086), 922–925.
- 2911 Rhine, E. D., R. L. Mulvaney, E. J. Pratt, and G. K. Sims (1998). Improving
2912 the Berthelot reaction for determining ammonium in soil extracts and water.
2913 *Soil Science Society of America Journal* 62(2), 473.
- 2914 Rogers, A. (2014). The use and misuse of V_{cmax} in Earth System Models. *Photo-*
2915 *tosynthesis Research* 119(1-2), 15–29.
- 2916 Rogers, A., B. E. Medlyn, J. S. Dukes, G. B. Bonan, S. Caemmerer, M. C.
2917 Dietze, J. Kattge, A. D. B. Leakey, L. M. Mercado, Ü. Niinemets, I. C.
2918 Prentice, S. P. Serbin, S. Sitch, D. A. Way, and S. Zaehle (2017). A roadmap
2919 for improving the representation of photosynthesis in Earth system models.
2920 *New Phytologist* 213(1), 22–42.
- 2921 Saathoff, A. J. and J. Welles (2021). Gas exchange measurements in the un-
2922 steady state. *Plant Cell and Environment* 44(11), 3509–3523.

- 2924** Saleh, A. M., M. Abdel-Mawgoud, A. R. Hassan, T. H. Habeeb, R. S. Yehia,
2925 and H. AbdElgawad (2020). Global metabolic changes induced by arbuscular
2926 mycorrhizal fungi in oregano plants grown under ambient and elevated levels
2927 of atmospheric CO₂. *Plant Physiology and Biochemistry* 151, 255–263.
- 2928** Saxton, K. E. and W. J. Rawls (2006). Soil water characteristic estimates by
2929 texture and organic matter for hydrologic solutions. *Soil Science Society of
2930 America Journal* 70(5), 1569–1578.
- 2931** Schaefer, K., C. R. Schwalm, C. Williams, M. A. Arain, A. Barr, J. M. Chen,
2932 K. J. Davis, D. Dimitrov, T. W. Hilton, D. Y. Hollinger, E. Humphreys,
2933 B. Poulter, B. M. Racza, A. D. Richardson, A. Sahoo, P. Thornton, R. Var-
2934 gas, H. Verbeeck, R. Anderson, I. Baker, T. A. Black, P. Bolstad, J. Chen,
2935 P. S. Curtis, A. R. Desai, M. C. Dietze, D. Dragoni, C. M. Gough, R. F.
2936 Grant, L. Gu, A. K. Jain, C. Kucharik, B. E. Law, S. Liu, E. Lokipitiya,
2937 H. A. Margolis, R. Matamala, J. H. McCaughey, R. Monson, J. W. Munger,
2938 W. Oechel, C. Peng, D. T. Price, D. Ricciuto, W. J. Riley, N. Roulet,
2939 H. Tian, C. Tonitto, M. Torn, E. Weng, and X. Zhou (2012). A model-
2940 data comparison of gross primary productivity: Results from the North
2941 American Carbon Program site synthesis. *Journal of Geophysical Research:*
2942 *Biogeosciences* 117(G3), G03010.
- 2943** Schneider, C. A., W. S. Rasband, and K. W. Eliceiri (2012). NIH Image to
2944 ImageJ: 25 years of image analysis. *Nature Methods* 9(7), 671–675.
- 2945** Scott, H. G. and N. G. Smith (2022). A Model of C4 Photosynthetic Acclimation
2946 Based on Least-Cost Optimality Theory Suitable for Earth System Model
2947 Incorporation. *Journal of Advances in Modeling Earth Systems* 14(3), 1–16.

- 2948 Shi, M., J. B. Fisher, E. R. Brzostek, and R. P. Phillips (2016). Carbon cost
2949 of plant nitrogen acquisition: Global carbon cycle impact from an improved
2950 plant nitrogen cycle in the Community Land Model. *Global Change Biology*
2951 *22*(3), 1299–1314.
- 2952 Shi, M., J. B. Fisher, R. P. Phillips, and E. R. Brzostek (2019). Neglecting
2953 plant–microbe symbioses leads to underestimation of modeled climate im-
2954 pacts. *Biogeosciences* *16*(2), 457–465.
- 2955 Smith, B., D. Wärllind, A. Arneth, T. Hickler, P. Leadley, J. Siltberg, and
2956 S. Zaehle (2014). Implications of incorporating N cycling and N limitations
2957 on primary production in an individual-based dynamic vegetation model.
2958 *Biogeosciences* *11*(7), 2027–2054.
- 2959 Smith, N. G. and J. S. Dukes (2013). Plant respiration and photosynthesis in
2960 global-scale models: incorporating acclimation to temperature and CO₂.
2961 *Global Change Biology* *19*(1), 45–63.
- 2962 Smith, N. G. and T. F. Keenan (2020). Mechanisms underlying leaf photosyn-
2963 thetic acclimation to warming and elevated CO₂ as inferred from least-cost
2964 optimality theory. *Global Change Biology* *26*(9), 5202–5216.
- 2965 Smith, N. G., T. F. Keenan, I. C. Prentice, H. Wang, I. J. Wright, Ü. Niinemets,
2966 K. Y. Crous, T. F. Domingues, R. Guerrieri, F. oko Ishida, J. Kattge, E. L.
2967 Kruger, V. Maire, A. Rogers, S. P. Serbin, L. Tarvainen, H. F. Togashi,
2968 P. A. Townsend, M. Wang, L. K. Weerasinghe, and S.-X. Zhou (2019).
2969 Global photosynthetic capacity is optimized to the environment. *Ecology*
2970 *Letters* *22*(3), 506–517.
- 2971 Smith, N. G., D. L. Lombardozzi, A. Tawfik, G. B. Bonan, and J. S. Dukes

- 2972 (2017). Biophysical consequences of photosynthetic temperature acclimation
2973 for climate. *Journal of Advances in Modeling Earth Systems* 9(1), 536–547.
- 2974 Smith, N. G., S. L. Malyshev, E. Shevliakova, J. Kattge, and J. S. Dukes
2975 (2016). Foliar temperature acclimation reduces simulated carbon sensitivity
2976 to climate. *Nature Climate Change* 6(4), 407–411.
- 2977 Smith, S. E. and D. J. Read (2008). *Mycorrhizal Symbiosis*. Academic Press.
- 2978 Soil Survey Staff (2022). Web Soil Survey.
- 2979 Soudzilovskaia, N. A., J. C. Douma, A. A. Akhmetzhanova, P. M. van Bode-
2980 gom, W. K. Cornwell, E. J. Moens, K. K. Treseder, and J. H. C. Cornelissen
2981 (2015). Global patterns of plant root colonization intensity by mycorrhizal
2982 fungi explained by climate and soil chemistry. *Global Ecology and Biogeog-
2983 raphy* 24(3), 371–382.
- 2984 Stocker, B. D., H. Wang, N. G. Smith, S. P. Harrison, T. F. Keenan, D. San-
2985 doval, T. Davis, and I. C. Prentice (2020). P-model v1.0: An optimality-
2986 based light use efficiency model for simulating ecosystem gross primary pro-
2987 duction. *Geoscientific Model Development* 13(3), 1545–1581.
- 2988 Stocker, B. D., J. Zscheischler, T. F. Keenan, I. C. Prentice, J. Peñuelas, and
2989 S. I. Seneviratne (2018). Quantifying soil moisture impacts on light use
2990 efficiency across biomes. *New Phytologist* 218(4), 1430–1449.
- 2991 Sulman, B. N., D. T. Roman, K. Yi, L. Wang, R. P. Phillips, and K. A.
2992 Novick (2016). High atmospheric demand for water can limit forest car-
2993 bon uptake and transpiration as severely as dry soil. *Geophysical Research
2994 Letters* 43(18), 9686–9695.

- 2995** Sulman, B. N., E. Shevliakova, E. R. Brzostek, S. N. Kivlin, S. L. Malyshev,
2996 D. N. L. Menge, and X. Zhang (2019). Diverse mycorrhizal associations
2997 enhance terrestrial C storage in a global model. *Global Biogeochemical Cy-*
2998 *cles* 33(4), 501–523.
- 2999** Sweet, S. K., D. W. Wolfe, A. DeGaetano, and R. Benner (2017). Anatomy
3000 of the 2016 drought in the Northeastern United States: Implications for
3001 agriculture and water resources in humid climates. *Agricultural and Forest*
3002 *Meteorology* 247, 571–581.
- 3003** Taylor, B. N. and D. N. L. Menge (2018). Light regulates tropical symbiotic
3004 nitrogen fixation more strongly than soil nitrogen. *Nature Plants* 4(9), 655–
3005 661.
- 3006** Terrer, C., S. Vicca, B. A. Hungate, R. P. Phillips, and I. C. Prentice (2016).
3007 Mycorrhizal association as a primary control of the CO₂ fertilization effect.
3008 *Science* 353(6294), 72–74.
- 3009** Terrer, C., S. Vicca, B. D. Stocker, B. A. Hungate, R. P. Phillips, P. B. Reich,
3010 A. C. Finzi, and I. C. Prentice (2018). Ecosystem responses to elevated CO₂
3011 governed by plant–soil interactions and the cost of nitrogen acquisition. *New*
3012 *Phytologist* 217(2), 507–522.
- 3013** Thieurmel, B. and A. Elmarhraoui (2019). suncalc: Compute sun position,
3014 sunlight phases, moon position, and lunar phase.
- 3015** Thomas, R. Q., E. N. J. Brookshire, and S. Gerber (2015). Nitrogen limita-
3016 tion on land: how can it occur in Earth system models? *Global Change*
3017 *Biology* 21(5), 1777–1793.

- 3018** Thomas, R. Q., S. Zaehle, P. H. Templer, and C. L. Goodale (2013). Global patterns of nitrogen limitation: confronting two global biogeochemical models
- 3019**
- 3020** with observations. *Global Change Biology* 19(10), 2986–2998.
- 3021** Thornton, P. E., J.-F. Lamarque, N. A. Rosenbloom, and N. M. Mahowald
- 3022** (2007). Influence of carbon-nitrogen cycle coupling on land model response
- 3023** to CO₂ fertilization and climate variability. *Global Biogeochemical Cycles* 21(4), GB4018.
- 3024**
- 3025** Tingey, D. T., D. L. Phillips, and M. G. Johnson (2000). Elevated CO₂ and
- 3026** conifer roots: effects on growth, life span and turnover. *New Phytologist* 147(1), 87–103.
- 3027**
- 3028** Udvardi, M. and P. S. Poole (2013). Transport and metabolism in legume-
- 3029** rhizobia symbioses. *Annual Review of Plant Biology* 64, 781–805.
- 3030** USDA NRCS (2022). The PLANTS Database.
- 3031** Uselman, S. M., R. G. Qualls, and R. B. Thomas (2000). Effects of increased
- 3032** atmospheric CO₂, temperature, and soil N availability on root exudation of
- 3033** dissolved organic carbon by a N-fixing tree (*Robinia pseudoacacia* L.). *Plant*
- 3034** and *Soil* 222, 191–202.
- 3035** van Diepen, L. T. A., E. A. Lilleskov, K. S. Pregitzer, and R. M. Miller (2007).
- 3036** Decline of arbuscular mycorrhizal fungi in northern hardwood forests ex-
- 3037** posed to chronic nitrogen additions. *New Phytologist* 176(1), 175–183.
- 3038** Vance, C. P. and G. H. Heichel (1991). Carbon in N₂ fixation: Limitation or
- 3039** exquisite adaptation. *Annual Review of Plant Physiology and Plant Molec-*
- 3040** *ular Biology* 42(1), 373–392.

- 3041** Viet, H. D., J.-H. Kwak, K.-S. Lee, S.-S. Lim, M. Matsushima, S. X. Chang,
3042 K.-H. Lee, and W.-J. Choi (2013). Foliar chemistry and tree ring $\delta^{13}\text{C}$ of
3043 *Pinus densiflora* in relation to tree growth along a soil pH gradient. *Plant*
3044 and *Soil* 363(1-2), 101–112.
- 3045** Vitousek, P. M., K. Cassman, C. C. Cleveland, T. Crews, C. B. Field, N. B.
3046 Grimm, R. W. Howarth, R. Marino, L. Martinelli, E. B. Rastetter, and
3047 J. I. Sprent (2002). Towards an ecological understanding of biological nitro-
3048 gen fixation. In *The Nitrogen Cycle at Regional to Global Scales*, pp. 1–45.
3049 Springer Netherlands.
- 3050** Vitousek, P. M. and R. W. Howarth (1991). Nitrogen limitation on land and in
3051 the sea: How can it occur? *Biogeochemistry* 13(2), 87–115.
- 3052** Vitousek, P. M., S. Porder, B. Z. Houlton, and O. A. Chadwick (2010).
3053 Terrestrial phosphorus limitation: mechanisms, implications, and nitro-
3054 gen–phosphorus interactions. *Ecological Applications* 20(1), 5–15.
- 3055** Walker, A. P., A. P. Beckerman, L. Gu, J. Kattge, L. A. Cernusak, T. F.
3056 Domingues, J. C. Scales, G. Wohlfahrt, S. D. Wullschleger, and F. I. Wood-
3057 ward (2014). The relationship of leaf photosynthetic traits - V_{cmax} and J_{max}
3058 - to leaf nitrogen, leaf phosphorus, and specific leaf area: a meta-analysis
3059 and modeling study. *Ecology and Evolution* 4(16), 3218–3235.
- 3060** Wang, H., I. C. Prentice, T. F. Keenan, T. W. Davis, I. J. Wright, W. K.
3061 Cornwell, B. J. Evans, and C. Peng (2017). Towards a universal model for
3062 carbon dioxide uptake by plants. *Nature Plants* 3(9), 734–741.
- 3063** Wang, W., Y. Wang, G. Hoch, Z. Wang, and J. Gu (2018). Linkage of root mor-
3064 phology to anatomy with increasing nitrogen availability in six temperate

- 3065** tree species. *Plant and Soil* 425(1-2), 189–200.
- 3066** Weatherburn, M. W. (1967). Phenol-hypochlorite reaction for determination of
- 3067** ammonia. *Analytical Chemistry* 39(8), 971–974.
- 3068** Wellburn, A. R. (1994). The spectral determination of chlorophylls a and b, as
- 3069** well as total carotenoids, using various solvents with spectrophotometers of
- 3070** different resolution. *Journal of Plant Physiology* 144(3), 307–313.
- 3071** Wen, Z., P. J. White, J. Shen, and H. Lambers (2022). Linking root exuda-
- 3072** tion to belowground economic traits for resource acquisition. *New Phytolo-*
- 3073** *gist* 233(4), 1620–1635.
- 3074** Westerband, A. C., I. J. Wright, V. Maire, J. Paillassa, I. C. Prentice, O. K.
- 3075** Atkin, K. J. Bloomfield, L. A. Cernusak, N. Dong, S. M. Gleason, C. Guil-
- 3076** herme Pereira, H. Lambers, M. R. Leishman, Y. Malhi, and R. H. Nolan
- 3077** (2023). Coordination of photosynthetic traits across soil and climate gradi-
- 3078** ents. *Global Change Biology* 29(3), 1–29.
- 3079** Wieder, W. R., C. C. Cleveland, W. K. Smith, and K. Todd-Brown (2015).
- 3080** Future productivity and carbon storage limited by terrestrial nutrient avail-
- 3081** ability. *Nature Geoscience* 8(6), 441–444.
- 3082** Wieder, W. R., D. M. Lawrence, R. A. Fisher, G. B. Bonan, S. J. Cheng, C. L.
- 3083** Goodale, A. S. Grandy, C. D. Koven, D. L. Lombardozzi, K. W. Oleson,
- 3084** and R. Q. Thomas (2019). Beyond static benchmarking: using experimental
- 3085** manipulations to evaluate land model assumptions. *Global Biogeochemical*
- 3086** *Cycles* 33(10), 1289–1309.
- 3087** Wright, I. J., P. B. Reich, and M. Westoby (2003). Least-cost input mixtures

- 3088 of water and nitrogen for photosynthesis. *The American Naturalist* 161(1),
3089 98–111.
- 3090 Wright, I. J., P. B. Reich, M. Westoby, D. D. Ackerly, Z. Baruch, F. Bongers,
3091 J. Cavender-Bares, T. Chapin, J. H. C. Cornelissen, M. Diemer, J. Flexas,
3092 E. Garnier, P. K. Groom, J. Gulias, K. Hikosaka, B. B. Lamont, T. Lee,
3093 W. Lee, C. Lusk, J. J. Midgley, M.-L. Navas, Ü. Niinemets, J. Oleksyn,
3094 N. Osada, H. Poorter, P. Poot, L. Prior, V. I. Pyankov, C. Roumet, S. C.
3095 Thomas, M. G. Tjoelker, E. J. Veneklaas, and R. Villar (2004). The world-
3096 wide leaf economics spectrum. *Nature* 428(6985), 821–827.
- 3097 Xu-Ri and I. C. Prentice (2017). Modelling the demand for new nitrogen fixation
3098 by terrestrial ecosystems. *Biogeosciences* 14(7), 2003–2017.
- 3099 Zaehle, S., B. E. Medlyn, M. G. De Kauwe, A. P. Walker, M. C. Dietze, T. Hick-
3100 ler, Y. Luo, Y. P. Wang, B. El-Masri, P. Thornton, A. Jain, S. Wang,
3101 D. Warlind, E. Weng, W. Parton, C. M. Iversen, A. Gallet-Budynek, H. Mc-
3102 carthy, A. C. Finzi, P. J. Hanson, I. C. Prentice, R. Oren, and R. J. Norby
3103 (2014). Evaluation of 11 terrestrial carbon-nitrogen cycle models against
3104 observations from two temperate Free-Air CO₂ Enrichment studies. *New
3105 Phytologist* 202(3), 803–822.
- 3106 Zaehle, S., S. Sitch, B. Smith, and F. Hatterman (2005). Effects of parame-
3107 ter uncertainties on the modeling of terrestrial biosphere dynamics. *Global
3108 Biogeochemical Cycles* 19(3), GB3020.
- 3109 Zhu, Q., W. J. Riley, J. Tang, N. Collier, F. M. Hoffman, X. Yang, and G. Bisht
3110 (2019). Representing nitrogen, phosphorus, and carbon interactions in the
3111 E3SM land model: development and global benchmarking. *Journal of Ad-*

- 3112** *vances in Modeling Earth Systems* 11(7), 2238–2258.
- 3113** Ziegler, C., M. E. Dusenge, B. Nyirambangutse, E. Zibera, G. Wallin, and
3114 J. Uddling (2020). Contrasting Dependencies of Photosynthetic Capacity
3115 on Leaf Nitrogen in Early- and Late-Successional Tropical Montane Tree
3116 Species. *Frontiers in Plant Science* 11, 1–12.
- 3117** Ziehn, T., J. Kattge, W. Knorr, and M. Scholze (2011). Improving the pre-
3118 dictability of global CO₂ assimilation rates under climate change. *Geophys-
3119 ical Research Letters* 38(10), L10404.